Application of the Layer-by-Layer Technology in Nucleic Acid Sensing Systems

Inaugural-Dissertation
to obtain the academic degree
Doctor rerum naturalium (Dr. rer. nat.)

submitted to the Department of Biology, Chemistry and Pharmacy
of Freie Universität Berlin

by

Jing Kang

from Taiyuan, China

Berlin, 2011

The work presented herein was carried out in the research group of Priv.-Doz Dr. Lars Dähne in Capsulution Nanoscience AG from May 2007 to October 2008 and in Surflay Nanotec GmbH from November 2008 until December 2010.

Reviewer 1: Priv.-Doz. Dr. L. Dähne, Freie Universität Berlin/Surflay Nanotec GmbH

Reviewer 2: Prof. Dr. E. Rühl, Freie Universität Berlin

Date of defense: 26.04.2011

Abstract

Polyelectrolyte multilayers assembled by the Layer-by-Layer (LbL) technique exhibit unique properties such as nano-thickness/roughness, semipermeability, tuneable physical properties and the versatility of surface modification on a wide range of substrates.

The aim of this work was to exploit the outstanding properties of the LbL films for construction of a novel nucleic acid detection system based on colloidal particles. LbL films were deposited on particle surface where oligodeoxyribonucleotides (ODNs) were covalently immobilised as probe molecules for selective binding of target DNA (hybridisation assay). The detection of the hybridisation was realized by Fluorescence Resonance Energy Transfer (FRET) between a fluorescent donor dye on the particle and an acceptor dye on the target DNA sequence. This method allowed the determination of hybridisation events without washing non-bound DNA away as it is normally necessary for other DNA hybridisation assays. Further advantages of the LbL-ODN system over conventional particle based DNA sensing systems as low non-specific binding and extraordinary high target binding capacity were determined. This was thanks to the specific surface properties of the LbL films such as roughness, flexibility and exact dye molecule positioning in the nanometer scale.

An undesired decrease of fluorescence quantum yield as well as changes in the absorption and emission spectra of certain FRET fluorophores were observed after the dye molecules were coupled onto the polyelectrolytes due to formation of non-fluorescent H-aggregates. A mechanism of the dye H-aggregate formation was proposed and a new synthesis route of dye labelled polyelectrolytes was developed. As a result, the dye H-aggregates could be minimised, allowing a better applicability of dye labelled polyelectrolyte in fluorescence sensing structures.

Furthermore, when the stability of the LbL-ODN system was tested against several external parameters such as temperature, ionic strength and the presence of surfactants, it was discovered that some LbL films were strongly responsive to cationic surfactants. The structural changes of the LbL film upon interaction with several cationic surfactants were investigated and a mechanism of the responsive behaviour was derived. By crosslinking the polyelectrolyte layers, a strategy was developed to stabilise the film. On the other hand, it was shown that cationic surfactants can be used as an efficient trigger for controlled release of the LbL film encapsulated substances.

The aforementioned findings allowed successful exploitation of the LbL technology for the preparation of a particle based nucleic acid detection system as a homogeneous diagnostic assay.

Table of Contents

Acknowledgement

I would like to express my sincere appreciation to all people who helped me for completion of this work.

Firstly I would like to acknowledge Dr. Lars Dähne for giving me the opportunity to work on my PhD thesis in his group as well as for his valuable discussions, guidance and supervision. At the same time, I would like to thank Prof. Dr. Eckart Rühl for accepting me as a PhD student in the department of Chemistry, Free University of Berlin. Without his kind help and advice, I would not be able to start on my PhD journey.

I would like to express my gratitude to Prof. Dr. Gleb Sukhorukov (QueenMary, University of London, UK), who introduced me to the interesting field of polyelectrolyte multilayer films as well as to the great people in Department of Interfaces, Max-Planck Institute. I am also deeply grateful to Prof. Helmuth Möhwald (Department of Interfaces, Max-Planck Institute, Golm, Germany) for giving me the opportunity for AFM and SEM measurements in his department, accepting me as an attendant in their summer schools and his kind support and discussions.

I express my sincere gratitude to all our project partners for the great collaboration, inspiring ideas and scientific discussions held within the consortium work: Prof. Dr. Andreas Herrmann, Dr. Anna Arbuzova and Martin Loew from Department of Molecular Biophysics, Humbolt University of Berlin; Prof. Dr. Jürgen Liebscher and his group members from Institute of Chemistry, Humboldt University of Berlin; Dr. Ioanna Andreou from Qiagen GmbH (Hilden, Germany); Prof. Dr. Daniel Huster and his group members from Institute of Medical Physics and Biophysics, University of Leipzig.

Many thanks to all my colleagues in Surflay GmbH and Capsulution Phama AG for providing the friendly and harmonic working environment. They have made my time in Germany delightful and unforgetful. I especially thank Mrs Barbara Baude for her great care to me at work and patience to all my small questions throughtout the entire time. I would also like to thank my office mate Dr. Gabriella Egri for all the sharing moments of happiness as well as problems at work and in life; and also for her useful technical tips for mastering graphic softwares.

Finally, I would like to thank my husband Vineet and my parents for their love, encouragement and supports. I would not be able to accomplish this work without them.

This work was funded by the Federal Ministry of Education and Research, Germany (BMBF project INUNA FKZ 0312027A).

List of Abbreviations

A_{21}	21-mer polyadenosine oligonucleotide
AFM	atomic force microscopy
BAC	alkyldimethylbenzylammonium chloride
BSA	bovine serum albumin
CDI	1,1'-Carbonyldiimidazol
CeTAB	cetyltrimethylammonium bromide
CLSM	confocal laser scanning microscopy
Cy3	1-methyl-1'-(5-carboxypentyl)-Cy3
Cy3-PMAA	1-methyl-1'-(5-carboxypentyl)-Cy3 labelled poly(methacrylic acid sodium salt)
Cy5	1-methyl-1'-(5-carboxypentyl)-Cy5
Cy5-PAH	1-methyl-1'-(5-carboxypentyl)-Cy5 labelled poly(allylamine hydrochloride)
DACl	diallyldimethylammonium chloride
DIC	diisopropyl carbodiimide
disulfo-Cy5	1-(4-sulfobutyl)-1'-(5-carboxypentyl)-6'-sulfonate-Cy5
disulfo-Cy5-PAH	1-(4-sulfobutyl)-1'-(5-carboxypentyl)-6'-sulfonate-Cy5 labelled poly(allylamine hydrochloride)
DMF	dimethylformamide
DMSO	dimethylsulfoxid
DNA	deoxyribonucleic acid
DoTAB	dodecyltrimethylammoniumbromide
dsODN	double stranded oligonucleotide
EDC	1-(3-dimethylaminopropyl)-3-ethylcarbodiimide hydrochloride
EDTA	ethylenediaminetetraacetic acid disodium salt
FACS	fluorescence activated cell sorting
FITC	fluorescein isothiocyanate
FITC-dextran	fluorescein isothiocyanate-labelled dextran
Flu	fluorescein-amine

$FluA_{21}$	21-mer polyadenosine oligonucleotide labelled with fluorescein at 5' end
FluODN	fluorescein labelled oligonucleotide
Flu-PMAA	fluorescein labelled poly(methacrylic acid sodium salt)
FRET	Förster resonance energy transfer
FSC	forward scatter
HEPES	4-(2-hydroxyethyl)-1-piperazine ethanesulfonic acid
I_{FRET}	fluorescence intensity of the acceptor fluorophore induced by excitation of the donor fluorophore
LbL	layer-by-layer
LbL-ODN	amine modified oligonucleotide covalently coupled on layer-by-layer films
LUVs	large unilamellar vesicles
MF	melamine formaldehyde
mRho	methacroyloxyethylthiocarbamoyl rhodamine B
NaSS	sodium styrene sulfonate
ODN	oligodeoxyribonucleotides
PAH	poly(allylamine hydrochloride)
PDA	poly(diallyldimethylammonium chloride)
PMAA	poly(methacrylic acid sodium salt)
PMT	photomultiplier tube
PMV	photomultiplier voltage
PNA	peptide nucleic acid
PSS	poly(styrenesulfonate sodium salt)
PVA	poly(vinylamine)
QCM	quartz crystal microbalance
$RhoA_{20}$	20-mer polyadenosine oligonucleotide labelled with rhodamine at 5' end
Rho-PAH	tetramethylrhodamine isothiocyanate labelled poly(allylamine hydrochloride)
Rho-PDA	diallyldimethylammonium chloride-methacroyloxyethylthiocarbamoyl rhodamine B copolymer
Rho-PSS	styrenesulfonate-methacroyloxyethylthiocarbamoyl rhodamine B copolymer

Rho-PVA	tetramethylrhodamine isothiocyanate labelled poly(vinylamine)
$RhoT_{20}$	20-mer polythymidine oligonucleotide labelled with rhodamine at 5’ end
ROI	region of interest
SDS	sodium dodecyl sulfate
SSC	side scatter
ssDNA	single stranded deoxyribonucleic acid
SNP	single nucleotide polymorphism
sulfo-NHS	*N*-hydroxysulfosuccinimide
T_{20}	20-mer polythymidine oligonucleotide
$T_{20}Rho$	20-mer polythymidine oligonucleotide labelled with rhodamine at 3’ end
THF	tetrahydrofuran
TRIS	2-amino-2-hydroxymethyl-1,3-propanediol
TRITC	tetramethylrhodamine isothiocyanate
UV/Vis	ultraviolet/visible

1 Introduction

The design of advanced functional materials with control in the micro/nanometer scale is highly desirable in many applications, especially in the ever expanding and demanding biomedical community. Due to the fast growing needs in rapid disease diagnosis, gene sequencing, food and environmental analysis, specific detection of nucleic acids has drawn great attention from researchers worldwide to develop nucleic acids diagnostic kits having high detection speed, specificity and sensitivity.[1-3]

Nucleic acid detection is usually based on hybridisation of a target DNA to synthetic probe ODNs immobilised on a solid support, e.g. microarray slides,[4] gold nanoparticles,[5-7] quantum dots (QDs)[8, 9] or other particle based systems.[10] Detection of the hybridisation events is mainly performed by optical[11] or electrochemical methods.[12] One advanced optical method is based on FRET, in which the fluorescence from one fluorophore is transferred to another of lower excitation energy when they are in close proximity within the Förster radius (a few nanometers).[13, 14] FRET has been well recognised as a molecular ruler for studying structure and conformational changes of nucleic acids,[15] proteins[16] and for numerous sensing applications.[17] Some FRET systems for DNA detection are applied in solution, such as the Molecular Beacon method[18, 19] and the method of using water soluble conjugated polymers as donor due to the light-harvesting effect[20-22] or the super-quenching property.[23] However, the sensitivity of single particle detection can hardly be achieved by these solution based systems. Particle based FRET systems have the advantage as homogeneous assays without the requirement of particle separation from the analyzing solution. Such systems based on QDs have been prepared for nucleic acid detection, in which the QDs have been used as substrates for biomolecules immobilisation and donor for FRET.[19, 24-28] However, QDs require surface modifications with a relatively thick layer of polymers or other materials to obtain stability against aggregation and enable immobilisation of probe molecules. This enlarges the distance between the QD and the target molecules, which strongly restricts the FRET efficiency.[29, 30] In order to ensure a high FRET signal with a low background fluorescence, the donor dye molecule needs to be located directly on the diagnostic particle surface. For high sensitivity it might be promising to use only a few particles in the micrometer range, on which the whole amount of probe molecules are attached. In contrast to nanoparticles in solution such microparticles can be analyzed with high sensitivity by

Confocal Laser Scanning Microscopy (CLSM) or Flow Cytometry. However, it is difficult to couple simultaneously a high amount of donor dyes and probe ODNs on the surface without using spacer molecules.

Polyelectrolytes represent water soluble polymers including biocompatible macromolecules such as proteins, enzymes, nucleic acids, and carbohydrates etc.[31, 32] They can be labelled with fluorescent tags, and they have been intensively exploited in recent years for biosensing and drug delivery applications. In 1991 a novel surface modification method has been developed, enabling the exact deposition of nanometer-thick layers of polyelectrolyte on planar or colloidal surfaces.[33, 34] This so-called LbL technology uses the self-controlled adsorption of e.g. a polycation to a negatively charged surface. After deposition of a polycation layer of 1-2 nm thickness the surface charge is reversed to positive and a polyanion layer can be adsorbed sequentially in the same manner. Multilayer of polyelectrolytes can be consecutively built up on the surface. A wide range of macromolecules can be employed as the wall build-up materials and the property of the film is tuneable after the assembly by external parameters.[35, 36]

Inspired by the unique properties of the LbL films, it has been evaluated to exploit these properties for the development of a novel DNA detection system based on microparticles modified by the LbL films and covalently coupled with probe ODNs (LbL-ODN particles). The scheme of one such particle is presented in Figure 1.1.

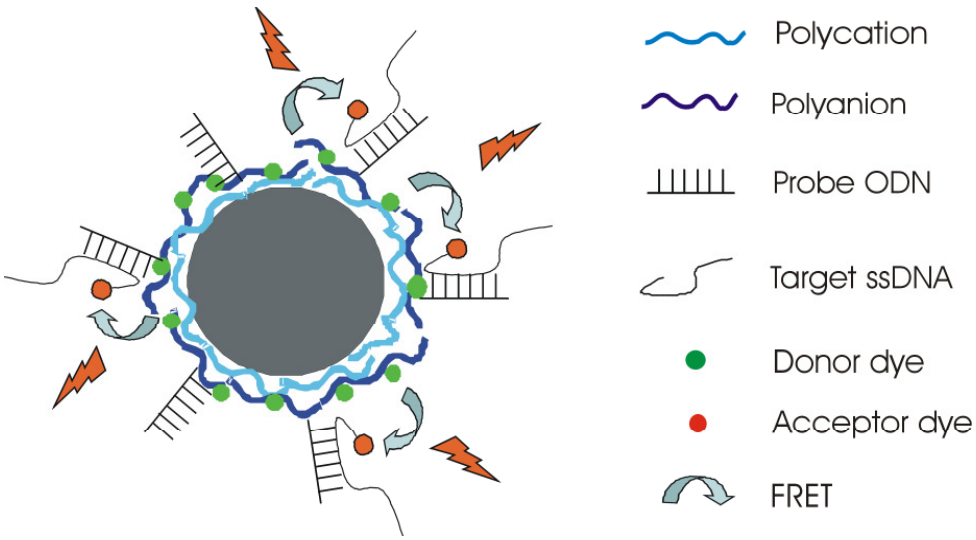

Figure 1.1 Scheme of a single LbL particle with covalently bound probe ODN for ssDNA hybridisation detection via FRET.

Due to the versatility of the LbL process and coupling chemistry there are several possibilities to construct such a system. Different parameters for the preparation have been evaluated and optimised to achieve efficient binding to the target molecules with highest specificity, sensitivity and stability. The developed system is characterised by different methods and the properties as a nucleic acid detection system are evaluated from several key perspectives. Stability and structural changes of the LbL films upon addition of disturbing substances such as cationic surfactants are particularly investigated.

For the development of the detection system, fluorophore labelled polyelectrolytes are prepared and intensively studied. The changes of the absorption spectra and fluorescence quantum yield of the fluorophores upon covalent attachment to the polyelectrolyte are investigated to improve their applicability in fluorescence sensing.

Finally it has been shown that the LbL-technology enables construction of fluorescence based DNA sensing system that exhibit several advantageous features over known commercial systems.

2 Literature review

2.1 Polyelectrolytes

Polyelectrolytes[31, 32, 37-39] are polymers bearing dissociated ionic groups; thus they have dual character of electrolytes and macromolecules. They can be classified into natural (e.g. DNA), modified natural (e.g. cellulose), and synthetic polymers (e.g. poly(diallyldimethylammonium chloride (PDA)). In terms of their charge, they can be divided into polycations, polyanions and polyampholytes (Figure 2.1). Depending on the charge density and acidity of the functional groups, they are classified as strong and weak polyelectrolytes. Strong polyelectrolytes have permanent charges and they are fully ionized over the whole pH range in solution, whereas the degree of dissociation of the ionisable groups on weak polyelectrolytes is highly dependent on the pH.

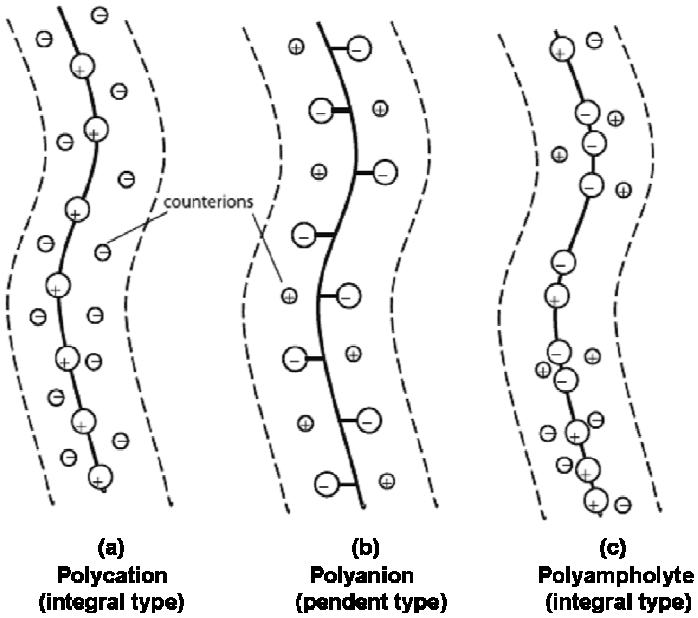

Figure 2.1 Classification of polyelectrolytes into polycations (a), polyanions (b), and polyampholytes (c).[39]

2.2 Polyelectrolyte complexes

One feature of polyelectrolytes is the formation of complexes with oppositely charged large molecules such as polyelectrolytes and surfactants.

2.2.1 Polyelectrolyte complexes with oppositely charged polyelectrolytes

Mixing a polycation solution and a polyanion solution leads to the formation of polyelectrolyte complexes.[31, 32, 39-42] This process is entropy-driven because of the release of counterions that are not restricted to the polymer backbone chain. The process is very fast and mainly controlled by counterion diffusion. When polyelectrolytes with weak ionic groups and large differences in molar mass are used and mixed in a non-stoichiometric ratio, water soluble polyelectrolyte complexes can be formed (homogenous one phase system). When polyelectrolytes with strong ionic groups and similar molar mass are mixed together near 1:1 stoichiometry, complexes are precipitated (phase-separated system, including turbid dispersions). The formation of polyelectrolyte complexes is dependent on the electrostatic interactions of oppositely charged groups. Increase of the ionic strength of the solution leads to a decrease of the ionic interactions between the polyelectrolytes due to screening of the charges. A further increase of salt concentration can even result in complex dissolution. In addition to electrostatic forces, inter-macromolecular interactions are also involved in polyelectrolyte complex formation such as hydrogen bonding, Van der Waals forces, hydrophobic and dipole interactions.

2.2.2 Polyelectrolyte complexes with oppositely charged surfactants

Polyelectrolytes do not only form complexes with oppositely charged polyelectrolytes but also with oppositely charged surfactants.

Generally, surfactants are amphiphiles due to possession of both hydrophobic chain and hydrophilic head groups. They can be divided into non-ionic and ionic ones. The latter one with charged head groups are of special interest for interaction with polyelectrolytes. The interaction between polyelectrolytes and oppositely charged surfactants is mainly driven by electrostatic and hydrophobic forces. Hence the interactions are mainly determined by the properties of the polyelectrolyte such as chemical composition, linear charge density, location of the charges and backbone flexibility (i. e. persistence length) of the polymers.[43-46]

It is well known that surfactant molecules associate at a critical concentration, the so-called critical micellisation concentration (*cmc*), and form spherical micelles containing ten to hundreds of surfactant molecules. It is observed that the presence of polyelectrolytes induces aggregation of oppositely charged surfactants above a surfactant critical aggregation concentration (*cac*) that is lower than the *cmc*. The surfactant aggregates formed in polyelectrolyte solutions are structurally similar to free micelles (Figure 2.2).[39, 47-49]

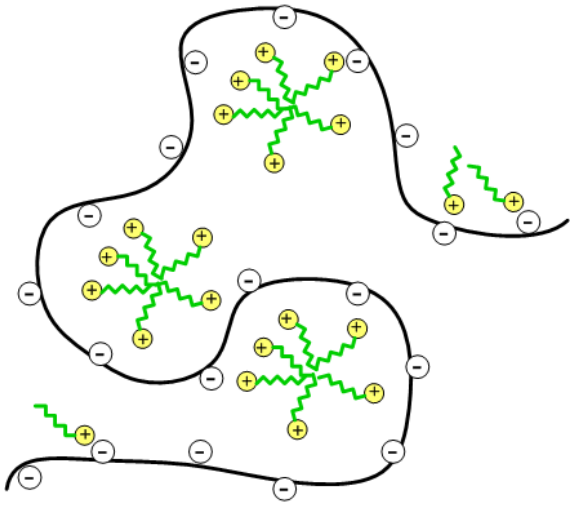

Figure 2.2 Model of polyelectrolyte surfactant aggregates.

In general, the *cac* increases with increasing surfactant chain length. Adding salt reduces the binding affinity between surfactants and oppositely charged polyelectrolytes, which also increases the *cac*. A linear relationship between binding affinity and the ion strength has been observed in several systems.[50, 51] Hydrophobic interactions also play an important role in the complexation: for example, poly(styrenesulfonate) (PSS) leads to much smaller *cac* than other flexible polyelectrolytes due to its hydrophobic backbone.[45, 52] For very hydrophobic polyelectrolytes, where the most repeat units form microdomains, the number of surfactant aggregation domains is proportional to the surfactant concentration. On the contrary, hydrophilic polyelectrolytes bind surfactants cooperatively above the *cac*, and the surfactant aggregation number is nearly independent on the surfactant concentration. Therefore, a higher surfactant concentration is needed for a stronger binding of surfactants with shorter chain length. Detailed description and investigation on polyelectrolyte-surfactant complexes can be found in a few review papers.[46, 53-54]

2.3 Layer-by-Layer electrostatic self-assembly

2.3.1 Assembly of LbL thin films on substrates

Multilayers of polyelectrolytes can be assembled on charged surfaces by the so called Layer-by-Layer (LbL) technology. The first report of the LbL technology can date back to 1966 when Iler prepared a multilayer structure by electrostatic interactions between colloidal anionic and cationic particles.[55] The technology was however not systematically established

until 1990. Decher and Hong started to prepare multilayers of oppositely charged polyelectrolytes on charged substrates.[33-35] As shown in Figure 2.3, when a substrate with positive surface charge is immersed in the aqueous solution of an anionic polyelectrolyte for several minutes, a thin layer of polyanions is adsorbed onto the substrate and the surface charge of the substrate is reversed to be negative. When a defined surface charge is achieved, no further polymers can be adsorbed. Hence, the self-limiting process leads to homogeneous and well reproducible layers of defined thickness on charged surfaces. Non-adsorbed polyelectrolytes are removed by washing the substrate with water. A polycation layer can be assembled onto this negatively charged surface in the same manner. When this cycle is repeated, a multilayer of polyelectrolyte thin film is formed. This process is normally referred to as self-assembly of multilayer films based on electrostatic forces between oppositely charged polyelectrolyte. There are other candidates that can be used besides the polyelectrolytes for the LbL film assembly such as proteins,[56] nucleic acids,[57] lipids,[58] viruses,[59] inorganic nanoparticles,[60] organic dye molecules etc.[61] Moreover, interactions beyond electrostatic forces such as hydrophobic interactions, hydrogen-bonding, covalent bonding, DNA hybridisation and steric interactions between polymers can also be employed for multilayer film assembly.[62-67]

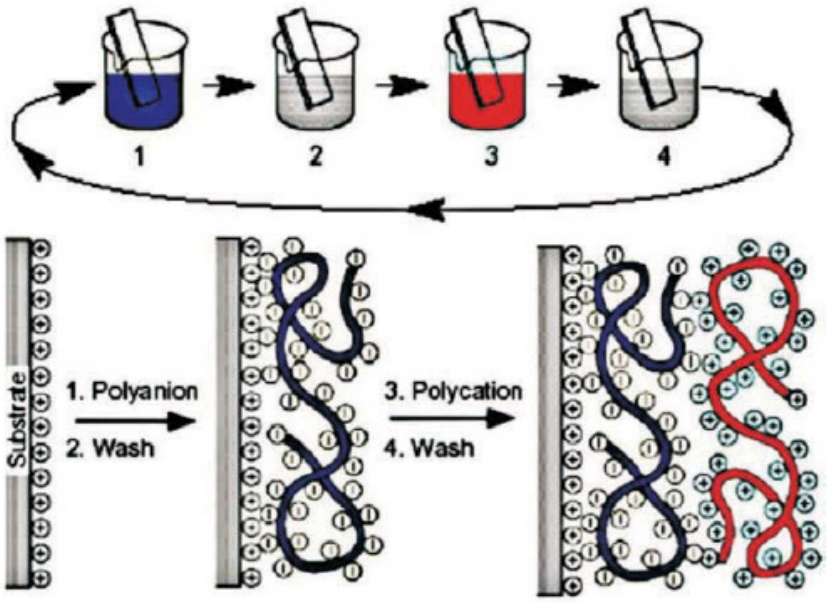

Figure 2.3 Scheme of self-assembly of LbL film on a planar surface.[34]

2.3.2 The structure and growth pattern of the LbL film

When a multilayer film is composed of two simple polyelectrolytes, a pair of oppositely charged homopolyelectrolyte, the film can be subdivided into three distinct zones as shown in Figure 2.4.[68] Zone I is comprised of one or a few polymer layers that are close to the substrate. Zone III is comprised of one or a few layers that are close to the solution or to the air. In this zone, the multilayer is highly influenced by the interface to the solution or to air. Zone II represents the film in a range that is not influenced by either interface. In the simple picture, Zone II is neutral and Zone I and Zone III are charged (with small gradients of excess charges and neutralized by small counterions). Therefore, the physicochemical behavior of the neutral and charged zones is distinguished different. Zone II is charge compensated and thus can behave like a polyzwitterion, while regions of film where there is an excess of charges should behave more like a polyelectrolyte.

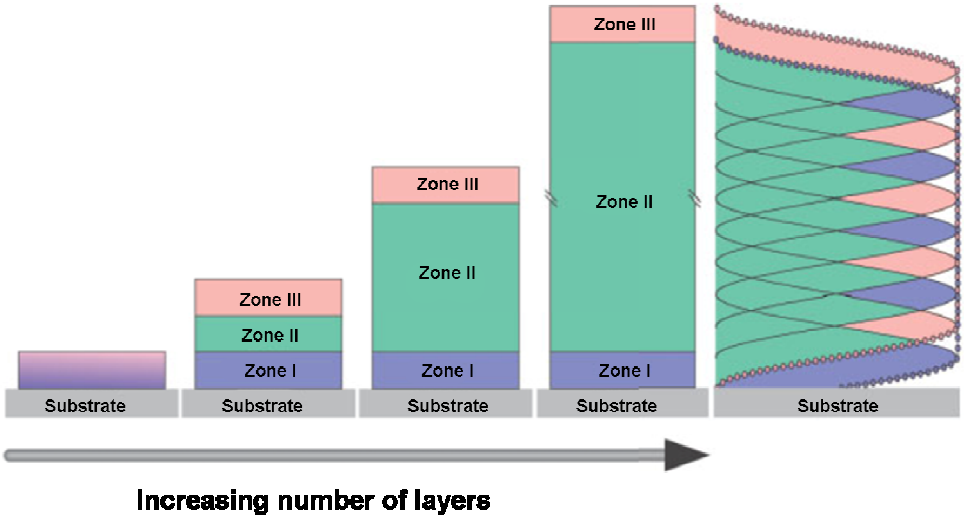

Figure 2.4 The zone model of polyelectrolyte multilayer films.[68]

For LbL films composed of strong polyelectrolytes, such as the combination of (Poly(allylamine hydrochloride)(PAH)/PSS), the film grows linearly with the number of deposition layers. On the contrast, multilayer films composed of weak polyelectrolytes show exponential growth. A model of polyions not being kinetically trapped in the position where they have been deposited but diffusing inside the film has been proposed by Picart *et al.* to explain the nonlinear growth behavior.[69]

2.3.3 Preparation of hollow capsules

In the similar way on planar surfaces, LbL films can be assembled onto colloidal particles by using ultrafiltration or centrifugation to separate the coated particles from excessive polyelectrolyte in the coating solution.[70, 71] Freestanding polyelectrolyte multilayer films can be prepared by dissolving the colloidal template particles after the LbL assembly. The film keeps in the template shape as hollow capsules.[72, 73] The LbL assembly on colloidal particles as well as the core dissolution process is schematically presented in Figure 2.5.

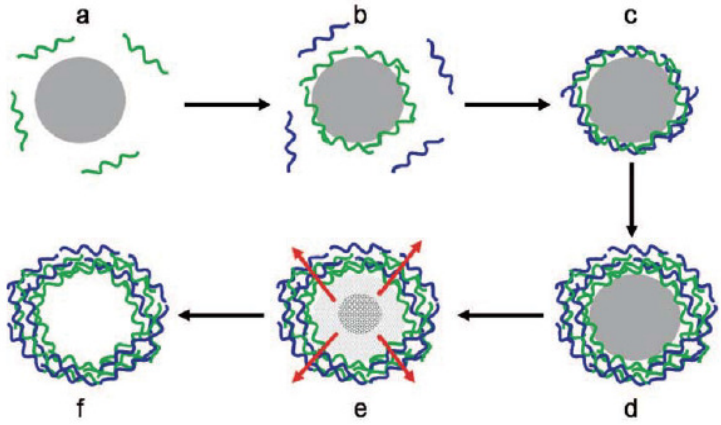

Figure 2.5 Schematic presentation of LbL assembly on colloidal particles and preparation of polyelectrolyte capsules by dissolving the core materials.[73]

The first hollow capsules were made templating on weakly crosslinked melamine formaldehyde (MF) cores that are available in uniform diameters between 100 nm -10 µm, spherical shape and smooth surface (Microparticles GmbH, Berlin).[73] After the LbL film assembly, the cores can be decomposed by 0.1 M HCl or treatment with DMF or DMSO without destroying the polyelectrolyte shell. Polystyrene beads are also used as core material for microcapsule preparation that can be dissolved in tetrahydrofuran (THF) or DMF. However, there are fundamental disadvantages of using organic resins as template materials. The rather large polymer or oligomer molecules induce high osmotic pressure during the dissolution process, because they are only slowly diffusing out of the capsules. This leads to a temporary strong swelling of the capsules.[74] Although the capsules shrink back to the original size, deformations of the shell or pore formation can not be avoided. Especially for thicker LbL films, this process can lead to complete rupture of the shells. Furthermore, there are residual polymers trapped in the shell, which affects the properties of the capsules,[75] and the dissolution in organic solvents can affect the property and stability of the polyelectrolyte

shells.[76] Alternatively, inorganic materials such as SiO_2, $CaCO_3$ or $MnCO_3$ can be adopted as microcapsules templates. Silica particles, in particular, have the advantages of smooth surface, spherical shape, monodispersity, biocompatibility and complete core dissolution by HF treatment. Moreover, they are available in a wide size range with defined porosities. Therefore, polyelectrolyte capsules obtained from SiO_2 template are widely employed for studying the physical properties of freestanding polyelectrolyte multilayer films.[77-79]

Other special types of core materials including blood cells, crystalline proteins, oil or even gas are also encapsulated. In such cases, they are mainly used as functional materials being protected by the LbL film, and the LbL films are often destroyed later to release the functional core materials for the specific applications.[80-83]

2.4 Multifunctional properties of the LbL films

2.4.1 Multifunctional LbL films

Thanks to the broad range of materials that are available to be incorporated into the multilayer films and to the stepwise assembling process, multifunctional properties can be introduced to the LbL film. A simple case is shown in Figure 2.6, where a bi-functional polymer easily functionalizes the surface of the film with group -F. This –F group can present a fluorescent label or some specific functional group. Besides, the –F groups can be used in the next step to change the interaction of deposition; e.g. from ionic to covalent or to donor/acceptor and etc.[56] This can be very useful when a certain multifunctional materials would be otherwise very difficult to prepare.

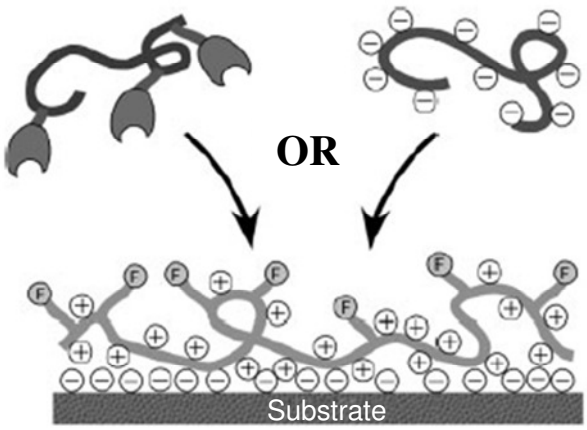

Figure 2.6 Schematic presentation of a polycation with two different functional groups (positive charges and functional groups –F) deposited onto a negatively charged substrate. In the next layer one can either adsorb a polyanion or a polymer capable of binding to –F.[36]

2.4.2 Responsive polyelectrolyte films

In dependence on the composition of the LbL films its structure can be influenced by environmental parameters such as pH, ion strength, temperature, solvent and humidity etc.[84-118] The structure changes are associated with a response of the multilayer films properties such as layer density, permeability and morphology, which may lead to swelling or shrinking of freestanding polyelectrolyte films. Such responses of the polyelectrolyte films have been explored for encapsulation and release of drugs or other substances of interest (section 2.4.3). Polyelectrolyte films that contain weak polyelectrolytes respond to external pH. Formation of pores induced by pH has been experimentally demonstrated for both hollow weak polyelectrolyte capsules and weak polyelectrolyte films on a solid substrate.[88, 89] For LbL films composed of at least one weak polyelectrolyte, reversible porosity can be created if the pH is shifted from the pH of preparation.[89] By that excess charges are created which increases the osmotic pressure in the film by adsorbed counterions. In consequence the water content increases, the film swells and the permeability increases. The switching of permeability has been utilized for binding and releasing low molecular weight compounds such as dyes and drugs,[90-92] encapsulation of water soluble polymers and proteins.[88, 92] For example, Park *et al.* demonstrated that crosslinked weak polyelectrolyte films showed reversible selective ion permeability for both cationic and anionic probe molecules by adjusting external pH.[93] Hiller and Rubner reported reversible swelling of (PAH/PSS) films when large amount of charged groups were deposited during the self-assembly step.[94] Later, Mauser *et al.* prepared pH responsive (PAH/ Poly(methacrylic acid)(PMAA)) microcapsules that were stable over a wide pH range (2.5-11.5) and exhibited reversible swelling and shrinking properties.[78]

Besides pH, ion strength is also a powerful parameter to control permeability of polyelectrolyte films and it is not restricted to weak polyelectrolyte. Ibarz *et al.* showed that capsules permeability could be reversibly switched from impermeable to permeable by variation of ion strength in a low concentration range of 10^{-3} to 10^{-2} M.[95] Antipov *et al.* showed that permeability of fluorescent dye to the (PAH/PSS) capsules was strongly enhanced in 0.5 M NaCl solution.[96]

Earlier approach to prepare temperature responsive polyelectrolyte films was to use thermal responsive polymers for the film assembly.[97-100] Quinn *et al.* demonstrated that film morphology of hydrogen bonded poly(N-isopropylacrylamide)(PNIPAM)/polyacrylic acid multilayers underwent considerable changes at elevated temperatures, which highly

enhanced the absorption of dye and release capability.[100] Leporatti *et al.* initially reported on the swelling and shrinking behavior of (PDA/PSS) microcapsules in response to temperature changes.[101] Ibarz *et al.* studied the influence of annealing of (PAH/PSS) capsules at different temperatures and created a model of the influence on their permeability.[102] Later on, Köhler intensively investigated on thermal behavior of (PDA/PSS) microcapsules and developed it into a versatile method for encapsulation based on the temperature induced rearrangement of the shells.[103-104]

Interaction of microcapsules with electromagnetic waves such as ultrasound, microwaves and light have also been investigated in order to achieve remote activation/opening of the capsules.[105-108] Gold/silver nanoparticles or IR dyes have often been included in the polyelectrolyte films to enable the optical responsiveness of the multilayer microcapsules.[109-112] Incorporation of magnetic particles into the polyelectrolyte multilayer films allows using magnetic field as another stimulus for delivery systems in biomedical applications.[113, 114] Lu *et al.* demonstrated using pulsed magnetic field to change the permeability of the microcapsules. The magnetic field in this case induced the magnetic particles to rotate in the film and irreversibly increase the permeability of film by damaging the shell.[114] Other specific stimuli such as enzyme[115] biotin[116] or other molecules[117-121] can be used to react with LbL films that are embedded or conjugated with DNA, avidin or other specific binding substances, so that the structure and properties of the LbL film are changed. Enzyme-mediated biodegradation of the LbL film is a highly promising method for biomedical applications.

2.4.3 Encapsulation of substances and the controlled release

Encapsulation of drugs or biomolecules and triggered release of the substance at desired time or location has high importance in biomedical applications. Polyelectrolyte microcapsules show semi-permeable properties. They are permeable for small polar molecules but not for macromolecules. The cutoff for molecular weight depends strongly on the material and the layer number. Due to the special properties of the capsules, they have been intensively studied during the last 11 years for encapsulation of various materials and their sustained or controlled release by different triggers.[89-92, 95, 100, 102-105, 115-129]

Substances of interest can be encapsulated into polyelectrolyte microcapsules by different strategies.[74] The most widely applied ones are: 1. Preloading materials into the template particles prior to LbL coating. Porous particles are often employed as templates in this method.[119-121] So far various substances such as drugs, proteins or nucleic acids have been

successfully encapsulated into the capsules in this manner.[122-126] 2. Polymerization of polymeric materials inside the capsules while the monomers can diffuse in but the resulting polymers after the reaction are trapped inside.[127] 3. Preparation of capsules with double shells, whereas the inner shell can be selectively destroyed with the remaining materials encapsulated.[95, 96] 4. Reversibly switching the permeability of the capsule shell via changing environmental parameters as described in section 2.4.2, creating pores temporarily to allow the inward diffusion of macromolecules for encapsulation.[89-92, 102-104, 115-117]

The various parameters that can change the permeability of the polyelectrolyte multilayer films mentioned in 2.4.2 are generally employed for controlled or triggered release of the encapsulated materials at desired conditions. The continuous rapid development of exploiting the polyelectrolyte films as drug carriers with triggered release properties is leading to new strategies in constructing LbL microstructures that can respond to multiple stimuli and deliver multiple active molecules in the controlled way.[130-147]

2.4.4 Surface modification

Due to the easy manipulation of polyelectrolyte multilayer coatings on substrates, LbL films have been used for surface modification, introducing versatile functionalities to a wide range of surfaces.

Great efforts have been devoted towards the functionalisation of material surfaces that are used in biomedical applications in order to provide biocompatibility or new functional biological properties. For example, polyelectrolyte films containing collagen were used to coat cytotoxic materials to provide biocompatibility.[148] Cell surfaces could be coated with LbL films to modify and control the cell functions, such as viability, morphology and proliferation.[149] Bactericidal and virucidal LbL films were synthesized by using polyelectrolyte with microbiocidal activity.[150]

On the more technical side LbL films with superhydrophobic,[151] anticorrosion,[152] antireflection[153-155] or other functions[156-158] have been demonstrated. Due to the vast development of polyelectrolyte multilayer films in varied applications, a number of reviews were published concerning different aspects of the LbL films.[74, 84, 142, 147, 159-170]

2.5 Nucleic acid detection systems

Due to the arisen demand in disease diagnostic and treatment, great attentions from researchers worldwide are paid to the development of nucleic acid assays with high speed, specificity and sensitivity.[171-172] The underlying methods are described in the next chapters.

2.5.1 Immobilisation methods

Probe ODN immobilisation on a surface is the first and critical step in DNA sensor preparation. The attachment should be stable while the probes remain functional. Adsorption, covalent immobilisation and avidin-biotin interactions are the frequently used methods to immobilise probe molecules on the substrates in DNA sensors.[173-178]

To enable covalent immobilisation, probe ODN is modified with functional groups such as thiol, amine or other groups. For example, thiol-modified probe DNA was covalently attached onto gold surfaces due to the strong affinity of the thiol groups on noble metal surfaces.[179, 180] Amine modified ODNs were coupled to carboxylic acid modified surfaces via carbodiimide mediation.[181, 182] 1-(3-dimethylaminopropyl)-3-ethylcarbodiimide (EDC) reaction was found to be very efficient for ODN immobilisation on carboxyl-terminated polymers.[11, 183, 184] Further development can be found in covalent immobilisation of DNA onto versatile substrates for wider applications.[185-188]

2.5.2 Nucleic acid hybridisation detection

Nucleic acid hybridisation can be detected by optical, electrochemical or gravimetric methods.[12, 19, 189, 190] Among these methods, optical sensors are best suited for repetitive analysis and continuous monitoring binding events in real time. Optical imaging methods, based on fluorescence labelled molecules are widely adapted to measuring microarrays of recognition events.

2.5.2.1 Fluorescence based DNA biosensors

When the DNA target is labelled with a fluorophore, its hybridisation with a probe can be measured by an imaging fluorescence apparatus. For example, an optical fiber based nucleic acid sensor was composed of single-stranded DNA (ssDNA) probes immobilised on the surface of an optical fiber. Hybridisation with complementary target DNA was detected through the use of fluorescently labelled target sequences[191] or intercalating dyes that exhibited enhanced fluorescence intensity upon hybridisation.[192]

A significant disadvantage of a single labelled probe was that quantification and visualization of the target was difficult by the strong fluorescence background of the unbound probes, which required an extra step for the removal of unhybridised DNA.[193] Therefore, new generations of fluorescent probes emerged with interesting properties have been exploited to develop DNA biosensors with higher detection limit, selectivity and background discrimination.

The Molecular Beacons (MBs) are specifically designed DNA hairpin structures that are widely used as fluorescent probes. MBs are ssODNs that possess a stem-loop structure in the absence of a target. A fluorophore and a quencher are located at opposite ends of the MB. The formation of the stem-loop structure brings the quencher and fluorophore in close proximity that the fluorophore is quenched effectively. In the presence of a target DNA molecule, hybridisation between the target and the loop sequence of the MB opens the stem helix, which spatially separates the fluorophore and quencher, resulting in restoration of the fluorescence (Figure 2.7). MB probes have the advantages of easy synthesis, molecular specificity and structural tolerance to various modifications. They are better alternatives to conventional linear probes for mismatch discrimination. Therefore they have been widely used for DNA detection.[194, 195] Despite of the relevant advantages of MBs, when employed in complex biological environments, they often give false signals most likely due to the disruption of the hairpin structure from interaction with proteins, membranes or intercalating agents in the cell cytoplasm. Another challenge is that it is not possible to visualize the insertion process of MBs into the cell due to the dark state in the absence of the target.[196, 197]

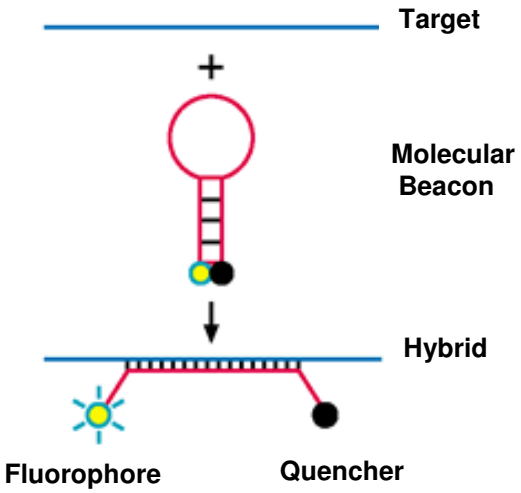

Figure 2.7 Scheme presentation of a MB structure before and after binding to the target.

Quantum dots (QDs) are semiconductor nanocrystals that have broad absorption spectra and exhibit narrow size tunable photoluminescence spectra. They can be excited by a single excitation wavelength and are more photostable than most organic fluorophores. Due to their unique electro-optical properties, QDs have been widely employed in bioassays and biosensors development.[27, 198-202]

The preparation of QD-ODN conjugate, using QDs not only as substrates for probe DNA immobilisation but also as donor for FRET detection, has been reported by several groups for DNA sensor applications.[8, 27, 203, 204] Wang *et al.* prepared as pioneers a single QD based DNA nanosensor, of which the detection limit was 100-fold higher than dye-based MBs.[27] The novel DNA biosensor consisted of two target-specific probe ODNs, which contained a reporter probe labelled with a fluorophore and a capture probe labelled with biotin, as well as a QD conjugation with streptavidins (Figure 2.8). The QDs acted as both FRET energy donor and target concentrator that amplified the target signal by confining several targets. Sejdic *et al.* designed a simple DNA sensor based on FRET between blue luminescent CdTe QDs and dye labelled ssDNA.[203] A cationic polymer was used as a linker to achieve efficient energy transfer from QD donor to dye acceptor. The different interaction of single-stranded and double-stranded DNA with CdTe resulted in different changes of FRET efficiency. Recently, Fan *et al.* reported a quick preparation of compact QD-DNA probes for sensitive DNA detection by FRET.[28] The radius of final QDs was only around 3 nm after applying the functional coating, resulting in a highly efficient energy transfer. Nearly 70% transfer efficiency could be achieved with only a few DNA molecules on each QD and that the FRET based DNA detection could be performed in a few minutes with a detection limit of $1.0 \cdot 10^{-9}$ M. These findings presented the possibility of using QDs to construct a homogeneous DNA assay.

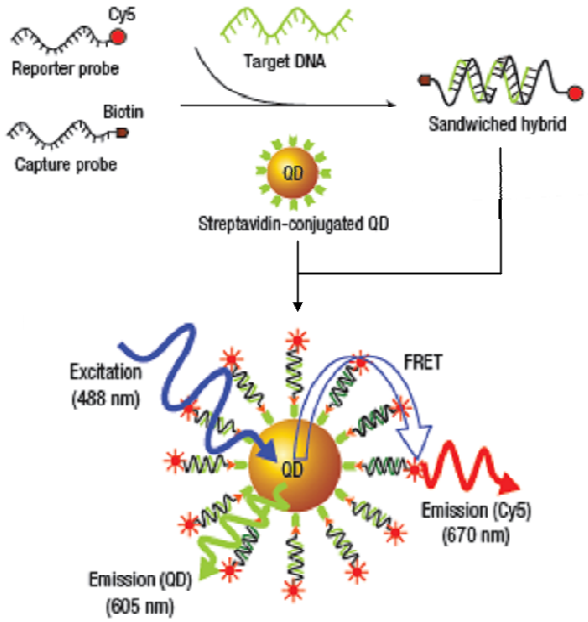

Figure 2.8 Scheme presentation of a single QD based DNA nanosensor prepared by Fang *et al.*[28]

Conjugated polymers (CPs) are characterised by a delocalized electronic structure. They have been widely used in optoelectronic devices such as light emitting diodes, field effect transistors and photovoltaic devices. In recent years, there is an increasing trend of using water soluble conjugated polymers for optical biosensor development due to their ability to gain signal in response to interactions with analytes by excitation energy transfers.[8, 20, 204-219] They are often referred to as amplifying fluorescent polymers or superquenching polymers. Cationic conjugated polymers (CCPs), in particular, have been employed for strand-specific DNA detection. The signal transduction mechanisms of CPs for biosensing are based on FRET, electron transfer, analyte induced aggregation of CPs or analyte induced conformational changes of CPs.

Whitten and coworkers have discovered fluorescence superquenching of conjugated polyelectrolyte for biosensing applications in 1998.[206] The initial superquenching based DNA hybridisation assay was a competition assay between a target ssDNA and a quencher functionalized target ssDNA to form the dsDNA duplex with the probe ssDNA that was immobilised on the fluorescent polyelectrolyte via biotin-avidin interactions.[207] A two step assay in which the sensor was first incubated with the target ssDNA and ssDNA-quencher was added in the second step resulted in a sensitive quench inhibition assay. An improved

assay using the biotinylated PNA instead of the biotinylated probe DNA was reported by their group with improved specific binding properties.[208]

Whitten *et al.* also intensively investigated the superquenching properties of J-aggregated polymers.[209] J-aggregate structure can be characterised by a sharp red-shifted absorption and the similar red-shifted enhanced fluorescence intensity. They have been exploiting such polymers in biosensing applications. Recently, they reported the preparation of a new label free, real time sequence specific DNA detection based on supramolecular selfassembly. A cationic phenylene ethinylene oligmer (OPE) formed a J-dimer or J-aggregate with DNA by a combination of electrostatic and hydrophobic interactions. The self-assembled complexes between OPE and dsDNA was characterised by the J-aggregate properties as the absorption changes and increased fluorescence intensity. The complex of OPE/ssDNA was less readily formed compared to OPE/dsDNA, but it showed a strong induced circular dichroism (CD) signal. This signal decreased steadily with addition of the complementary ssDNA over time, which allowed the monitoring of DNA hybridisation in real time. Introduction of mismatches in the target ssDNA sequence slowed down the signal decrease process, which enabled the system for SNP test without modification of the DNA.[210]

Leclerc *et al.* pioneered DNA detection with conjugated polymers based on the electrostatic attraction between a CCP and DNA.[211] They found that water soluble imidazolium substituted poly(thiophene) was highly sensitive to the presence of ODNs by forming a duplex structure and its color changing from yellow to red in 5 min. After adding the complementary ssODN sequence, a triplex structure was obtained, and the color of the solution changed back to red. This process could be followed by fluorometry and detect label free specific ssDNA with high sensitivity and selectivity. However, the reaction must be carried out at high temperature. This group has since then developed homogenous DNA assays with improved sensing property in sensitivity, selectivity and applicability over years by modified methods.[212] In one of their latest work, they reported a detection limit of 5 target DNA molecules in a 3 ml sample solution by tagging the capture ssDNA with a donor fluorophore for FRET analysis.[213]

In contrast to the electron transfer based superquenching approach, Bazan *et al.* developed an energy transfer based DNA sensor that possessed high signal amplification due to efficient energy transfer from a cationic conjugated polymer to a dye labelled probe molecule.[214] The method used the light harvesting luminescent conjugated polymer and a peptide nucleic acid (PNA) probe labelled with a fluorescein reporter. Addition of the solution of target DNA with the complementary sequence to the PNA yielded a duplex.

Electrostatic interactions brought the cationic conjugated polymer and the PNA/ssDNA duplex in close proximity so that the energy transfer from the conjugated polymer to the fluorescein occured (Figure 2.9). The resulting fluorescence intensity was 25 fold enhanced compared with that obtained from direct excitation of the PNA-fluorescein. DNA sensor based on similar principle involving usage of dsDNA, intercalated dye ethidium bromide (EB) as the acceptor or fluorescein as an intermediate signal enhancing 'FRET gate' have been developed based on a signal amplification observed upon specific hybridisation to the target DNA.[215-217] The group have modified the structure of their cationic conjugated polymers for wider application and improved sensitivity and specificity.[218-221]

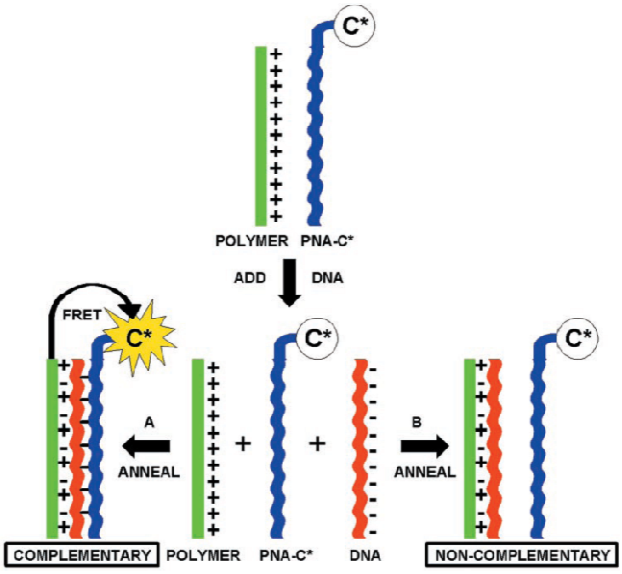

Figure 2.9 Scheme presentation of using a water soluble CP with a specific PNA (labelled with a fluorescent reporter C*) for DNA detection.[214]

2.5.2.2 Other optical DNA biosensors

There are several other optical DNA sensing methods based on nonfluoresent detection such as surface-enhanced raman scattering spectroscopy,[222] chemiluminescent detection,[223] colorimetric detection,[224] dual polarization interferometry[225] and surface plasmon based detection.[226] The development for DNA sensing is a rapid growing field, in which tailored methods should be applied in different application conditions. Progress in a diversity of nucleic acid sensing systems with highly desired properties will continue to be made.

2.6 Förster resonance energy transfer (FRET)

FRET is a quantum phenomenon occurring between two fluorescent molecules when the emission energy of the donor overlaps with the absorption energy of the acceptor and the molecules are in a close proximity (typically 10-100 Å).[13, 227, 228] Energy is transferred from a donor to an acceptor fluorophore through dipole-dipole interaction without emission of a photon. As a result, the intensity of the donor fluorescence, lifetime and quantum efficiency decrease, and the fluorescence intensity of the acceptor increase. Figure 2.10 illustrates the energy transfer process by Jablonski diagram.

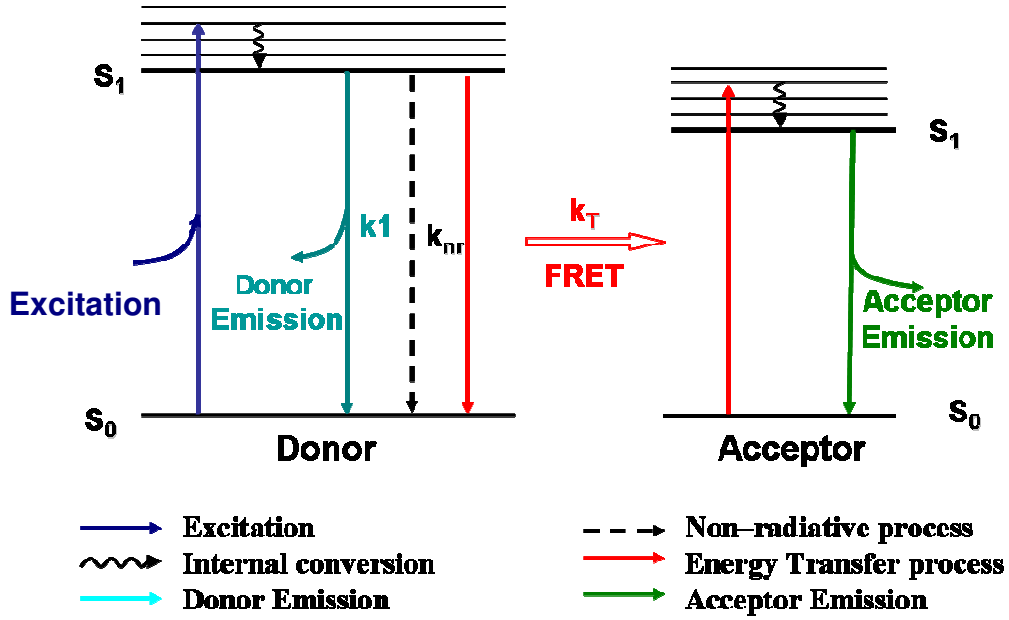

Figure 2.10 Scheme of the principle of FRET by Jablonski diagram.

The rate of FRET K_T, is related to several quantum mechanical and optical properties of the donor and acceptor molecules and the distance between them. According to the theory of Föster, K_T can be described by

$$K_T = \frac{Qk^2}{\tau_D r^6}\left(\frac{9000\ln(10)}{128\pi^5 N n^4}\right)J(\lambda) \qquad \text{(Equation 2.1)}$$

where k^2 is the factor describing the relative orientation of the transition dipoles of donor and acceptor. For random orientation of the donor and acceptor, i.e. freely rotating dyes, k^2 is 2/3. n is the refractive index of the medium; Q is the quantum yield of the donor in absence of the acceptor; τ_D is the life time of the donor in the excited state in the absence of the acceptor; r is the separation distance between the donor and acceptor; N is the Avogadro's

number and *J* describes the degree of spectral overlap between donor emission and acceptor excitation:

$$J(\lambda) = \int_0^\infty F_D(\lambda)\varepsilon_A(\lambda)\lambda^4 d\lambda \qquad \text{(Equation 2.2)}$$

where $F_D(\lambda)$ is the donor emission as a function of the λ, and $\varepsilon_A(\lambda)$ is the extinction coefficient of the acceptor.

The efficiency of energy transfer *E*,

$$E=K_T/(K_T+ K_1+K_{nr}) \qquad \text{(Equation 2.3)}$$

where K_1 is the donor emission. K_{nr} is the non-radiative relaxation process, which is inversely proportional to the distance *r* between donor and acceptor. It is extremely sensitive to distance changes described by:

$$E = \frac{1}{1+(r/R_0)^x} \qquad \text{(Equation 2.4)}$$

where R_0 is the Förster distance between the donor and acceptor at which *E* is 50%. For a single donor molecule transferring energy to a single acceptor molecule *x* is equal to 6.

Experimentally, *E* can be determined in a few different ways. It is often evaluated by: [229]

$$E = 1 - I_{DA}/I_D \qquad \text{(Equation 2.5)}$$

where I_{DA} and I_D are the donor fluorescence intensities in the presence and absence of the acceptor respectively. *E* can also be estimated by comparing the ratio of emission from the acceptor to the emission of the donor,[230] or through the increase of acceptor emission in the presence of the donor.[228] An evaluation and validation of the present vast number of FRET efficiency strategies was performed by Danuser *et al.* based on a surface FRET system, in which the absolute and relative fluorophore concentrations can be controlled. They classified the different methods in terms of data, equipment requirements and their validity of applied concentration range of the donor or acceptors.[231]

However, accurate FRET quantification accounting for random distribution of donor and acceptor positions with multiple donor-acceptor interactions is not simple to achieve. Several models to analyse FRET in 2D systems such as membranes, lipid-protein complexes have been proposed earlier already in 1980s,[232, 233] however such models can only allow for interactions between one donor and multiple acceptors. Moreover, Monte Carlo simulation has been used to calculate FRET efficiency for more complicated system.[231]

The theory of FRET was first described by Förster in the late forties, its application to measure distances between donor and acceptor molecules came decades later. FRET is now widely utilized for a variety of applications. Conventional microscopy has a spatial

resolution limit of 200 nm, which limits the direct observation of intra/inter-molecular interactions in the nanometers range, e.g. protein-protein interactions, DNA conformational changes and etc. The strong dependence of FRET on the distance between donor-acceptor molecules in a few nanometers range enables researchers to use it as a 'molecular ruler'. Besides the mentioned utilization of FRET in DNA sensing applications, FRET can be incorporated into chromatographic assays, electrophoresis, microscopy and flow cytometry for sensitive and specific analysis to obtain information on biomolecules interactions, conformational changes or structure information that are otherwise difficult to achieve.[234-242]

3. Experimental Part and Methods

In this chapter, the materials used are listed. The synthesis of dye labelled polyelectrolytes and other sample preparations are described. The basic principles of the used techniques are briefly explained with the emphasis on their practical applications, particularly how they are used for sample measurement.

3.1 Materials

Poly(diallyldimethylammonium chloride) (PDA) (M_w=200-350 kDa), poly(allylamine hydrochloride) (PAH) (M_w=70 kDa), sodium poly(styrenesulfonate) (PSS, M_w=70 kDa), sodium poly(vinylphosphate) (PVPho, M_w=70 kDa), sodium styrene sulfonate (NaSS), diallyldimethylammonium chloride (DACl, 65% w.t.%), Vazo44, potassium persulfate ($K_2S_2O_8$), methanol, ethanol, dimethylformamide (DMF), hydrofluoric acid (HF), sodium borate, sodium acetate, acetic acid, 4-(2-hydroxyethyl) piperazine-1-ethanesulphonic acid (HEPES), tris(hydroxymethyl)methylamine (TRIS), hydrogen peroxide (H_2O_2) (30%), ammonium hydroxide (NH_4OH) (25%), 1-(3-dimethylaminopropyl)-3-ethylcarbodiimide hydrochloride (EDC), 1.1'-carbonyldiimidazol (CDI), N-hydroxysulfosuccinimide sodium salt (sulfo-NHS), rhodamine B, tetramethylrhodamine isothiocyanate (TRITC) and fluoresceinisothiocyanate-dextran (FITC-dextran) (M_w=150 kDa), and were purchased from Sigma-Aldrich (Germany). Polyvinylamine (PVA) (M_w=45 kDa) was kindly supplied by BASF (Weinheim, Germany under the product name Lupamin 5095). Poly(methacrylic acid sodium salt) (PMAA) (M_w=100 kDa) was purchased from Polysciences Inc (Eppelheim, Germany). Sodium hydroxide (NaOH), hydrochloric acid (HCl), sodium chloride (NaCl), ethylenediaminetetraacetic acid disodium salt (EDTA) were obtained from Merck (Darmstadt, Germany). Monodisperse silica particles of 4.3 µm were purchased from microparticles GmbH (Berlin, Germany). Dodecyltrimethylammoniumbromide (DoTAB), Alkyldimethylbenzylammonium chloride (BAC) and cetyltrimethylammonium bromide (CeTAB) were purchased from Fluka (Steinheim, Germany). The lipophilic ODN modified liposomes, i.e. large unilamellar vesicles (LUVs) were kindly provided by Professor Herrmann (Department of Biology, Humboldt University of Berlin).

All chemicals were used without further purification. Solutions were prepared with water from a three stage Millipore Milli-Q Plus 185 purification system with a resistivity higher than 18 MΩ·cm. The structural formulas of polyelectrolytes are presented in Figure 3.1.

The ODNs used in this work and their suppliers are listed in Table 3.1. ODN stands for single stranded DNA sequence in the present work unless specified as dsODN that stands for double stranded DNA helix.

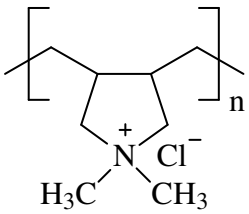

PDA

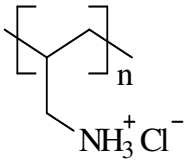

PAH

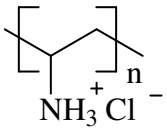

PVA

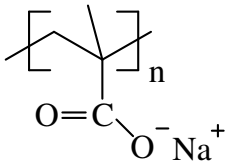

PMAA

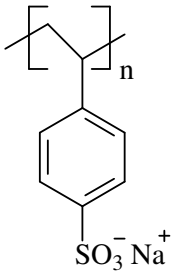

PSS

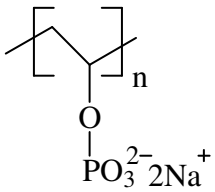

PVPho

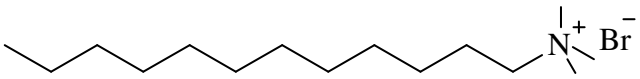

DoTAB

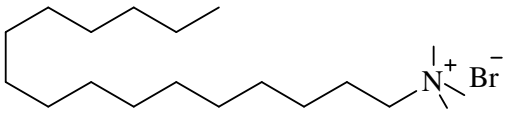

CeTAB

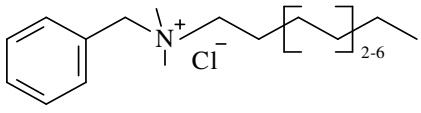

BAC

Figure 3.1 Structural formulas of polyelectrolytes and cationic surfactants used.

Table 3.1 Overview of ODNs used.

Probe ODNs for covalent coupling	**Abbreviation**	**Supplier**
5'-NH_2-AAA AAA AAA AAA AAA AAA AAA-3'	A_{21}	BioTez*
5'-NH_2-AAT(Flu)AAA AAA AAA AAA AAA AAA AAA-3'	$FluA_{21}$	
5'-NH_2-Cy3-CACTACGGTGCTGAAGCGACAAA-3'	Cy3ODN	TIB**
ODNs for DNA hybridisation	**Abbreviation**	**Supplier**
5'-TTT TTT TTT TTT TTT TTT TT-3'	T_{20}	BioTez
5'-T(Rho)TT TTT TTT TTT TTT TTT TT-3'	$RhoT_{20}$	
5'-TTT TTT TTT TTT TTT TTT TT(Rho)-3'	$T_{20}Rho$	
5'-TTT TTG TCG CTT CAG CAC CGT AGT G-Cy5-3'	3'Cy5ODN	TIB
ODNs for the single-nucleotide polymorphism (SNP) study	**Abbreviation**	**Supplier**
5' NH_2-CACTACGGTGCTGAAGCGACAAA-3'	Probe	TIB
5'-TTTTTGTCGCTTCAGCACCGTAGTG-3'	$Target^0$	
5'-TTTTTGTCGCTTCAGCACCGTAGTG-Rho-3'	$Target^0Rho$	
5'-TTTTTGTCGCTTTAGCACCGTAGTG-Rho-3'	$Target^1Rho$	
5'-TTTTTGTAGCTTCAGCAGCGTAGTG-Rho-3'	$Target^2Rho$	

* Biotez GmbH, Berlin, Germany; ** TIB Molbiol GmbH, Berlin, Germany.

3.2 Synthesis of fluorescently labelled polyelectrolytes

Different polyelectrolytes with varied label degrees of defined dyes were self-synthesized (the overview is given in Table 3.3). Fluorescent dyes involved in polymer labelling with their abbreviation are listed in Table 3.2.

Table 3.2 Overview of fluorescent dyes involved in polymer labelling.

Fluorophore	**λ_{abs}***	**λ_{em}**	**Abbreviation**	**Supplier**
tetramethylrhodamine- isothiocyanate	556	582	TRITC	Sigma-Aldrich (US)
methacryloxyethylthiocarbamoyl-rhodamine B	548	570	mRho	Polyscience Inc (US)
1-methyl-1'-(5-carboxypentyl)-Cy3	543	557	Cy3	kindly provided by Prof. Liebscher**
NHS ester of 1-methyl-1'-(5-carboxypentyl)-Cy5	638	657	Cy5	
NHS ester of 1-(4-sulfobutyl)-1'-(5-carboxypentyl)-6'-sulfonate-Cy5	644	669	disulfo-Cy5	FEW Wolfen (Germany)
fluorescein-amine	490	519	Flu	Sigma-Aldrich (US)

* Absorption spectra measured in 10 mM TRIS buffer (pH 7.0)

** Department of Chemistry, Humboldt-University of Berlin

Table 3.3 Overview of self-synthesized fluorescent dye labelled polyelectrolyte.

Polyelectrolyte	Mw / kDa	Abbreviation	Label Degree*
TRITC labelled PAH	70	Rho-PAH	90
Cy5 labelled PAH	70	Cy5-PAH	230/350/840/1500
disulfo-Cy5 labelled PAH	70	disulfo-Cy5-PAH	320/500
mRho-DA copolymer	N/A	Rho-PDA	210
Flu labelled PMAA	100	Flu-PMAA	350
mRho-SS copolymer	N/A	Rho-PSS	220
TRITC labelled PVA	45	Rho-PVA	80
FITC labelled dextran	150	FITC-dextran	N/A
Cy3 labelled PMAA	100	Cy3-PMAA	130/260/500

* Label degree defined as the number of monomer units/dye units on the polymer chain

3.2.1 Preparation of Flu-PMAA

200 mg PMAA was dissolved in 3.8 ml borate buffer (50mM, pH 8.0); thereafter 60 mg of EDC and 30 mg of sulfo-NHS were added into the polymer solution. 30 min was allowed for this reaction before 1200 µl fluorescein-amine (20 mM) in acetone was added to the activated polymer solution. The reaction mixture was stirred for 24 hours at room temperature. The molar extinction coefficient value of ε_{Flu}= 80.000 $M^{-1}cm^{-1}$ was used for determination of the Flu dye concentration.

3.2.2 Preparation of Cy3-PMAA

Cy3-PMAA was prepared in a two-step procedure: Cy3 carboxylate was converted to amine-Cy3 in the first step before it was labelled onto PMAA to produce Cy3-PMAA.

3.2.2.1 Preparation of amine-Cy3

109 mg (0.2 mmol) Cy3 carboxylate was dissolved in 2.5 ml DMSO followed by addition of 64.8 mg (0.4 mmol) CDI. The activation step was carried out at room temperature for one hour. Thereafter, 600 mg (10 mmol) ethylendiamine was added to the activated dye solution. The reaction mixture was stirred at 70 ^{o}C for 24 hours overnight.

3.2.2.2 Preparation of Cy3-PMAA

6 mmol PMAA was dissolved in 3 ml borate buffer (50mM, pH 8.0) before addition of 1.2 mmol freshly prepared EDC. 30 min was allowed for this reaction and amine-Cy3 solution was added to the activated polymer solution. Varied molar ratio between monomer unit of

the polymer and dye molecules was used for producing Cy3-PMAA with different label degrees. The reaction mixture was stirred for 24 hours at room temperature. The molar extinction coefficient value of ε_{Cy3}= 134.000 $M^{-1}cm^{-1}$ was used for determination of the Cy3 dye concentration.

3.2.3 Preparation of Rho-PAH and Rho-PVA

1 g (10 mmol of the amine function groups) of PAH or PVA was dissolved in 10 ml borate buffer (50 mM, pH 8.5) and mixed with a solution of 120 mg (0.3 mmol) TRITC in 20 ml of DMF. The reaction mixture was stirred for 24 hours at room temperature. The extinction coefficient for TRITC ε_{TRITC} was taken as 100.000 $M^{-1}cm^{-1}$ at 556 nm.

3.2.4 Preparation of Cy5-PAH

PAH was dissolved in borate buffer (50mM, pH 8.0) to a final concentration of 1.0 M and the NHS ester of Cy5 (or disulfo-Cy5) was dissolved in DMF to a final concentration of 0.1 mol/l. A mixture solvent consisted of 75% borate buffer and 25% DMF was used to synthesize Cy5-PAH and disulfo-Cy5-PAH. A mixture of 25% borate buffer and 75% DMF was used to synthesize PAH-Cy5 II. Varied molar ratio between monomer unit of the polymer and dye molecules was used for producing Cy5-PAH with different label degrees. The reaction was performed under stirring at room temperature for 24 hours. The extinction coefficient for Cy5, ε_{Cy5} was determined and taken as 230.400 $M^{-1}cm^{-1}$ at 640 nm, while $\varepsilon_{disulfoCy5}$ was taken as 187.000 $M^{-1}cm^{-1}$ (FEW Wolfen) at 645 nm in water.

3.2.5 Preparation of Rho-PSS and Rho-PDA

Because of the difficulty for coupling substances to sulfonate and quaternary amine groups Rho-PSS and Rho-PDA were synthesized by copolymerisation of dye molecules and monomers. 1 M of monomer solution NaSS and DACl in water and 40 mM mRho in methanol were prepared. 1 M Vazo44 or 0.15 M $K_2S_2O_8$ initiator was prepared in water. The rhodamine dye and monomers were mixed in a molar ratio of 1:100. The mixture was flushed with nitrogen for 15 min before incubation in the oven for 24 hours at 60 ^oC. The extinction coefficient for mRho ε_{mRho} was taken as 100.000 $M^{-1}cm^{-1}$ at 550 nm.

The labelled polymers were dialyzed against MilliQ water using a cellulose membrane (Mwco= 15 kDa) for one week and thereafter filtered and lyophilized. The label degree of dye molecules on the polymer chain was determined by UV-Vis spectrometer in 10 mM TRIS buffer (pH 7.0).

3.3 Other sample preparation

3.3.1 LbL film assembly on colloidal particles

4.3 µm silica particles were employed as the templates for coating with polymer layers. Alternating layers of positively charged polycations and negatively charged polyanions were adsorbed on the particles from solution (1 g/l polyelectrolyte, 0.2 M NaCl, 50 mM acetate buffer pH 6.2) respectively. After 20 min of each adsorption step, the particles were washed with deionized water for three times to remove the non-adsorbed polyelectrolyte. 1 min of centrifugation at 3000 rpm was applied for the separation of particles from the solution during each coating/washing cycle.

3.3.2 Coupling of probe ODNs onto LbL particles by EDC activation

Amine modified ODNs were covalently bound to carboxylic groups on the LbL particles by EDC alone or with sulfo-NHS (Figure 3.2).[243] In a one-step coupling process, amine-ODNs, EDC, sulfo-NHS and the LbL particles were mixed at the same time. In a two-step coupling procedure, as the first step 10 µl EDC (50 mg/ml) and 10 µl sulfo-NHS (50 mg/ml) was used to activate 50 µl silica particles (2 w.t.%, 4.3 µm) coated with two double layers of PDA and PMAA. 30 min was allowed for the activation before amine-ODNs were added to the LbL particle suspension as the second step. The reaction concentration of ODNs was kept at 1.5 µM and the mixture was incubated at room temperature for 1 hour before thoroughly washed with water. 50 mM borate buffer (pH 8.0) was used in the coupling step.

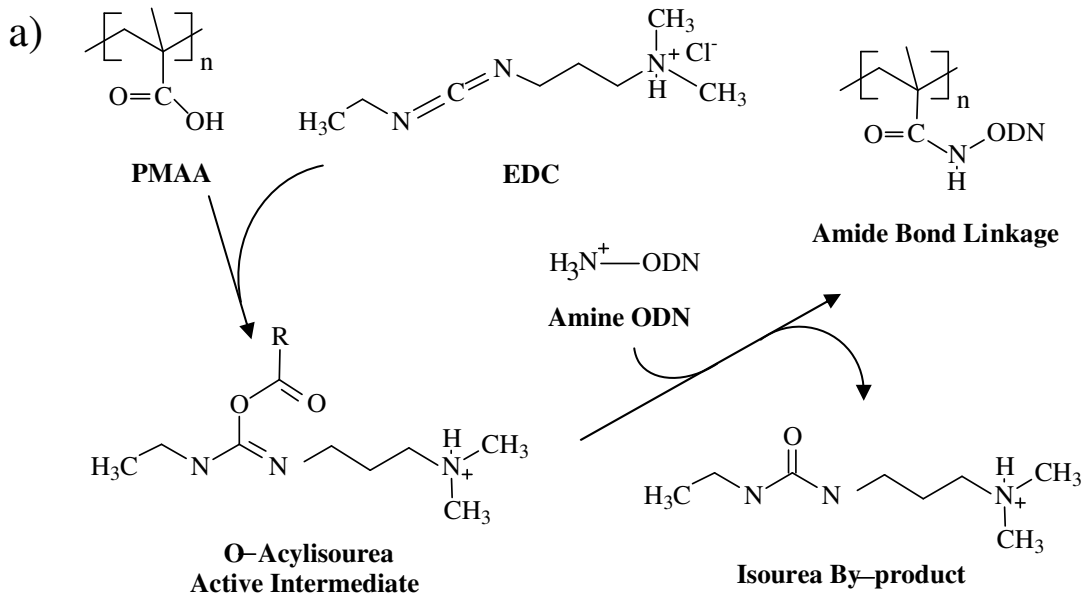

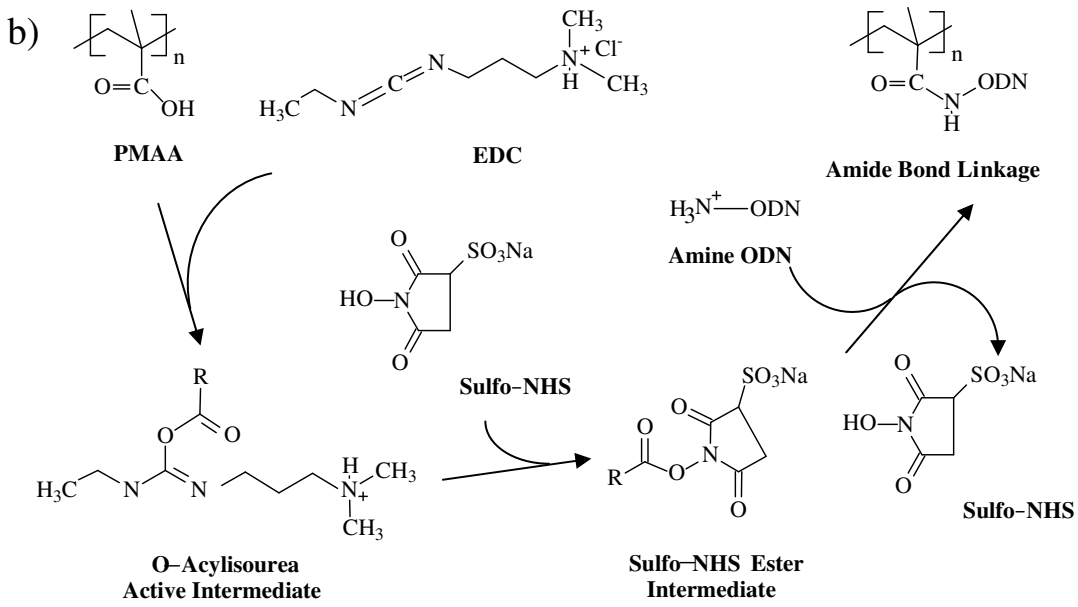

Figure 3.2 Scheme of coupling mechanism of amine-ODNs to PMAA in aqueous solution: a) by crosslinker EDC only; b) by EDC plus sulfo-NHS.

3.3.3 Coupling of probe ODNs onto LbL particles by CDI activation

Amine-ODNs were also covalently bound to carboxylic groups on the LbL particles by mediation of CDI in organic solvent DMSO (Figure 3.3).[243] The LbL particles were washed by water free DMSO five times for solvent exchange. 10 µl of CDI solution (100 mg/ml dissolved in water free DMSO) was used to activate 50 µl silica particles (2 w.t.%, 4.3 µm) coated with two double layers of PDA and PMAA. 60 min at 35 ^{o}C (oil bath) was allowed for the activation of the LbL particles before addition of amine-ODNs (dissolved in DMSO and water mixture due to poor solubility of the ODNs in water free DMSO). The reaction concentration of ODNs was kept at 1.5 µM and the mixture was incubated at room temperature for two hours before thoroughly washed with water.

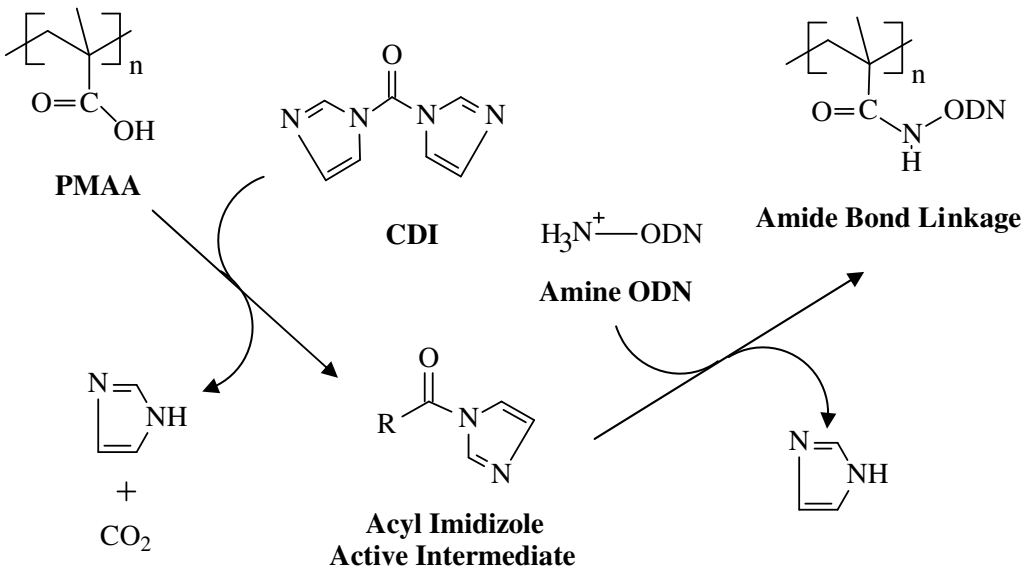

Figure 3.3 Scheme of coupling mechanism of amine-ODNs to PMAA in organic solvent by crosslinker CDI.

3.3.4 Hybridisation of complementary ODNs onto the LbL-ODN particles

For polyadenosine/polythymidine (poly dA/T) ODNs, the dsODN was obtained by mixing complementary ODNs and the LbL-ODN particles in 10 mM HEPES buffer (pH 7.4, 500 mM NaCl) at room temperature ($C_{particle}$= 2.5%). The hybridisation time allowed was 30 min. When ODN sequence from Escherichia coli (*E. coli.*) DNA was used, the same hybridisation buffer was used but temperature of 60 ^{o}C was applied for 15 min before cooling down to room temperature.

For storage of the LbL-ODN particles, 10 mM TRIS buffer containing 0.1% EDTA (pH 7.0) was used to prevent cleavage of ODN sequence by DNases that might be present in the suspension.

3.3.5 LbL-ODN particles for single-nucleotide polymorphism (SNP)

The ODN sequence used in SNP test as probe DNA (Probe) and hybridisation sequence as target DNA with different mismatch numbers (Target^{n}) are listed in Table 3.1. LbL-ProbeODN particles were prepared and hybridised with Target-ODNs firstly. Then the fluorescence of the LbL-Probe/Target(Rho) particles ($C_{particles}$=1 mg/ml) as a function of base pair mismatch were measured at 25 ^{o}C and 60 ^{o}C respectively by fluorometry in order to establish whether mismatch in the target sequence can be detected by fluorescence spectra changes. The temperature of the particle suspension was controlled by an external heating system on the fluorometer built in house.

3.3.6 Recycling of the LbL-ODN particles

The complementary ODNs hybridised onto the LbL-ODN particles were removed by heating up the particles above the melting temperature of the duplex so that the probe ODN on the particle was again single stranded. This was achieved by incubating the LbL-dsODN particle suspension in water bath at 75 ^{o}C for 15 min. Thereafter, the particles were centrifuged at 5000 rpm for 30 seconds, and the supernatant containing the free complementary ODNs was removed. Then the LbL-ssODN particles were washed with MilliQ water three times before used again for the next hybridisation cycles.

3.3.7 Preparation of polyelectrolyte capsules

Microcapsules consisting of 4 double layers of (PAH/PSS), (PVA/PSS), (PDA/PSS) and (PAH/PMAA) were prepared by dissolving the templates after the LbL film assembly. After polyelectrolytes were deposited on the surface, the silica particles were dissolved in 0.1 M hydrofluoric acid. For pH sensitive (PAH/PMAA) capsules, the particles were dissolved in 0.2 M ammonium fluoride in acetate buffer (pH 5.0). The capsules were washed with water until the suspension reached a pH value of 6.

3.3.8 Crosslinking of the $(PAH/PSS)_4$ capsules

Crosslinking of the (PAH/PSS) films was performed during or after LbL coating on the template particles prior to the core dissolution. Freshly prepared 2.5% glutaraldehyde solution was added to particles suspension (after each PAH coating layer or after complete 8 polyelectrolyte layer coating) yielding a final concentration of around 0.2% glutaraldehyde. 30 min of incubation time was allowed for the crosslinking process. The particles were thereafter thoroughly washed with Milli-Q water.

3.3.9 Preparation of multilayer liposomes on LbL-ODN surface

To attach liposomes to the LbL-ODN particles via hybridisation, complementary lipophilic ODNs were incorporated into lipid membranes.[244] 1-palmitoyl-2-oleoyl-sn-glycerophosphocholine (POPC) was used to prepare the liposomes and adenosine/thymidine based ODNs conjugated with two tocopherol moieties were incorporated into the outer leaflet of the lipid vesicles. The size of the liposomes is approximately 100 nm controlled by filters.

The hybridisation between the ODNs on the liposomes (LUVs-ODN) and the probe ODNs on the LbL surface was carried out in the same condition as described in 3.3.4; and for the

hybridisation of LUVs-ODNs on the LbL-ODN particles, 20 min of centrifugation at 500 rpm was applied instead of 1 min at 3000 rpm to separate the particles from the unhybridised LUVs-ODN and water in the washing cycles.

Gold coated quartz crystals were used as the substrate for assembly of polyelectrolyte films, ODN conjugation system and specific binding of liposomes on planar surfaces, which was carried out and analyzed by QCM (see section 3.4.5).

3.4 Methods and measurement conditions

3.4.1 UV-Vis spectroscopy

In the ultraviolet and visible (UV-Vis) region of the electromagnetic spectrum (λ = 200 – 800 nm), most organic molecules absorb photons and undergo electronic transitions. The absorption spectroscopy measures transitions from the ground state to the excited states of the molecules. The method is often used to quantitatively determine concentrations of an absorbing species in solution, following the Beer-Lambert law:

$$A = -\log_{10}(I/I_0) = \varepsilon\, cL \qquad \text{(Equation 3.1)}$$

where A is the measured absorbance, I_0 is the intensity of the incident light at a given wavelength, I is the transmitted intensity, L the pathlength through the sample, and c the concentration of the absorbing species. For each species and wavelength, ε is a constant known as the molar absorptivity or extinction coefficient.[245]

The absorption spectra were recorded by a Cary 50 Scan UV-VIS spectrometer (Varian Inc., USA). Quartz cuvette with a path-length of 1 cm was used for determination of ODNs concentration.

3.4.2 Fluoresence spectroscopy

Fluorescence spectroscopy measures the emission of radiation of the molecules from their electronic excited states to the ground state. In the fluorescence spectrometer (often called fluorometer), the species is firstly excited by absorbing a photon from its ground electronic state to one of the vibrational states in the excited electronic state. The energy of the electronic transition can be lost either by non-radiative relaxation or by the emission of a photon (fluorescence). The wavelength of this photon depends on the vibrational state of the electronic ground state where the transition finishes. Some energy is lost through the relaxation process so that the emission wavelength is always longer than the excitation

wavelength. The difference between the excitation and emission wavelength is called the Stokes shift. Figure 3.4 illustrates the different processes of energy relaxation after absorption of light in a Jablonski diagram.

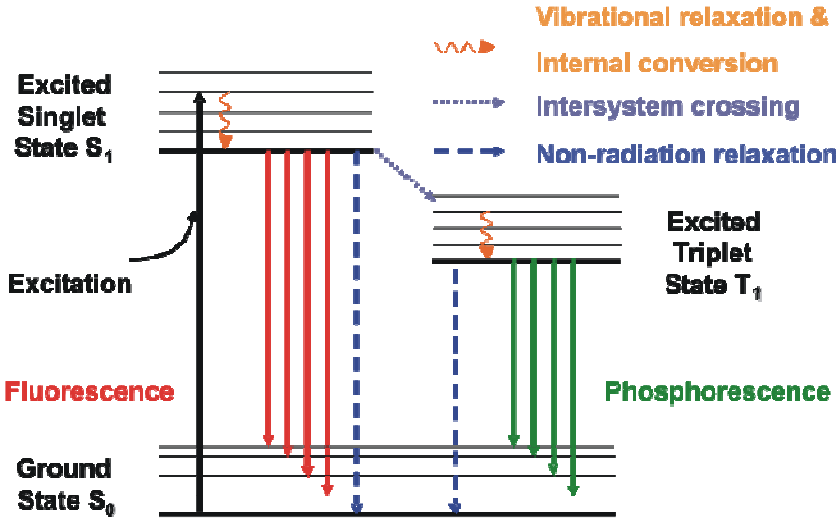

Figure 3.4 Jablonski diagram of the absorption and subsequent radiative or non-radiative energy decay processes.[13]

The main advantage of fluorescence detection compared to absorption measurement is the higher sensitivity and the ability to separate compounds on the basis of their excitation and emission spectra as opposed to a single spectrum. This advantage is further enhanced by commercial fluorescence dyes that have narrow and distinctly separated excitation and emission spectra. A typical fluorometer contains an excitation light source, two monochromators, sample cell, fluorescence detector and recorder (Figure 3.5).

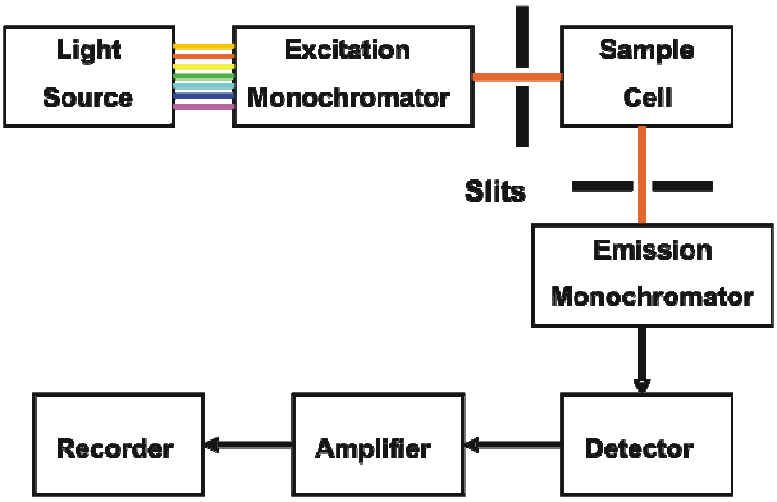

Figure 3.5 Scheme of the set-up of a fluorometer.

In the present study, fluorescence was recorded by a Cary Eclipse spectrometer (Varian Inc., USA) for one of the following purposes: 1. determination of ODNs immobilised on the substrates by recording the fluorescence in the supernatant; 2. kinetic measurement of fluorescence intensity changes of fluorescent capsules upon addition of surfactants; 3. the fluorescence quantum yield comparison of free dye molecules and dye molecules immobilised on polymers; 4. determination of FRET by simultaneous collection of emission data at desired excitation and emission wavelength. The program of 'Advanced Read' was used with 5 nm monochromator slit width for excitation and 10 nm for emission light. Quartz cuvettes with a path length of 1 cm were used for measurement of particle based samples. Magnetic stirrer of 8 mm length was used to prevent particle sedimentation.

3.4.3 Confocal laser scanning microscopy (CLSM)

Confocol laser scanning microscopy (CLSM) is a fluorescence based technique for obtaining high-resolution optical images. The key feature of confocal microscopy is its ability to acquire in-focus images from selected depths with a resolution of the fluorescence wavelength, a process known as optical sectioning through the specimen that have a thickness ranging up to 50 µm or more. Images are acquired point-by-point and reconstructed with a computer. A scheme of the CLSM is shown in Figure 3.6.

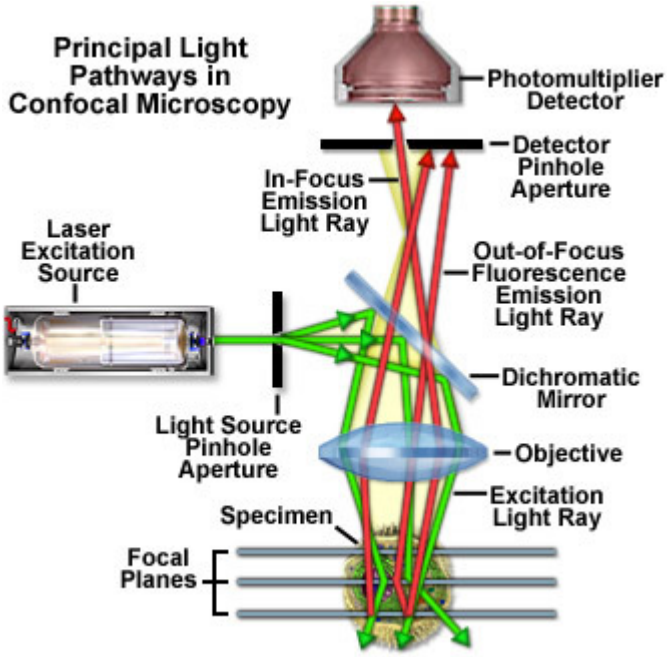

Figure 3.6 Scheme of the set-up of a confocal laser scanning microscopy.[246]

In the confocal laser scanning microscopy, a laser beam passes through a pinhole aperture situated in the confocal plane with a scanning point on the specimen and a second pinhole aperture positioned in front of the detector (usually a photomultiplier tube (PMT)). As the laser is reflected by a dichromatic mirror and scanned across the specimen in a defined focal plane, scattered and reflected laser light as well as any fluorescent light from the illuminated spot is then re-collected by the objective lens, passes through the dichromatic mirror and is directed to the second pinhole. Only the lights at points on the focal plane are confocal with the pinhole and will pass the pinhole aperture. After passing the pinhole, the light intensity is detected by the PMT, transforming the light signal into an electrical one that is recorded by a computer. In this way, the out-of-focus light is prevented from detection by the PMT and does not contribute to the resulting image. Thus sharper images can be obtained than those from conventional fluorescence microscopy techniques. Refocusing the objective shifts the excitation and emission points on a specimen to a new plane that is confocal with the pinhole apertures.[247]

A Leica TCS SP inverted confocal microscope (Leica, Germany) equipped with a 63x oil immersion objective was used to visually investigate the LbL particles or capsules. It was used to obtain informations on particle/capsule size, fluorescence intensity, permeability and relative fluorophore distribution in/on the particles/capsules. An Argon-ion (488 nm, 514 nm) and a helium-neon laser (543 nm) are the excitation sources that can be selected according to the fluorophores.

Quantification of the fluorescence intensity of LbL particles by CLSM can be conducted either by profile or by area analysis (Figure 3.7). The analysis by profile is simple and fast. However, it only measures two points on the particle surface, which is a drawback in case the fluorophore distribution on the particle is inhomogeneous. Therefore, analysis by area was used in the present work (Figure 3.7 b). A table such as Figure 3.6b was automatically given when the region of interest (ROI) was defined. The mean chain value was taken as the fluorescence intensity of each individual particle; e.g. the fluorescence intensity of the particle defined by ROI 1 was 53.08 (note that the particles need to be uniform in size for valid comparison of mean chain values). A minimum of 10 particles were analysed to give an average value for each sample. Note that the fluorescence intensity of the background must be negligible, otherwise the background intensity has to be deducted from the value obtained on the particles (e.g. the intensity of ROI 4 was 0).

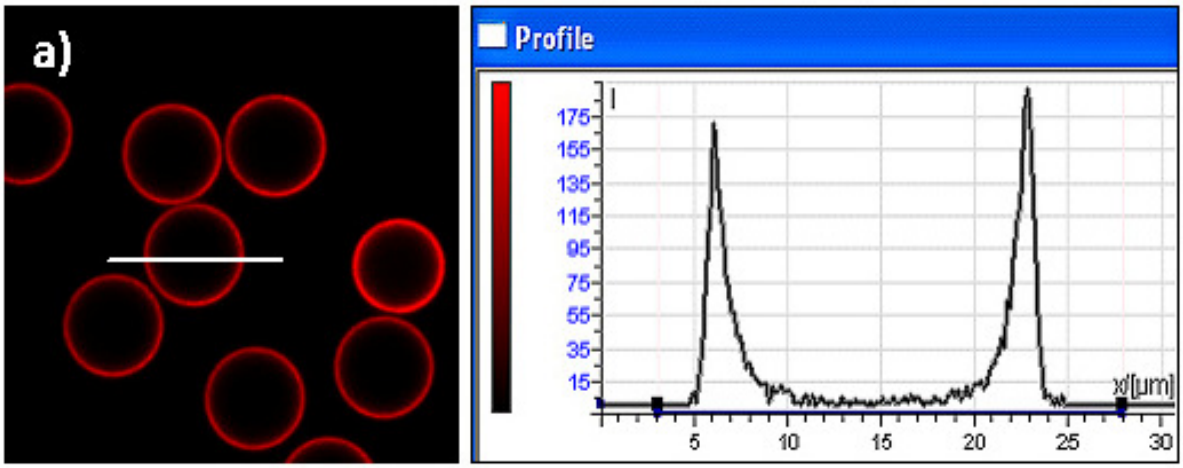

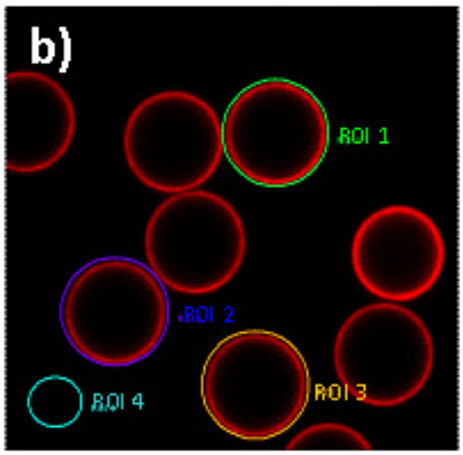

Region of Interest (ROI):	Area/ µm²	Intensity/(a.u.)	
		Mean Chain	Sum Chain
ROI 1:	268.97	53.08	594186
ROI 2:	276.71	40.82	470069
ROI 3:	274.06	42.68	486819
ROI 4:	62.23	0	1

Figure 3.7 Quantification of fluorescence intensity by CLSM: a) profile method, the fluorescence intensity along the profile is shown in the graph; b) area method, the fluorescence intensity sum in the region of interest and average value divided by the area are listed in the table.

The CLSM images were taken at different photomultiplier voltage (PMV) values for obtaining optimal visual brightness. In order to compare the fluorescence of the particles, the conversion factors between different PMVs of fluorescence intensities were determined. The amplification factor between PMVs normalised at PMV 450 is shown in Figure 3.8.

At each PMV, the CLSM has a display limit of fluorescence intensity. Above this limit, a different colour (e.g. blue colour in Figure 4.36) is shown instead of the emission colour of the fluorophore, indiciting that the fluorescence intensity of the sample is well above the display range by the CLSM at the defined PMV. Therefore, for the quantification of fluorescence intensity, PMV should be adjusted in a range so that the fluorescence of the samples is below the display limit of the CLSM.

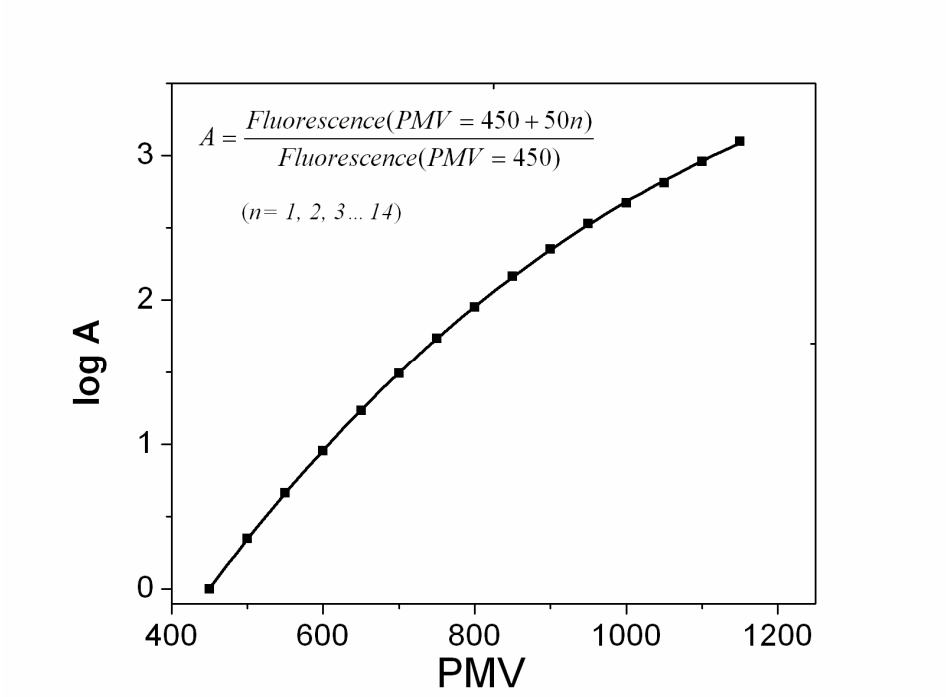

Figure 3.8 Fluorescence intensity amplification factors of different PMVs. The factor of 450 PMV was set to 1.

3.4.4 Flow cytometry

Flow cytometry, or Fluorescence Activated Cell Sorting (FACS), is a technology that simultaneously measures multiple physical characteristics of single particles or cells as they flow in a fluid stream through a beam of light (Figure 3.9). It uses the principles of light scattering and fluorescence to generate specific multi-parameter data from particles or cells in the size range of 0.5 μm to 40 μm. Lasers are often used as the light source in the flow cytometry. One unique feature of flow cytometry is that it measures signals per particle or cell. This is in contrast to the spectrophotometry, where the measurement is based on a bulk volume of sample.

A flow cytometer is made up of three main systems: fluidics, optics, and electronics. The fluidics system transports particles in a stream to the laser beam for interrogation. The optics system consists of lasers to illuminate the particles in the sample stream and optical filters to direct the resulting light signals to the appropriate detectors. These detectors collect different information of the particles: the forward scatter (FSC) intensity, correlated with the particle volume; the side scatter (SSC) intensity, depending on the internal and external structure of the particles; fluorescence intensity at specific wavelengths. The electronics system converts the detected light signals into electronic signals that can be processed by the computer.[248]

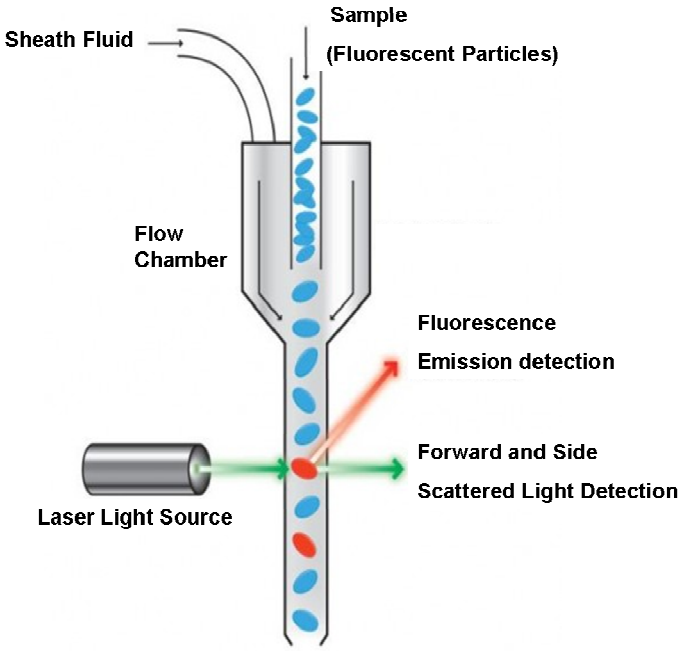

Figure 3.9 Scheme of the key features in a flow cytometer.

Flow cytometry was performed on LbL-dsODN particles to measure the fluorescence intensity using a FACScan (Becton Dickinson, San Jose, USA). It is equipped with an argon (488 nm) laser and can provide three fluorescent and two scatter properties. It has emission band filters of 530±30 nm, 585±42 nm and a long-path filter of > 670 nm, of which the first has been used in this work for the donor intensity measurement and the second for acceptor intensity both at λ_{ex}= 488 nm. For each data point 10.000 particles were measured. Data were analyzed using Cyflogic software (Cyflo Ltd), and they can be shown as dot plots with FSC and SSC intensity, out of which the population of single particles can be selected for exclusive fluorescence intensity analysis (Figure 3.10). Therefore, fluorescence signals from aggregates of particles were excluded from the FRET analysis.

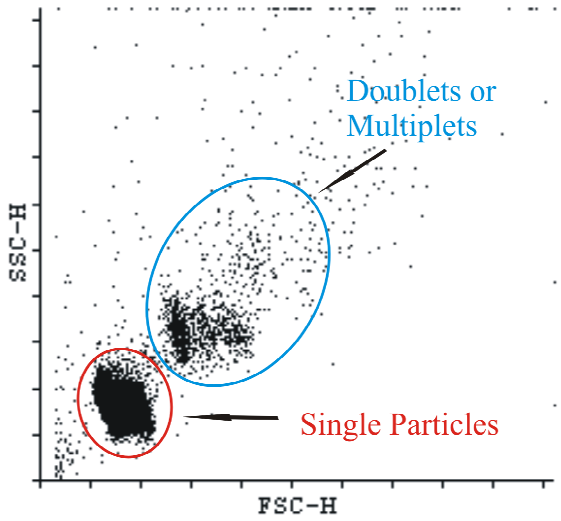

Figure 3.10 Dot plot of fluorescent LbL-dsODN particles by flow cytometry, of which the population of single particles are presented in the red circle and most of the doublets or multipletes population are presented in the blue circle.

3.4.5 Quartz crystal microbalance (QCM)

Quartz crystal microbalance (QCM) is an ultra-sensitive weighing device that measures a mass per unit area in the nanogram range.[249] It uses the principle that a piezoelectric quartz crystal changes its oscillation frequency when mass is deposited or removed from the crystal surface. In the most common configuration, a thin (~200-400 µm) circular crystal disc is sandwiched between a pair of circular metal electrodes (usually gold). When a thin film is attached to the crystal the resonance frequency decreases. If the deposited film is thin and rigid the decrease in the frequency is proportional to the mass of the film according to the Sauerbrey equation:[250]

$$\Delta f = -\frac{n}{C}\Delta m \qquad \text{(Equation 3.2)}$$

where C= 17.7 ng $Hz^{-1}cm^{-2}$ for a 5 MHz quartz crystal, and n =1, 3, 5, 7 is the overtone number. The thickness of the adhering film can also be estimated as below:

$$d_{eff} = \Delta m / \rho_{eff} \qquad \text{(Equation 3.3)}$$

where ρ_{eff} is the effective density of the thin film.

By collecting the resonance frequency of a quartz crystal, QCM technology can be used to characterise the formation of thin films (nm) such as proteins, polymers and cells onto surfaces, in liquid.[251-253]

A Q-Sense E4 apparatus from Q-Sense (Västra Frölunda, Sweden) was used in all experiments. All measurements were taken at 25 ^{o}C at the fundamental frequency as well as at the 3rd, 5th and 7th harmonic including the frequency shift and the dissipation. In this work only the results of the frequency changes at the 3rd harmonic (15 MHz) were used for calculation. The resonance frequencies of the crystal were measured with a precision of 1 Hz. QCM crystals with a fundamental frequency of 5 MHz were used in all experiments. In the present work, the QCM was used to quantify the assembly of LbL films, coupled ODNs and the built up of liposomes on the planar surface.

The crystals were cleaned by freshly prepared piranha solution that consisted of 3:1 H_2SO_4: H_2O_2 at room temperature for 20 min three times before being thoroughly rinsed with water. The measurement cell was cleaned with flowing water for half an hour at room temperature. Afterwards they were rinsed with water and dried with nitrogen. The polymer solutions (0.5 mg/ml) were injected into the system with a peristaltic pump for 30 min with a velocity of 0.5 ml/min for each layer and rinsed with water/buffer solution for 10 min before the following polymer coating solution. The ODN (1 mM) and liposome solution (2 mM) were injected into the chamber and incubated for 60 min before washing. Borate buffer (50 mM, pH 8.0) was used for washing before EDC activation step and during ODN coupling process. HEPES buffer (10 mM, pH 7.4) was used during the liposome assembly. Changes of the frequency and dissipation were continuously monitored and recorded.

3.4.6 Atomic force microscopy (AFM)

Atomic force microscopy (AFM) or scanning force microscopy (SFM) is a very high resolution type of scanning probe microscopy. For ideal samples (crystals) the AFM resolution is in the nanometer scale, more than 1000 times better than the optical diffraction limit.[254]

The AFM measures the forces acting between a fine tip and a sample. It consists of a piezocrystal that develops an electrical potential in response to mechanical pressure and the probe that is a cantilever with a fine tip at its end to scan the specimen surface. The cantilever is typically silicon or silicon nitride with a tip radius of curvature on the order of nanometers. When the tip is brought into proximity of the sample surface, forces between the tip and the sample lead to a deflection of the cantilever. Typically, the deflection is measured using a laser spot reflected from the top surface of the cantilever into an array of photodiodes. The principle of AFM is shown in Figure 3.11.

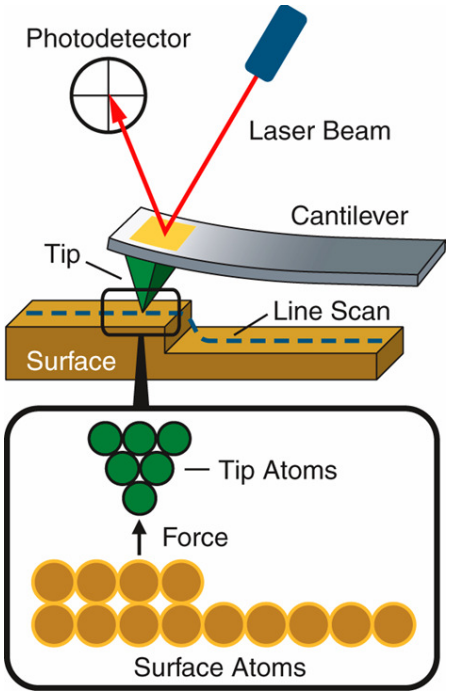

Figure 3.11 Schematic presentation of the AFM principle.[255]

AFM is operated as contact mode, non-contact mode or tapping mode. In contact mode, the tip makes a soft 'physical contact' with the surface of the sample. The deflection of the cantilever Δz is proportional to the force ΔF acting on the tip according to Hooke's law,

$$\Delta z = \Delta F / k_c \qquad \text{(Equation 3.4)}$$

where k_c is the spring constant. By using contact mode AFM, even 'atomic resolution' images can be obtained. The use of non-contact mode allows scanning without influencing the shape of the sample by the tip-sample forces. In tapping mode AFM the cantilever is oscillating close to its resonance frequency. An electronic feedback loop ensures that the oscillation amplitude remains constant, so that a constant tip-sample interaction is maintained during scanning. The advantage of the tapping mode is the elimination of a large part of permanent shearing forces and it causes the least damage to the sample surface. Tapping mode AFM can reach a lateral resolution as high as 1 nm.

AFM can image the non-conducting and conducting surfaces in various environment (air, liquid, vacuum), which enables its application on different types of materials. Nowadays AFM has been widely used as a technique leading to new discoveries in many fields including life science, materials science, polymer science, nanotechnology and biotechnology.[256-259]

AFM measurement was performed in air on LbL film coated planar surfaces (coupled with ODNs or without) using a Nanoscope III multimode AFM (Digital Instruments Inc., USA) operating in tapping mode. The AFM tip (PPP-NCH-W) from Nanosensors (Wetzlar, Germany) with a resonance frequency of 302-354 kHz and a stiffness of 25-42 Nm^{-1} was used.

3.4.7 Zeta potential measurement

Particles in a colloidal suspension or emulsion are usually electrically charged. The amount of charges on the particle surface determines the stability of the colloids, and therefore it is an important particle characteristic. It can be measured by the electrophoretic mobility of the particles in suspension. The suspension is in an electroneutral state because the charge on the surface of each particle is counterbalanced by opposite charges (ions) in the surrounding solution.[260] The charges on the particle surface are considered to be attached firmly to it, and they are so called bound ions that make the Stern layer. The surrounding charges are loosely attached in the diffuse layer. Within the diffuse layer, there is a notional boundary, where the ions and particles form a stable entity. Ions within this boundary move with the particles, whereas ions beyond this boundary do not travel with the particles. This boundary is called the surface of hydrodynamic shear or slipping plane, and the potential at this boundary is known as zeta potential (ζ). The model of surface charge layers and zeta potential is shown in Figure 3.12.

Zeta potential indicates the potential stability of a colloidal system. Particles with a zeta potential above |30mV| generally have no tendency to aggregate due to the electrostatic repulsion to each other, and they are considered stable. Zeta potential is highly dependent on the pH value and the ion strength.[261] Therefore, a zeta potential value needs to be measured at a known pH and ion strength.

The determination of Zeta potential ζ is based on the electrophoresis measurement according to the Henry equation:

$$U_E = \frac{2\varepsilon\zeta f(ka)}{3\eta} \qquad \text{(Equation 3.5)}$$

where U_E is the electrophoretic mobility, ε is the dielectric constant, η is the viscosity of the medium and $f(ka)$ is Henry's function that equals to 1.5 when the measurement is in aqueous media and at moderate electrolyte concentration.

Zeta potential measurement was performed on LbL film coated particles using a Malvern Zetasizer Nano-Z (Malvern Instruments Ltd., Worcestershire, UK). Each obtained value was

an average value of 30 measurements. 1 mM TRIS buffer (pH 7.0) was used in all zeta-potential measurements.

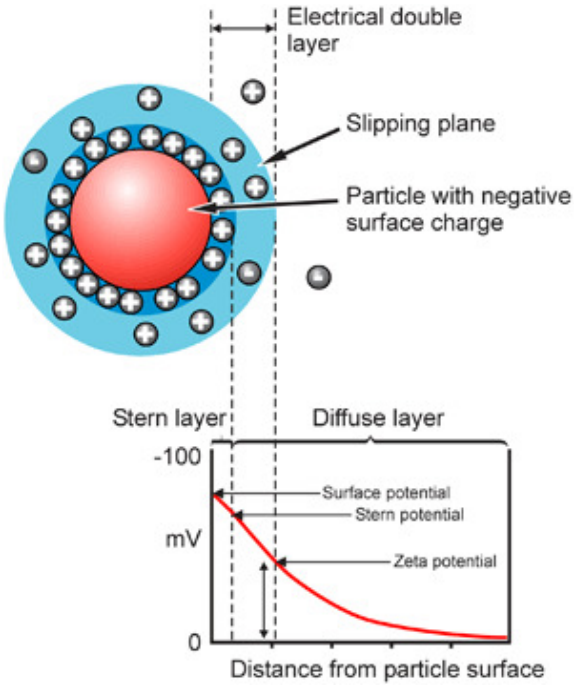

Figure 3.12 Schematic model of zeta potential.

3.4.8 Calculation of I_{FRET}

In this work, fluorescence intensity of the acceptor molecules induced by the 'energy transfer' from the near-by donor, denoted as I_{FRET} is used to evaluate the FRET efficiency in our LbL-ODN system. I_{FRET} was analyzed by fluorometry and flow cytometry; both methods allowed simultaneous fluorescence collection at different wavelength. The data were corrected for crosstalk between the dyes as described below. Crosstalk controls were 1) I_{Rho}, 2) I_{Flu}, (λ_{ex} = 488 nm, λ_{em} = 580 nm).

$$I_{FRET} = I - I_{Flu} - I_{Rho} \quad \text{(Equation 3.6)}$$

$$I_{Flu} = I_{0\,Flu(em580)} / I_{0\,Flu(em518)} * I_{Flu(em518)} \quad \text{(Equation 3.7)}$$

$$I_{Rho} = I_{0\,Rho(ex488)} / I_{0\,Rho(ex555)} * I_{Rho(ex555)} \quad \text{(Equation 3.8)}$$

where I is the fluorescence at 580 nm in the presence of donor and acceptor for λ_{ex} = 488 nm; $I_{0\,Flu\,(Em518)}$ and $I_{0\,Flu(em580)}$ is the donor fluorescence at 518 nm and 580 nm respectively in the absence of acceptor for λ_{ex} = 488 nm. $I_{0\,Rho\,(ex488)}$ and $I_{0\,Rho\,(ex555)}$ is the acceptor

fluorescence at 580 nm in the absence of donor for λ_{ex} = 488 nm and 555 nm respectively; $I_{Flu\ (em518)}$ is the donor fluorescence at 518 nm in the presence of acceptor for λ_{ex} = 488 nm and $I_{Rho\ (ex555)}$ is the acceptor fluorescence at 580 nm in the presence of donor for λ_{ex} = 555 nm. (Note: 1. In order to minimize the influence of light scattering of particles on the fluorescence signal, λ_{ex} = 480 nm was used in particles based fluorometry measurement; 2. Due to a single laser excitation source (488 nm) availability in the flow cytometer used, crosstalk control of I_{Rho} was neglected in the measurement by flow cytometry.)

4 Results and Discussion

This chapter is composed of three sub-sections: 1. the preparation and characterisation of the LbL-ODN system for DNA detection by FRET; 2. the investigation of photophysics of the FRET donor dye Cy3 covalently coupled to polyelectrolytes; 3. the stability of the LbL films to several cationic surfactants. In addition to the emphasis on their contribution to the development of the FRET-based DNA diagnostic system by the LbL technology, each section is discussed individually both from the fundamental point of view and the application aspects.

4.1 Preparation and characterisation of the LbL-ODN particles

In this section, the preparation of LbL film modified microparticles covalently coupled with ODNs (LbL-ODN particles) is reported. The properties as a FRET based nucleic acid detection system are evaluated from several key perspectives. In addition to the application in nucleic acid diagnostics, the possibility of specific assembly of other biomolecules or nanocontainers on the LbL-ODN structure was also demonstrated.

4.1.1 Preparation of the LbL-ODN particles

LbL particles were prepared by adsorption of layers of polycations and polyanions alternatively on 4.3 µm silica particles by the LbL technique. The first layer was a polycation as the template particles were negatively charged. The outermost layer had to be negatively charged in order to avoid non-specific binding of negatively charged DNA on the LbL particles. The probe ODN was modified with an amine linker; therefore the polyanion layer should contain carboxylate groups in order to covalently couple the ODN onto the LbL films by certain crosslinkers such as EDC, yielding an amide bond between carboxylate and amine groups (Figure 3.2 a).

During initial characterisation of the system, a 21-mer amine modified polyadenosine ODN with or without fluorescent dye label (i.e. 5'-NH_2-Flu-A_{21}-3' ($FluA_{21}$) and 5'-NH_2-A_{21}-3' (A_{21}) respectively) was used as probe ODN. Accordingly, the polythymidine ODN T_{20}, complementary to A_{21}, labelled with Rho either at 5´ or 3´ end, namely $RhoT_{20}$ or $T_{20}Rho$ respectively, were used as the target DNA models for the hybridisation test. By measuring

the fluorescence intensity of the ODN solution before and after the coupling to the activated LbL particles the amount of coupled ODNs was determined.

4.1.1.1 One-step or two-step coupling process

In one-step coupling, the LbL particles, crosslinking agent EDC and the probe ODN $FluA_{21}$ were mixed together at the same time. However, using this simple method the coupling efficiency was low. In a parallel control experiment, it was observed that pure $FluA_{21}$ in solution reacted already with EDC in the absence of the particles causing a strong reduction of fluorescence intensity of $FluA_{21}$ solution. This could be caused by activation of the carboxylate group in fluorescein or the phosphate groups from the ODNs by EDC leading to a self-crosslinking of the ODN via the amine group reducing the coupling efficiency. Therefore, a two step coupling process was developed, in which the probe ODNs were added as a second step after washing away the excess EDC when the activation on the particle surface was completed.

It is well known that EDC and the EDC-activated intermediate groups are hydrolysed quickly in aqueous solution.[243] Thus freshly prepared EDC was used and the time between activation and ODN addition in the two-step process was kept as short as possible. It is reported that in the presence of sulfo-NHS with EDC, the more stable NHS-ester is formed (Figure 3.2 b). However, the present study showed that the use of sulfo-NHS resulted in lower coupling efficiency and caused severe problems of non-specific binding (see section 4.1.1.3).

4.1.1.2 Selection of polyelectrolytes

Selection of polyelectrolyte for LbL coating on the particles should be considered under the following aspects:

1. Allowing maximal coupling efficiency of probe ODNs
2. No or negligible non-specific binding of non-target DNA on the LbL particles surface
3. Stability of polyelectrolyte layers under the hybridisation conditions

For the selection of polycations, PAH and PDA, which are commonly used in the LbL film assembly were tested. PDA consists of quaternary amine groups that do not react with activated carboxylate groups. Also the charge density of PDA is independent on pH. However, LbL films containing PDA showed lower thermal stability as reported by Köhler *et al.*[103] PAH consists of primary amine groups that generally yield more stable LbL films due to additional hydrogen bonding.[262] However, due to the interpenetration of

polyelectrolytes in the LbL films, there is competition between the amine groups on PAH and the amine-modified probe ODNs to react with EDC-activated carboxylate groups. Hence, the influence of primary amine groups on the coupling efficiency of the probe ODN was studied (Figure 4.1). 100 pmol of $FluA_{21}$ was used to couple on 1 mg of LbL particles coated with four polyelectrolyte layers of $(PAH/PMAA)_2$, (PAH/PMAA/PDA/PMAA) and $(PDA/PMAA)_2$ respectively. After identical coupling process, only one third of $FluA_{21}$ was coupled onto the particles coated with $(PAH/PMAA)_2$ compared to particles coated with $(PDA/PMAA)_2$. This is consistent to the measurement of fluorescence intensity by CLSM, which shows that the fluorescence intensity of $(PAH/PMAA)_2$-based LbL-$FluA_{21}$ particles was remarkably lower than the $(PDA/PMAA)_2$–coated ones.

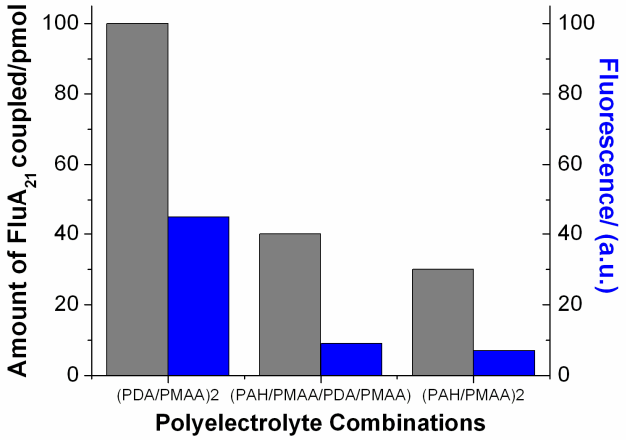

Figure 4.1 Amount of $FluA_{21}$ that can be coupled onto the particles coated with different polyelectrolyte combinations (left) and the fluorescence intensity of the respective LbL-$FluA_{21}$ particles measured by CLSM (right). PMV= 600.

The remarkably reduced coupling efficiency of $FluA_{21}$ onto the PAH containing LbL film can be ascribed to the consumption of activated carboxylic groups due to crosslinking between PAH and PMAA within the LbL layers. This effect can be especially pronounced for the two step coupling process used, because the NH_2-ODNs were added after the EDC activation process when the crosslinking of LbL film already took place. It is worth mentioning that, even when PAH was assembled 3 layers underneath (i.e. only used as the first coating layer) the effect was still remarkable, pointing to a rather strong interpenetration of the layers. Due to the strong decrease in activated carboxylate groups available for covalent linkage to probe ODNs, PAH was not suitable to be employed in the LbL film assembly.

For selection of polyanions, the following polyelectrolyte combinations were investigated as LbL film for covalent coupling of probe ODNs: $(PDA/PMAA)_2$, (PDA/PSS/PDA/PMAA), $(PDA/PSS)_2$, $(PDA/PVPho)_2$. The last two were used in the first instance as control samples. 500 pmol of $FluA_{21}$ was used for coupling on 1 mg of each type of LbL particles under identical coupling process. Surprisingly, $FluA_{21}$ was coupled on all four types of LbL particles including $(PDA/PSS)_2$ and $(PDA/PVPho)_2$-coated ones, though there have been so far limited reports on reactivity between polymeric sulfonate or phosphate groups and the carbodiimide crosslinker (Figure 4.2). All four samples yielded similar coupling efficiency (250 pmol per mg particles). The fluorescence intensity of each sample was quantified by the CLSM (method described in section 3.4.3).

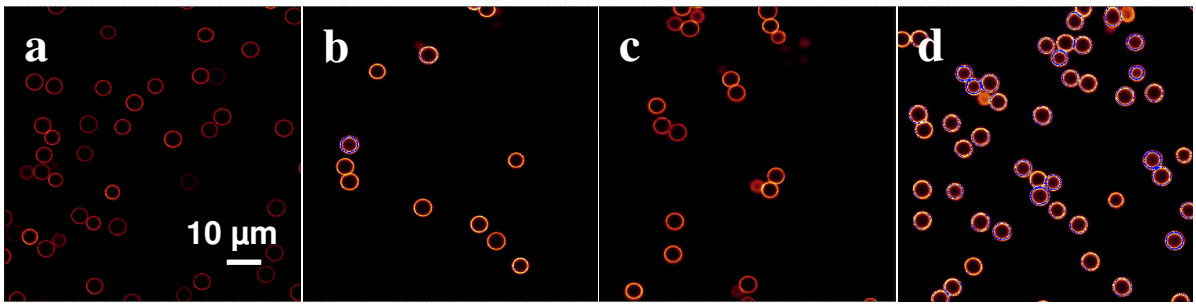

Figure 4.2 CLSM images of $FluA_{21}$ coupled onto LbL particles coated with four polyelectrolyte layers of a) $(PDA/PVPho)_2$, (PMV=500); b)$(PDA/PSS)_2$, (PMV=600); c) (PDA/PSS/PDA/PMAA), (PMV=550); d) $(PDA/PMAA)_2$, (PMV=600). The fluorescence intensities of each sample normalised at 600 PMV are: a) 72.3; b) 67.1; c) 101.2; d) 85.6.

4.1.1.3 Minimisation of non-specific binding

One important requirement of a DNA diagnostic kit is negligible non-specific binding, i.e. no non-target molecules bind onto the sensor. The non-specific binding test of LbL-ODN particles was carried out in 3 ways: 1) Affinity of ODNs to the LbL particles without EDC activation; 2) Affinity of ODNs (without amine-linker modification) to the LbL particles after EDC (plus sulfo-NHS) activation; 3) Affinity of non-complementary ODNs to the LbL particles coupled with probe ODNs by EDC (plus sulfo-NHS). All these tests were carried out under hybridisation conditions described in section 3.3.4.

Firstly, affinity of $RhoT_{20}$ (without amine-linker) to the LbL particles without any crosslinking agents was tested. No adsorption of ODNs on LbL film was expected due to the electrostatic repulsion between the negatively charged ODN and the LbL particles with a polyanion as the outermost coating layer. However, non-specific binding of $RhoT_{20}$ on $(PDA/PVPho)_2$ coated particles was observed (Figure 4.3 a), while no binding was found on

other polylelectrolyte combinations tested. Therefore, polyanions containing phosphate groups should be avoided in the LbL film for specific coupling of ODNs.

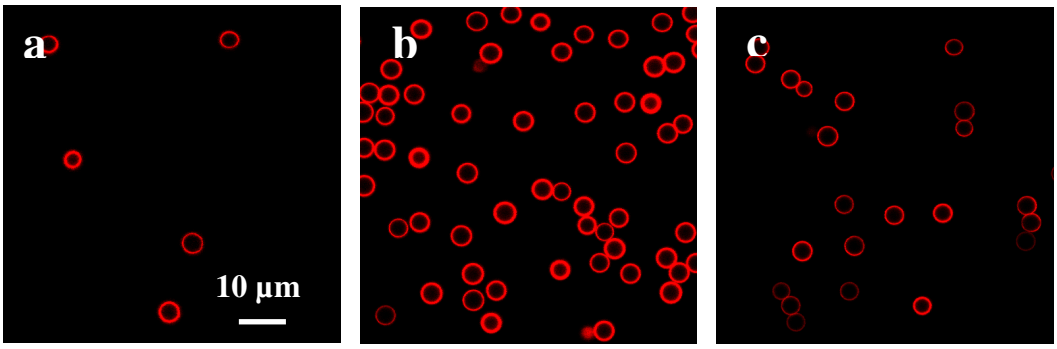

Figure 4.3 Non-specific binding of $RhoT_{20}$ on particles coated with a) $(PDA/PVPho)_2$ without EDC activation (PMV=700); b) $(PDA/PSS)_2$ after EDC (plus sulfo-NHS activation (PMV=700); c) $(PDA/PMAA)_2$ after EDC (plus sulfo-NHS) activation (PMV= 650). The fluorescence intensities of the particles normalised at 600 PMV are: a) 44.5; b) 47.5; c) 38.1.

Secondly, the affinity test of $RhoT_{20}$ (without amine linker) on particles coated with $(PDA/PSS)_2$ or $(PDA/PMAA)_2$ after EDC (plus sulfo-NHS) activation was tested by CLSM. Strong affinity of $RhoT_{20}$ was found on both surfaces (Figure 4.3 b, c). This can be ascribed to the positive charges on the surface produced by the crosslinking intermediate groups.

Thirdly, the affinity of $RhoA_{20}$ (without amine-linker) and $RhoT_{20}$ to the LbL-ODN particles, i.e. particles coated with $(PDA/PSS)_2$ or $(PDA/PMAA)_2$ and covalently coupled with $FluA_{21}$ was tested (Figure 4.4).

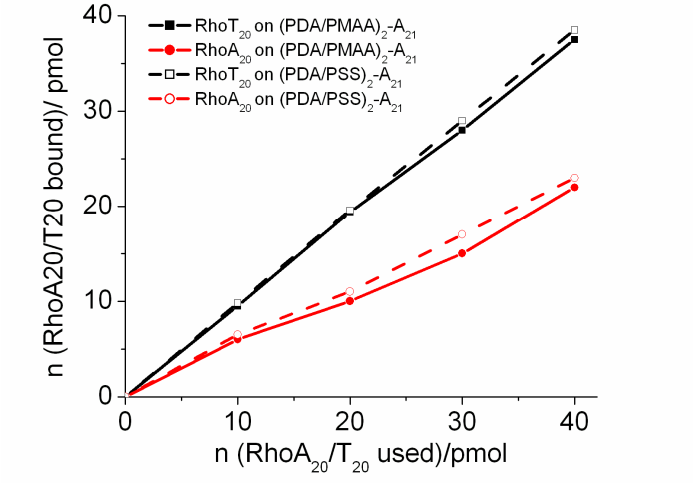

Figure 4.4 Amount of $RhoT_{20}$ (mainly specific via DNA hybridisation, black line) or $RhoA_{20}$ (non-specific, red line) bound onto LbL-A_{21} particles coated with polyelectrolyte layers of $(PDA/PMAA)_2$ (solid line) and $(PDA/PSS)_2$ (dashed line) and activated by EDC plus sulfo-NHS.

Figure 4.4 shows that $RhoA_{20}$ non-specifically bound onto the LbL-A_{21} particles, which indicats that the binding of $RhoT_{20}$ onto the LbL-A_{21} particles was not only via specific DNA hybridisation but also partially non-specific. This strong non-specific affinity of ODNs on LbL particles after EDC plus sulfo-NHS activation was mostly caused by remaining activated groups that were not used by specific coupling to probe ODNs. It is known that the EDC active intermediates undergo hydrolysis in aqueous solutions slowly and return to carboxylate groups. But even after several days, non-specific binding was still observed for the particles activated by EDC plus sulfo-NHS. Therefore, efforts were made to accelerate this process and to reverse the activated groups back to carboxylate groups after sufficient probe ODNs were coupled.

A range of substances were tried to deactivate the EDC/sulfo-NHS ester groups on LbL particles. The efficacy of deactivation was investigated by affinity test of NH_2-$FluA_{21}$ onto the LbL particle surface after the deactivation. 100 pmol $FluA_{21}$ was used for coupling onto 1 mg of particles coated with certain polyelectrolyte combinations, activated by EDC (with or without sulfo-NHS) and then treated by different solutions (shown in Table 4.1). for deactivation. The amount of $FluA_{21}$ coupled onto each type of LbL particles after treatment was analysed.

Table 4.1 Amount of $FluA_{21}$ bound (/pmol) on treated LbL particles*

	LbL film activated by EDC with sulfo-NHS			LbL film activated by EDC only
Deactivation Solution (pH) / Polyelectrolytes in the LbL film	1 M glutamic acid (8)	0.5 M $NH_2OH{\cdot}HCl$ (8)	0.5 M CH_3COOH (3)	0.1 M CH_3COOH (3)
$(PDA/PSS)_2$	34	35	76	9.5
(PDA/PSS/PDA/PMAA)	39	29.5	10	2-5
$(PDA/PMAA)_2$	40	27	5	0

*The LbL particles were firstly activated by EDC (alone or with sulfo-NHS) and then treated with the listed solution overnight. ($C_{particles}$ = 0.5 mg/ml)

As shown in Table 4.1, complete quenching of the activated carboxyl groups was only found on NHS-ester free $(PDA/PMAA)_2$ particles which were treated with acetate buffer (0.1 M CH_3COOH , pH 3.0). Further test revealed that one hour treatment with the acetic acid solution was sufficient to achieve complete deactivation. Therefore, in order to avoid non-specific binding, the LbL-A_{21} particles were treated with 0.1 M acetate buffer at pH 3.0 for one hour and washed with water and hybridisation buffer. Later their affinity to $RhoT_{20}$ and

$RhoA_{20}$ was tested. After addition of the LbL-A_{21} particles to the solution of a non-complementary ODN ($RhoA_{20}$), the supernatant fluorescence was the same as that of the corresponding $RhoA_{20}$ solution, meaning that almost all $RhoA_{20}$ molecules remained in the supernatant without binding onto the LbL-A_{21} particles. In contrast, addition of the complementary ODN $RhoT_{20}$ to 1 mg LbL-A_{21} particles resulted in negligible fluorescence of the supernatant up to 100 nM $RhoT_{20}$, indicating efficient specific binding via DNA hybridisation (Figure 4.5).

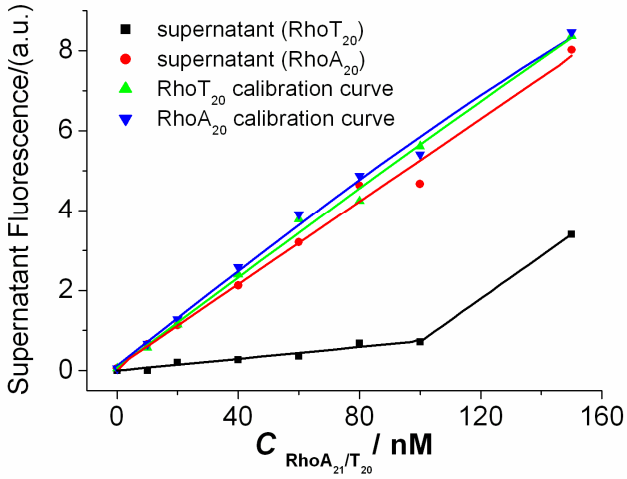

Figure 4.5 Fluorescence intensity of supernatant after addition of different concentrations of $RhoA_{20}$ (red line) or $RhoT_{20}$ (black line) to LbL-A_{21} particles ($C_{particle}$ = 1 mg/ml). The corresponding calibration curves of $RhoA_{20}$ or $RhoT_{20}$ solutions without particles are shown as blue and green lines, respectively.

4.1.1.4 Number of polyelectrolyte layers

Although use of polyelectrolyte combination (PDA/PMAA) yielded the least non-specific binding, which is essential for the LbL-ODN system, aggregation of the particles during the LbL film assembly was observed. The aggregation level increased with increasing number of (PDA/PMAA) layers coated on the particle surface. Since sufficient amount of probe ODNs can be coupled already onto particles coated with four layer of polyelectrolytes (see section 4.1.2.2), $(PDA/PMAA)_2$ was selected to modify the particle surface.

4.1.1.5 Optimisation of the coupling conditions

Optimisation of the parameters in the coupling procedure including the EDC activation time, concentration of EDC and the reaction time of probe ODNs with activated particles were carried out in order to obtain 1) LbL-ODN particles with the highest binding capacity to target molecules; 2) good stability; and 3) homogeneous ODN distribution. The optimal

coupling conditions were determined and used throughout this work (section 3.3.2). The amount of probe ODNs coupled on LbL particle was evaluated (section 4.1.2.2).

4.1.1.6 Stability of the LbL-ODN particles

The DNA hybridisation assay usually includes an intial incubation step above 60 °C in order to ensure complete melting of any existing dimer or duplex DNAs. High salt concentration (500 mM) is also used for efficient shielding of the repulsive ODN charges. In addition, other substances such as surfactants like SDS and proteins like BSA are often added in hybridisation buffers in order to prevent non-specific binding. The LbL-ODN particles should remain stable under these conditions. LbL films are known to be responsive to environmental changes such as temperature, ionic strength and surfactants, with possible conformational changes or partial dissolution of the polyelectrolyte layers in the film.[84-118] Therefore the stability of the LbL particles was investigated under different hybridisation conditions by varying the following parameters: room temperature/70 ^{o}C, HEPES buffer (pH 7.4), 0.5 M NaCl, 0.1% SDS and 1 mg/ml BSA. The LbL-ODN particles remained stable during hybridisation at room temperature under aforementioned parameters; whereas for particles incubated at 70 ^{o}C and in the presence of SDS, a partial release of the polyelectrolyte PMAA from LbL-ODN particles coated with $(PDA/PMAA)_2$ was observed. Different treatments were performed on the LbL particles prior to the ODN-coupling process in order to achieve most stable LbL films. The most effective method was incubation of the LbL particles in 50 mM borate buffer (pH 8.0) at 70 ^{o}C for 2 hours, by which all the excess PMAA was released during the treatment and a leakage of polyelectrolytes in the hybridisation step was not observed anymore. The treatment of the LbL particles did not influence the coupling efficiency for probe ODNs. However, heating for a longer time and at a higher temperature caused further loss of polyelectrolyte from the film and induced aggregation of the particles (see section 4.1.4.7). Furthermore a strong influence of cationic surfactants already at low concentration on the LbL films was observed. This is studied in detail and reported in section 4.3.

4.1.1.7 Alternative coupling methods

Beside EDC, there are alternative crosslinkers used for the coupling of amine-containing compounds to carboxyl groups such as N, N'-carbonyldiimidazole (CDI) and diisopropyl carbodiimide (DIC).[243] Both coupling agents require water free solvent to avoid almost instant hydrolysis or insolubility in water. LbL particles were washed with water free DMSO

five times and LbL-FluA$_{21}$ particles were successfully prepared by CDI activation (see section 3.3.3). This method has the advantage that deactivation of excess esters is not necessary because the activated esters undergo fast hydrolysis when the solvent is shifted back to aqueous solution. However, the coupling efficiency was slightly lower than that achieved by EDC activation in aqueous solution, most likely due to the presence of remaining water molecules in the LbL films that are highly hydrated due to the remaining charges.[36] Therefore, the solvent exchange inside the layers was not complete. Hence, covalent coupling of ODNs on LbL particles in the present work was performed mainly by EDC activation.

4.1.2 Characterisation of LbL-ODN particles

4.1.2.1. Zeta potential of LbL-ODN particles

Assembly of LbL layers onto the particle surface reverses the surface charge. Therefore, zeta potential measurement of the particles was employed to monitor the formation of each polyelectrolyte layer deposited sequentially on the particles (Figure 4.6).

The particles had an average zeta potential of +39.3 mV and –47.3 mV after PDA and sequential PMAA coating, respectively. This alternation of zeta potential quantitatively demonstrated a successful recharging of the particle surface by the deposition of each polyelectrolyte layer, indicating the step-wise layer growth on the particle surface. The surface charge of the particles with the outermost layer PMAA remained almost unaltered after covalent coupling of the negatively charged probe ODNs.

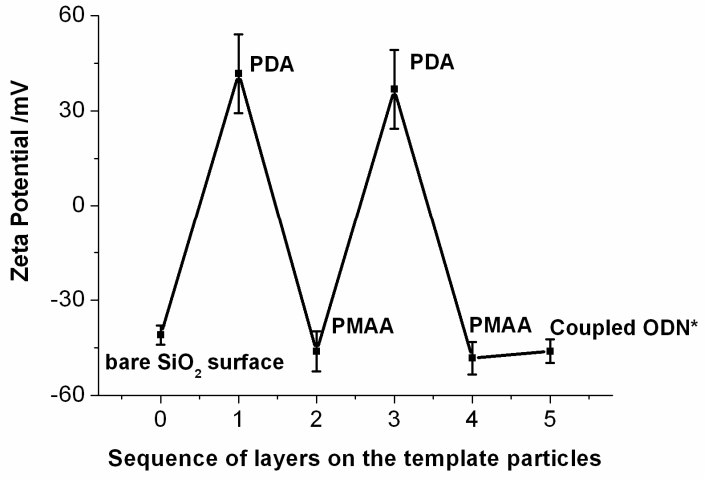

Figure 4.6 Zeta potential of the LbL particles after each layer of coating or coupling of the probe ODNs. (*: measurement from the LbL-ODN particles with ODN coupling density of 100 pmol/mg).

4.1.2.2. Coupling and hybridisation efficiency of ODNs

Coupling efficiency

The optimal amount of ODNs for coupling was analyzed by measuring the fluorescence of the supernatant solution after the coupling process using varing amount of probe ODNs (Figure 4.7). Up to 250 pmol $FluA_{21,}$ ODN molecules were all covalently coupled onto 1 mg of the LbL particles, i.e. $2x10^{-17}$ mole ODNs (i.e. $1.2x10^{7}$ ODN molecules) per particle. 250 pmol $FluA_{21}$ was the threshold vaule above which there was no further increasing coupling amount. By increasing the amount of EDC used for activation, the coupling capacity of probe ODNs can be further increased. However, this led to pronounced aggregation of the LbL particles during the activation step, which can be explained by loss of negative charges on the particle surface due to the creation of the positively charged active intermediate substance o-acylisourea (refer to Figure 3.2). Such aggregation remained even after the coupling of the ODNs and the deactivation of the acylisourea groups. Besides, for such high density of probe ODNs on the particle surface (approximately one ODN molecule per 5 nm^2 if neglecting the LbL film roughness) the hybridisation efficiency decreased, which was most likely caused by steric hindrance for DNA hybridisation (a double stranded DNA helix has a diameter of 2 nm).[263]

During further work unlabelled probe ODNs were also coupled onto the particles. When relative large batches were prepared, the amount of ODNs coupled could also be determined by UV/Vis due to the distinctive absorption of ODNs at 260 nm. The coupling efficiency for the unlabelled ODNs was consistent with the value obtained by the fluorescence method for the labelled ones. Hence, the label on the ODNs had no influence on the coupling efficiency. However, the fluorescence measurement offers much higher sensitivity than the absorption method and requires less amount of sample. Therefore, it was preferentially used in this work for quantification of the immobilised ODNs.

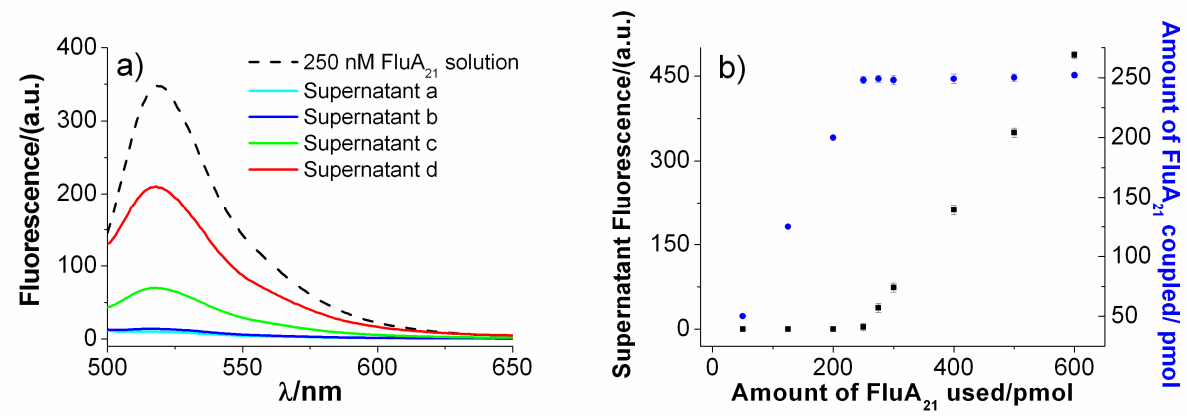

Figure 4.7 a) Fluorescence spectra of supernatant solution after coupling procedure. Amount of $FluA_{21}$ used for coupling: 125 pmol (cyan line), 250 pmol (blue line), 300 pmol (green line) and 400 pmol (red line). Fluorescence of 250 nM $FluA_{21}$ solution is shown as dashed line as reference. b) Supernatant fluorescence (black squares, left) and the coupled amount of $FluA_{21}$ (blue circles, right) in dependence on the amount of $FluA_{21}$ used. (Note: a constant amount of 1 mg LbL particles was used for each sample.)

Hybridisation efficiency

ssDNA containing the complementary sequence to the probe ODN can form double helices on the LbL-ODN particles via DNA hybridisation. The hybridisation efficiency is defined as the ratio between the amounts of ssDNA hybridised to the coupled ODNs per particle. When A_{21} was used as the probe ODN, $RhoT_{20}$ or $T_{20}Rho$ was used as target ssDNA to test the hybridisation. The amount of hybridised ODNs was determined in the same manner as for the coupling efficiency, by measuring the fluorescence or absorption intensity in the supernatant. As mentioned, a single 4.3 µm LbL particle can carry up to $2x10^{-17}$ mole probe ODNs. However, at such a high ODN density, the hybridisation efficiency of the complementary ODNs was less than 50%. To optimise the hybridisation efficiency of the LbL-ODN particles, the coupling amount of probe ODNs was reduced to 125 pmol per mg particles, resulting in a hybridisation yield of approximately 80% both for $RhoT_{20}$ and $T_{20}Rho$ (100 pmol T_{20} per mg LbL-A_{21} particles).

4.1.2.3 Comparison of LbL particles with conventional carboxylated particles

The LbL particles were compared with commercially available carboxylated polystyrene particles from Polyscience Inc. (4 µm) and MagSense Inc. (1.6 µm), respectively. By identical coupling procedure (section 3.3.2), only up to 20% $FluA_{21}$ was immobilised on the commercial particle surface without multilayer polymer modification. This was in agreement with the analysis by CLSM: the fluorescence of the Polyscience-ODN particles and the

MagSense-ODN particles was much weaker compared to the LbL-ODN ones (Figure 4.8). (Note that the PMV of 700 (used for Polyscience-FluA_{21} particles) and 800 (used for and MagSense-FluA_{21} particles) yields a 3.6 and 10.0 fold signal amplification compared to 600 PMV (used for LbL-FluA_{21} particles). The uneven distribution of fluorescence on the Polyscience-FluA_{21} particles revealed that the ODNs were inhomogeneously immobilised onto the particle surface.

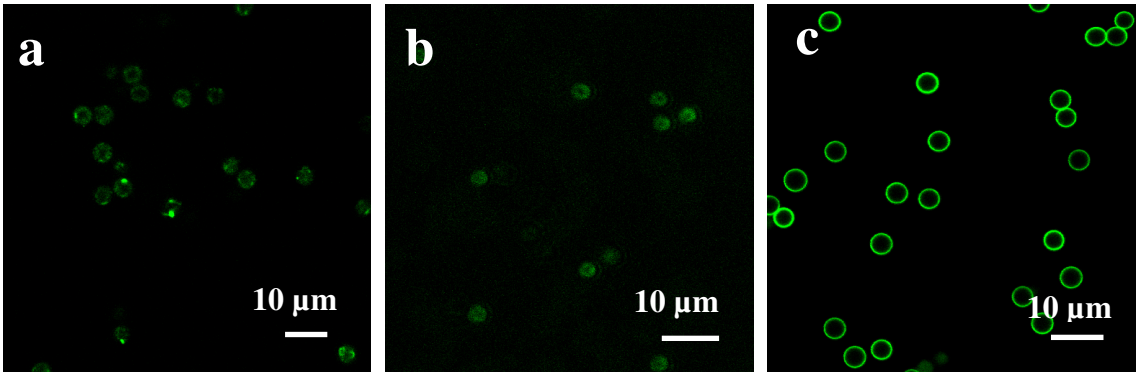

Figure 4.8 CLSM images of FluA_{21} coupled onto a) carboxylated polystyrene particles from Polyscience Inc., PMV: 700; b) MagSense Inc., PMV: 800; c) LbL particles, PMV: 600.

4.1.2.4 LbL-ODN system on planar surfaces

In order to obtain more quantitative information about the LbL-ODN structure, the deposited mass and morphology of the identical films were also investigated by QCM and AFM.

QCM is an advanced method that can quantitatively and time-dependently monitor the deposition of layers on surfaces. As the frequency of a QCM crystal is inversely proportional to the increase of the deposited mass on the crystal surface, the amount of polyelectrolyte and ODNs A_{21} immobilised on the surface was estimated (Figure 4.9). The polyelectrolytes PDA and PMAA were assembled in stepwise manner onto the crystal surface, and the thickness of each polyelectrolyte layer was determined to be between 1-3 nm corresponding to a mass of 105-315 ng cm^{-2}. The amount of A_{21} coupled onto the LbL film investigated by the QCM was approximately 180 ng cm^{-2} (1.8 mg m^{-2}). This number was in the same range as the amount coupled onto spherical particles. Full coupling capacity of ODN A_{21} on LbL particles was approximately 250 ng cm^{-2}.

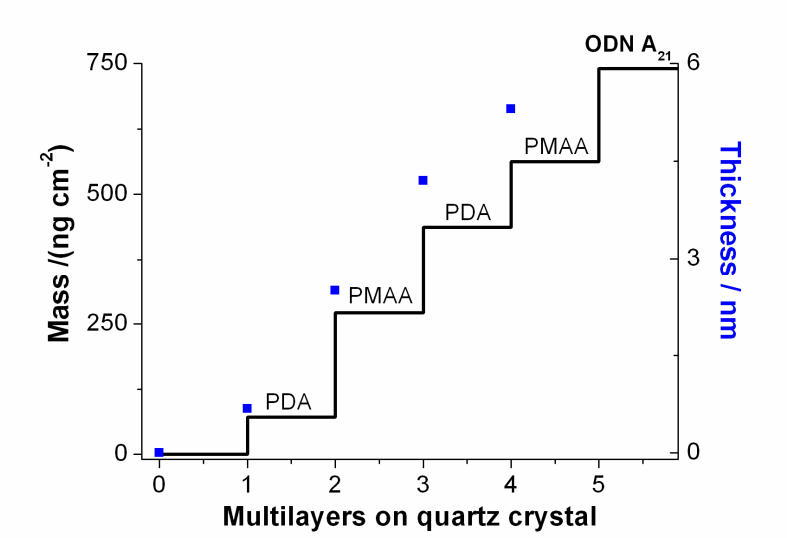

Figure 4.9 Plot of mass (black line, left Y-axis) and thickness (blue squares, right Y-axis) of the polyelectrolyte layers and the coupled A_{21} on planar substrate determined by QCM. Each data point was the average value from four measurements in parallel.

The morphology of the multilayer structure on the planar surface was further analyzed by AFM. The roughness of the multilayer surface changed drastically before and after the coupling of ODN onto the LbL surface (Figure 4.10 a↔b). The LbL film consisting of $(PDA/PMAA)_2$ showed a rather smooth surface with the roughness in the range below 10 nm. Whereas after covalent coupling of A_{21} onto the surface, the roughness of the LbL-ODN surface was in the range of approximately 100 nm, ten-fold bigger than before. This revealed that the ODN coupling process induced substantial conformational changes of the polyelectrolyte layers.

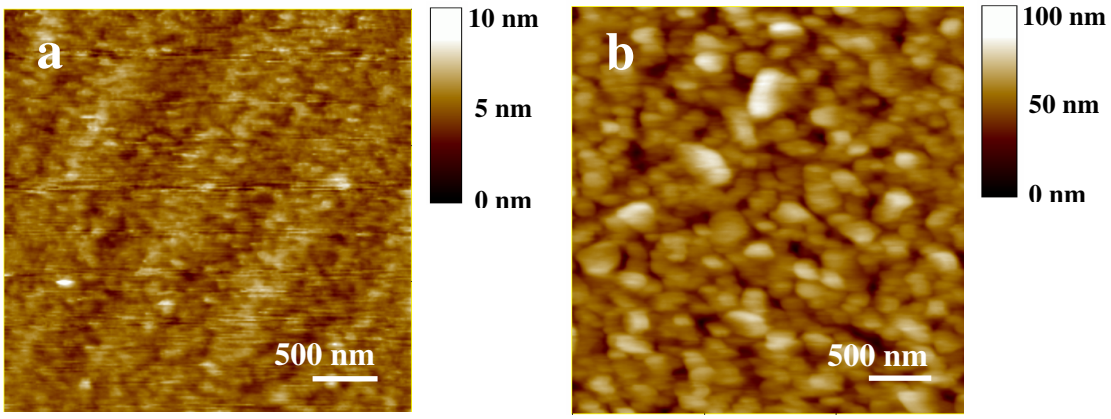

Figure 4.10 AFM images of (a): $(PDA/PMAA)_2$ film and (b): $(PDA/PMAA)_2$ film covalently coupled with A_{21}.

4.1.3 Controlled assembly of liposomes on LbL-ODN surfaces

The advantages of DNA sequence specific hybridisation for supramolecular assembly are well recognized. For example, DNA hybridisation was recently used for programming biomolecular self-assembly pathways, building crystals of nanoparticles and supramolecular polyhedra.[264-267] Based on the intrinsic property of dsDNA Watson-Crick pair formation, liposomes (i.e. LUVs) as nanocontainers were assembled on the LbL-ODN particles via DNA hybridisation.[268] This was achieved by utilizing complementary lipophilic ODNs that were incorporated into the lipid membranes.[244] Intact liposomes containing lipophilic ODN T_{20} were assembled onto the LbL-A_{21} particles and the resulting structure enabled further assembly of A_{20} modified liposomes as the second layer.

Such specific assembly of multilayer liposomes on LbL-ODN surface was also characterised by QCM. An obvious mass increase was observed as the solution of liposomes incorporated with T_{20} (LUVsT_{20}) was pumped through the QCM chamber on the crystal surface that was pre-assembled with LbL-A_{21} films (Figure 4.11). The behaviour of pure LUVs without inserted ODNs and LUVsA_{20} on LbLA_{21} films were also studied as control samples. Negligible amounts of LUVs without ODNs or LUVsA_{20} were attached onto the LbL-A_{21} film; whereas an average amount of 22 mg m^{-2} LUVs containing the complementary sequence T_{20} was assembled (Table 4.2). The quartz crystal has a diameter of 14 mm. Taking the surface area of the crystal as the effective area for binding of LUVs, the density of the LUVsT_{20} specifically bound on the surface was calculated. An adsorbed film consisting of a considerably high amount of water was sensed as mass uptake by the QCM. Liposomes were considered as vesicles of 100 nm in size (controlled during preparation) containing only water; the mass of the lipid wall was negligible compared to the mass of the water contained inside the vesicle.

Table 4.2 Density of liposomes assembled on the LbL-ODN surface via DNA hybridisation.

	Mass/ (mg m^{-2})	No. of LUVs/ 10^4 nm^2
coupled ODN A_{21}	1.77	--
1st Layer LUVs T_{20}	22	0.4
2nd Layer LUVs A_{20}	5.2	0.1
3rd Layer LUVs T_{20}	4.4	0.08

The amount of the second liposome layer ($LUVA_{20}$ on the first $LUVT_{20}$ layer via DNA hybridisation) was substantially lower compared to the first layer. This might be due to the softness of the liposome assembled onto the surface. As mentioned, the estimation of mass adsorbed on the crystal by Sauerbrey equation only applies to 'rigid film'. The structure of additional liposome layer assembled via DNA hybridisation between the lipophilic ODNs anchored to the membrane might not be rigid enough to be detected by the QCM.

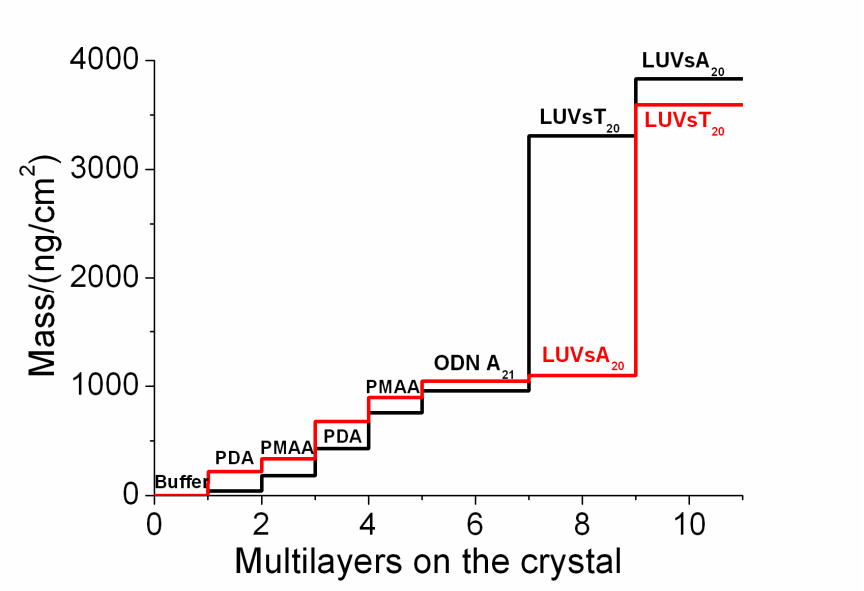

Figure 4.11 Assembly of liposomes on the planar LbL surface measured by QCM.

4.1.4 Target DNA hybridisation detection by FRET

FRET has been a widely used analysis method for DNA hybridisation. In order to ensure a high FRET efficiency and low background fluorescence in a particle-based assay, the donor dye needs to be located as close as possible to the probe DNA on the surface of the particle. For conventional carboxylated poly(styrene) or poly(methylmethacrylate) particles, it is difficult to couple simultaneously a high amount of donor dyes and probe ODNs on the surface without using spacer molecules. Similar problems lie with the Quantum Dots (QDs) based system, namely that limited spacer molecules can be used so that the acceptor dye can remain in the FRET radius to the QDs (donor) after binding onto the surface.

Due to the versatile and specific properties of the LbL film, the LbL-ODN particles can be a highly promising platform for FRET detection, where the donor dye is incorporated in the LbL-ODN particles surface (in different possible positions) and the acceptor dye is on the complementary ODNs. The preparation and the evaluation of such systems are demonstrated.

4.1.4.1 Flu-Rho FRET pair

As mentioned, two fluorophores that the emission spectra of the donor overlaps with the absorption spectra of the acceptor are essential for FRET to occur. Fluorescein (Flu) as donor and rhodamine (Rho) as acceptor were employed as the FRET pair in our study. The large overlapping of the integrated Rho absorption and Flu emission spectra are shown in Figure 4.12.

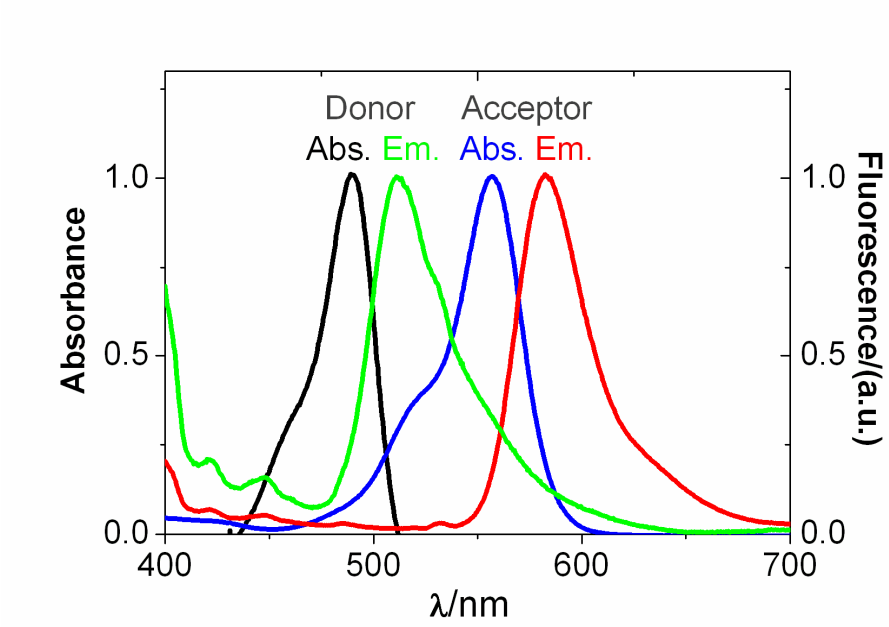

Figure 4.12 Spectra overlap between Rho absorption and Flu emission as a FRET pair: the absorption and emission spectra of Flu are shown as black and green lines, respectively; the absorption and emission spectra of Rho are shown as blue and red lines, respectively. TRIS buffer (10 mM, pH 7.0) was used as the solvent for the measurement.

4.1.4.2 FRET of dsODNs free in solution

As the first step to study the FRET between Flu-Rho, the behaviour of the dye pair-labelled ODNs free in solution was investigated. By using the combination of ODN FluA_{21} and T_{20}Rho/RhoT_{20}, the distance between the FRET pair was well defined for a convenient FRET analysis. To take into account the possible quantum yield changes of the fluorophores by DNA hybridisation, FluA_{21} was also hybridised with unlabeled ODN T_{20} and T_{20}Rho was hybridised with unlabeled ODN A_{21} as control samples, so that the quantification was always based on double stranded helices.

The fluorescence spectra of the hybridised dsODNs solution with varing dye position on the ODN sequence are shown in Figure 4.13.

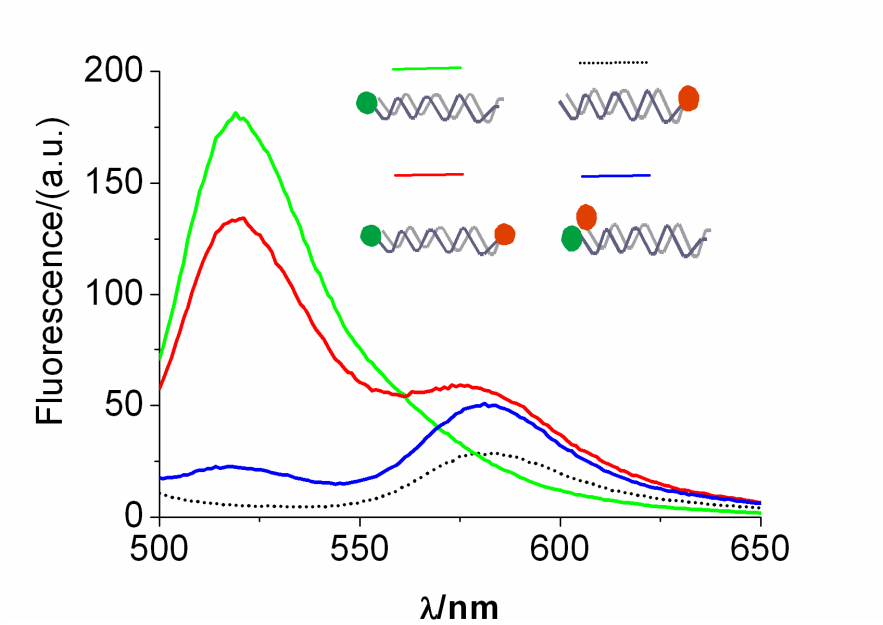

Figure 4.13 Fluorescence spectra of ODN hybrids free in solution (C_{dsODNs} = 50 nM). $FluA_{21}$-T_{20} (——), $FluA_{21}$-T_{20}Rho (——), $FluA_{21}$-RhoT_{20} (——), A_{21}-T_{20}Rho (----). Spectra were taken at λ_{ex} = 480 nm, slits width: 5/10 nm.

The evaluation of the spectra showed a decrease of donor emission by 26.0% when Flu and Rho dye molecules were 20 bps apart (i.e. 6.8 nm separation distance) on $FluA_{21}$-RhoT_{20} hybrids (approximately 130% of the Förster radius of Flu-Rho).[269] As comparison, when the FRET pair was directly close to each other (i.e. on $FluA_{21}$-T_{20}Rho hybrids), the quenching of the donor increased to 87.5%. Simultaneously with decreasing donor emission, an increase of fluorescence signal was observed at 580 nm, which clearly indicated occurrence of FRET. The spectrum of A_{21}-T_{20}Rho hybrid in solution was used as control value for FRET calculation. The detailed FRET characterisation is described in sections 3.4.8 and 4.1.4.4.

4.1.4.3 Two FRET systems of dsODNs on LbL particles

When the ODNs are immobilised on a solid support, the behaviour of the ODNs and the fluorophores can be very different from that in solution. For example, when probe ODNs $FluA_{21}$ are coupled onto the particle surface with a density of 125 pmol/mg particles, the Flu molecules are brought into a close distance below 4 nm, which can lead to self-quenching of the donor prior to hybridisation.

Two FRET systems based on LbL-ODN particles were prepared (Figure 4.14): in system 1, probe ODN was labelled with donor dye ($FluA_{21}$) and the outermost PMAA layer on the LbL particles was non-labelled; in system 2, the dye was coupled to the outermost polyelectrolyte layer (Flu-PMAA) and unlabelled probe ODN A_{21} was used. The latter

system is preferred for DNA diagnostics due to the possibility of using inexpensive unlabelled probe ODNs.

For FRET analysis, ODNs $RhoT_{20}$ or $T_{20}Rho$ were hybridised on the LbL-(Flu)-A_{21} particles. In its most common conformation, the DNA helix has 10 base pairs (bps) per turn and a pitch of 3.4 nm.[263] Therefore, in system 1, upon hybridisation with $T_{20}Rho$ the distance between donor and acceptor on each dsODN is smaller than 2.5 nm, which is below the Förster radius of Flu-Rho FRET pair: high FRET efficiency is expected (system 1B). Whereas upon hybridisation with $RhoT_{20}$, the distance is approximately 7 nm, which exceeds the Förster radius: lower FRET efficiency is expected (system 1A).

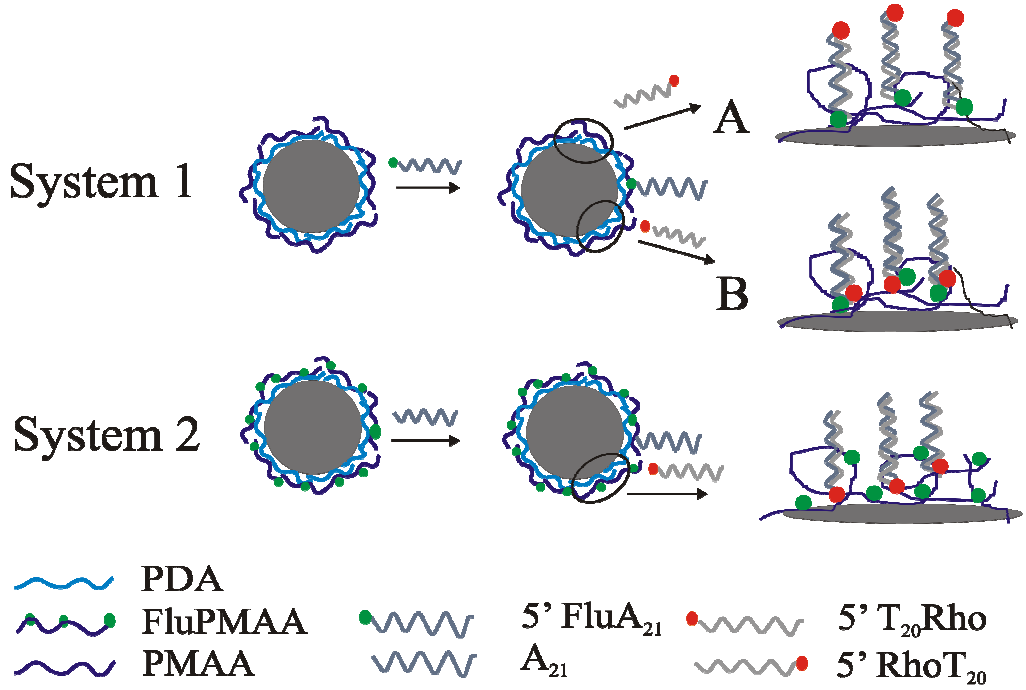

Figure 4.14 Scheme of two FRET systems based on LbL-ODN particles: 1) donor dye Flu coupled on probe ODN A_{21}; 5'$RhoT_{20}$ (A) and 5'$T_{20}Rho$ (B) were used as model target ssDNA to form ds-DNA; 2) donor dye coupled onto outermost polyelectrolyte layer, probe ODN unlabelled.

The fluorescence spectra of LbL-ODN particles from system 1 were firstly measured (Figure 4.15). The FRET difference caused by the Rho position (i.e. ODN hybrids $FluA_{21}$-$RhoT_{20}$ and $FluA_{21}$-$T_{20}Rho$) was much less pronounced for the ODN hybrids immobilised on the LbL surface than for the hybrids free in solution (refer to Figure 4.13). This effect can be explained by the nanoroughness and flexibility of the LbL surface resulting in multiple donor-acceptor interactions.

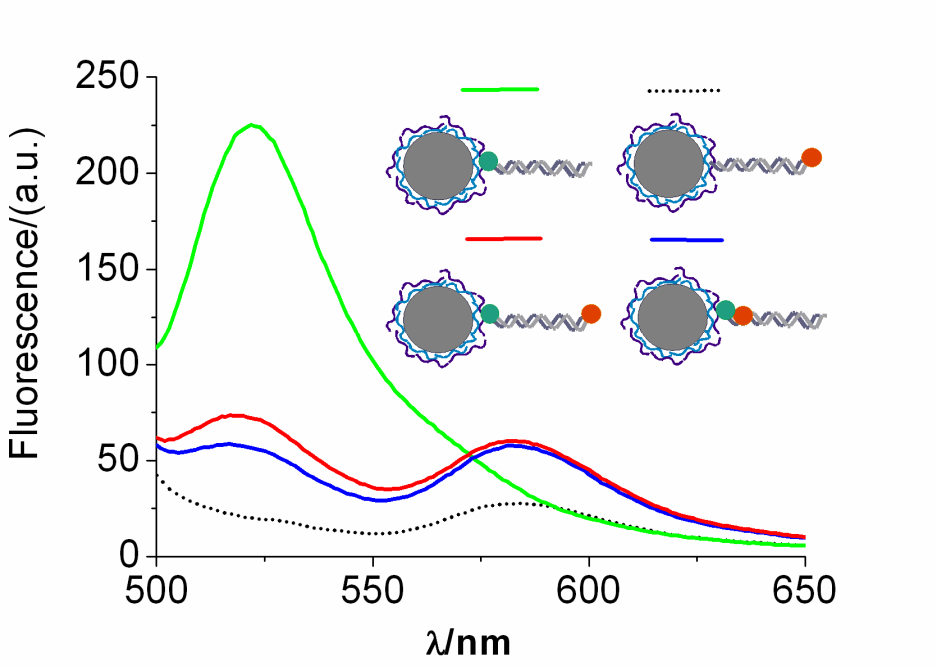

Figure 4.15 Fluorescence spectra of ODN hybrids coupled to the LbL particle surface ($C_{particle}$ = 1 mg/ml with 50 nM T_{20}Rho/RhoT_{20}). FluA_{21}-T_{20} (——), FluA_{21}-T_{20}Rho (——), FluA_{21}-RhoT_{20} (——), A_{21}-T_{20}Rho (----). Spectra were taken at λ_{ex} = 480 nm, slits width: 5/10 nm.

In system 2, unlabelled A_{21} was used as probe ODN and the donor dye Flu was integrated within the LbL films. dsODNs of A_{21} hybridised with T_{20}, RhoT_{20} or T_{20}Rho on the LbL particles (coated with Flu-PMAA as the outermost layer) were prepared. Surprisingly, the FRET difference caused by the position of Rho was almost negligible (Figure 4.16). This is ascribed to the random distribution of the donor dye molecules over the particle surface using the polyelectrolyte Flu-PMAA. The flexibility and nanoroughness of the outermost layer leads to a random distance between the FRET pair in the nanometer range, independent on using T_{20}Rho or RhoT_{20} (see Figure 4.26).

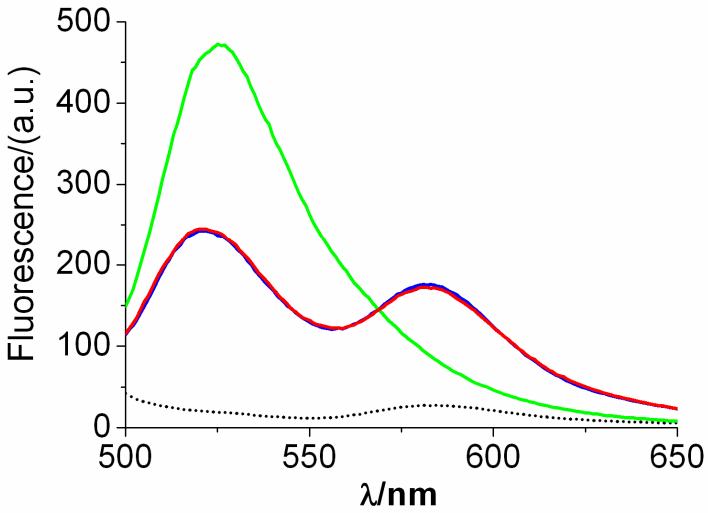

Figure 4.16 Fluorescence spectra of ODN hybrids coupled to the LbL(Flu-PMAA) particle surface ($C_{particle}$ = 1 mg/ml with 50 nM T_{20}Rho/RhoT_{20}). (Flu-PMAA)-A_{21}-T_{20} (——), (Flu-PMAA)-A_{21}-T_{20}Rho (——), (Flu-PMAA)-A_{21}-RhoT_{20} (——), (PMAA)-A_{21}-T_{20}Rho (----). Spectra were taken at λ_{ex} = 480 nm, slits width: 5/10 nm.

Comparing the two FRET systems from Figure 4.15 and Figure 4.16, it is apparent that the fluorescence intensity was remarkably higher when the donor dyes were linked to the polymer (system 2). Not only was the expected donor fluorescence higher, but also the fluorescence intensity collected at 580 nm with λ_{ex} = 480 nm, I_{em580}, a rough estimation of FRET, was almost three times higher than in system 1. In the presence of the same amount of acceptor dye molecules (i.e. same amount of target ODN T_{20}Rho/RhoT_{20} on the particle surface), the higher density of donor dye on the particle surface in system 2 by using the polymer Flu-PMAA (label degree of 1: 350) yielded higher FRET. As this system allows variation of donor density independent on the amount of probe ODNs, one can adjust the ratio between donor and acceptor dyes by using PMAA with varying label degrees.

CLSM images of LbL-A_{21}-T_{20}Rho particles using Flu-PMAA as the outermost layer in the LbL film are shown in Figure 4.17. The monodisperse LbL-Flu-PMAA-A_{21} particles exhibited almost homogenous fluorescence intensity (Figure 4.17 a) pointing to an even distribution of the donor dye on the particle surface. After T_{20}Rho was hybridised on the particles, the fluorescein intensity decreased drastically (Figure 4.17 b), indicating donor quenching due to FRET. The presence of fluorescence in the red channel (λ_{em} = 554-619 nm, Figure 4.17 c) was mainly due to FRET, with a small contribution from the tail of the donor fluorescence, which was only recognizable before hybridisation with 5 times amplification of the PMV.

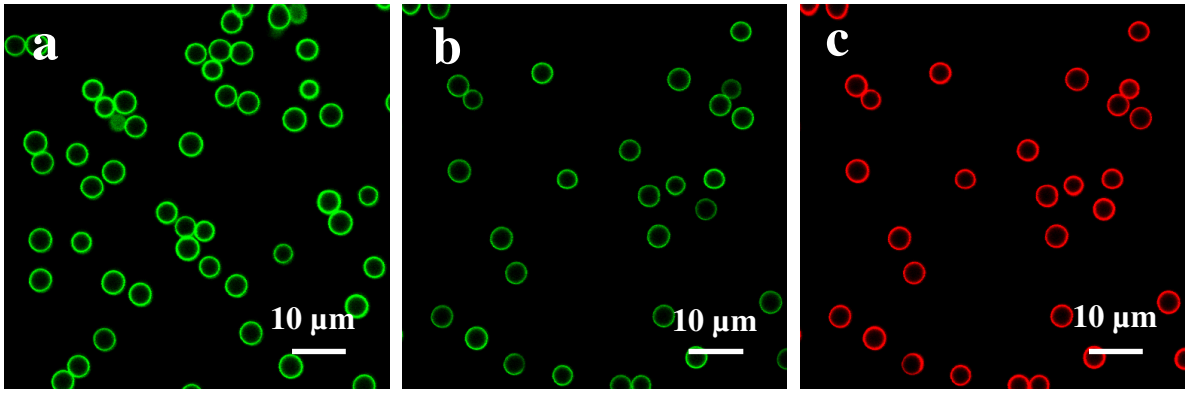

Figure 4.17 CLSM images of LbL-ODN particles (system 2): (a) LbL-Flu-PMAA-A_{21} particles at green channel (λ_{em} = 500-534 nm) before hybridisation, no acceptor present; (b) LbL-Flu-PMAA-A_{21}-T_{20}Rho particles after hybridisation at green channel (quenched donor signal) and (c) red channel (λ_{em} = 554-619 nm) (mainly FRET signal). All images were taken at λ_{ex} = 488 nm under identical PMV setting of 600.

4.1.4.4 Characterisation of FRET

FRET efficiency can be characterised from two points of view: 1. decrease of fluorescence of the donor dye; 2. increase of fluorescence of the acceptor dye induced by the excitation of the donor. The former one is widely used as a simple and basic method (Equation 2.7).[203] However, in realistic application, a decrease of donor fluorescence ('signal off') can occur due to other parameters rather than FRET, and the analysis from signals of acceptor fluorescence ('signal on') is more reliable.

In this work, the fluorescence intensity of the acceptor molecules induced by the 'energy transfer' from the near-by donor, denoted as I_{FRET} was used to evaluate the FRET efficiency for our LbL-ODN system. The calculation of I_{FRET} is described in section 3.4.8.

Data of quenched donor intensity and I_{FRET} obtained from (a) flow cytometry and (b) fluorometry shows that in system 1B, having donor dye directly close to the acceptor on each dsODN, the quenching of the donor was remarkably more pronounced than in system 2, having a random distribution of donor on the surface (Figure 4.18). In the latter system, not all of the donor molecules were in sufficiently close neighbourhood of an acceptor molecule, and the percentage of quenching was therefore smaller. However, in absolute values, more donor molecules were quenched in system 2 compared to system 1, resulting in a higher I_{FRET}. Evaluation of FRET by fluorometry and flow cytometry yielded slightly different results. The flow cytometry data showed a higher donor quenching and I_{FRET} for the same samples than that measured by fluorometry. This is due to that flow cytometry can

distinguish the fluorescence from singlet, doublet or other multiplets of particles, allowing for evaluation to be carried out exclusively on single particles. In the case of bulk measurements by fluorometry, the fluorescence spectra of particles in solution include some uncertainties due to light scattering and the presence of aggregated particles.

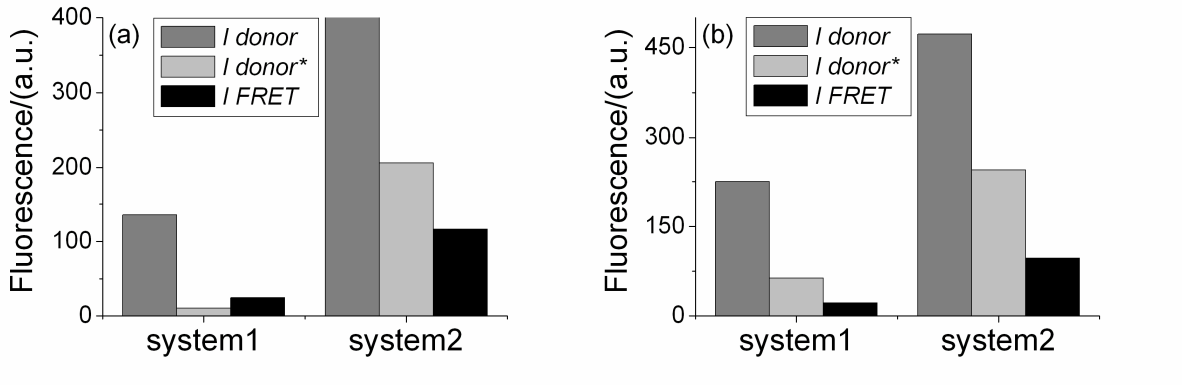

Figure 4.18 FRET comparisons between two systems. I_{donor} and I_{donor*} represents the donor fluorescence in the absence and presence of acceptor, respectively. Data collected from (a) flow cytometry, (b) fluorometry. The data of (a) were based on the average value measured from 10.000 particles of each sample. The standard deviation of data was negligible.

4.1.4.5 Detection limit by fluorometry

A low detection limit is one of the most important criteria for a successful and competitive nucleic acid assay. The sensitivity of our LbL-ODN system was investigated by fluorometry. To 1 ml of 1 mg LbL-Flu-PMAA-A_{21} particle suspension, with constant A_{21} coupling amount of 125 pmol, varied amounts of T_{20}Rho (0 nM-200 nM T_{20}Rho) were added for hybridisation. The fluorescence spectra are shown in Figure 4.19. Occurrence and changes in FRET were revealed by the gradual decrease of the donor intensity and increase of acceptor intensity. At 1 nM of T_{20}Rho, a small change in the spectrum was already detected and at 5 nM a distinct decrease of fluorescence at 520 nm by 5.6% and an increase of fluorescence at 580 nm by 19.0% was measured. Hence, the detection limit using a conventional fluorometer is ~1-5 nM target DNA.

The change was initially almost linear with the concentration of T_{20}Rho. Then it levelled off when the hybridisation was saturated at 100 nM T_{20}Rho, at which the T_{20}/A_{21} ratio was 0.8. This confirmed that 80% of the A_{21} ODNs coupled to the LbL particles were available for hybridisation. The analysis by I_{FRET} showed that the FRET efficiency increased with increasing amounts of T_{20}Rho until the hybridisation was saturated (Figure 4.20). Above the threshold concentration, I_{FRET} was even decreased apparently because free T_{20}Rho molecules

in the solution did not contribute to the FRET signal but they were considered in the crosstalk correction. The FRET efficiency E analyzed by donor quenching (Equation 2.7) revealed the same trend as the method by I_{FRET}.

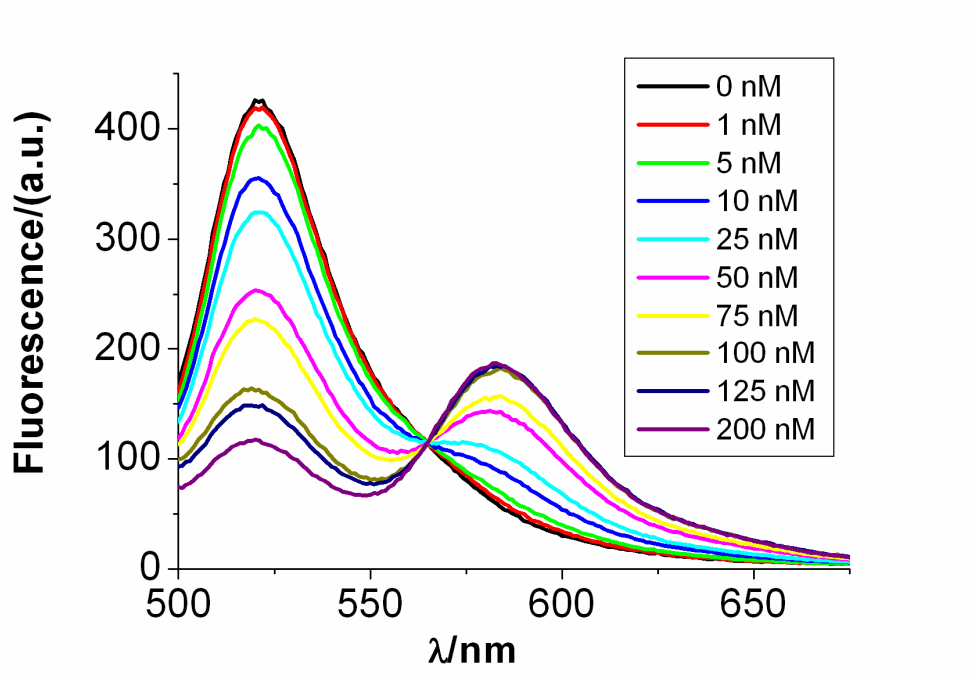

Figure 4.19 Fluorescence spectra of the LbL-A_{21}-T_{20}Rho particles at different T_{20}Rho concentrations. ($C_{particle}$ = 1 mg/ml). Spectra were taken at λ_{ex} = 480 nm, slits width: 5/10 nm.

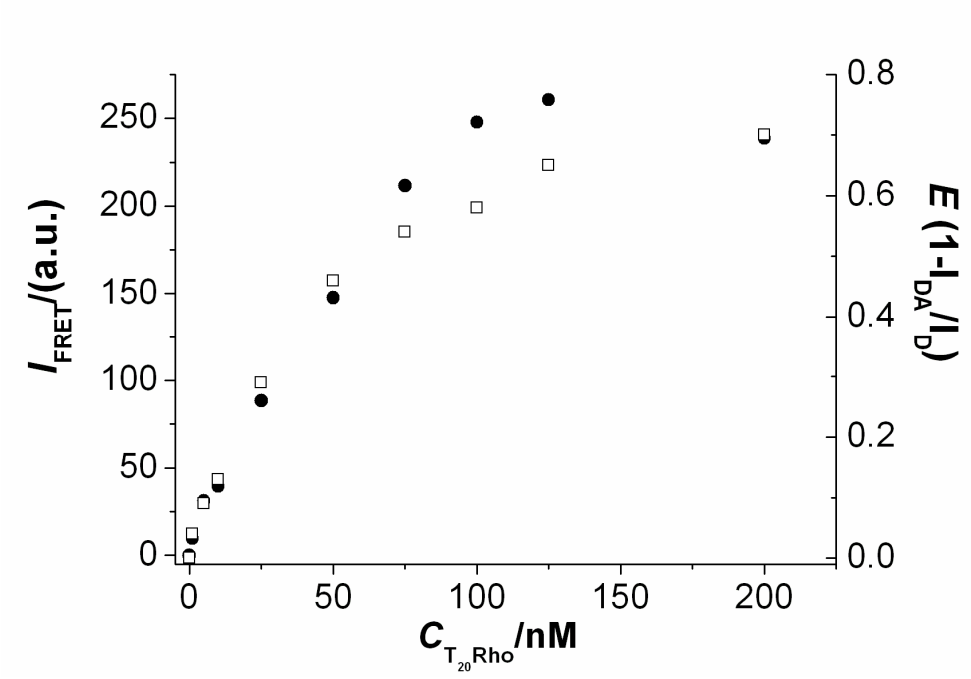

Figure 4.20 FRET efficiency evaluated by I_{FRET} (circles) and E (hollow squares) in dependence on the T_{20}Rho concentration.

4.1.4.6 Single nucleotide polymorphism (SNP) test

Nowadays, nucleic acid diagnostic systems have been mainly developed in two directions: specific detection of target by hybridisation assay and SNP for study of mutation.[270, 271] The applicability of the LbL-ODN system in SNP assays was therefore investigated.

The fluorescence spectra of LbL-Flu-PMAA-ODN particles as a function of base pair mismatch were measured at 25 °C and 60 °C, respectively. For this study ODNs with a sequence from *E. coli.* DNA were employed in order to work with a real system containing a defined sequence of the four nucleotide bases. The ODN sequence used as probe ODN and the complementary sequences as target DNA with different mismatch numbers are listed in Table 3.1.

In the SNP study, the LbL-ODN particles were firstly hybridised with target ssDNA having increasing number of mismatches. Then the hybridised particles were heated to defined temperatures and the melting of the dsODN duplex was detected by decrease of the FRET signal. At 25 °C near room temperature, the differences in fluorescence spectra were negligible in dependence on the number of mismatches (Figure 4.21 a). In contrast, at 60 °C, near the melting point T_m for the fully matched DNA hybrids, hybrids containing base pair mismatches were denatured. The increasing number of mismatches led to the decrease of the hybrid's stability; the donor fluorescence restored its intensity as the acceptor dye-labelled Target ODN was separated from the probe ODN, i.e. the donor and acceptor molecules were no longer in the Förster radius (Figure 4.21 b). The donor intensity gradually increased as the mismatch number increased from 0 to 1 and 2. The results revealed that the nucleic acid detecting system based on LbL particles can also be applied in SNP studies.

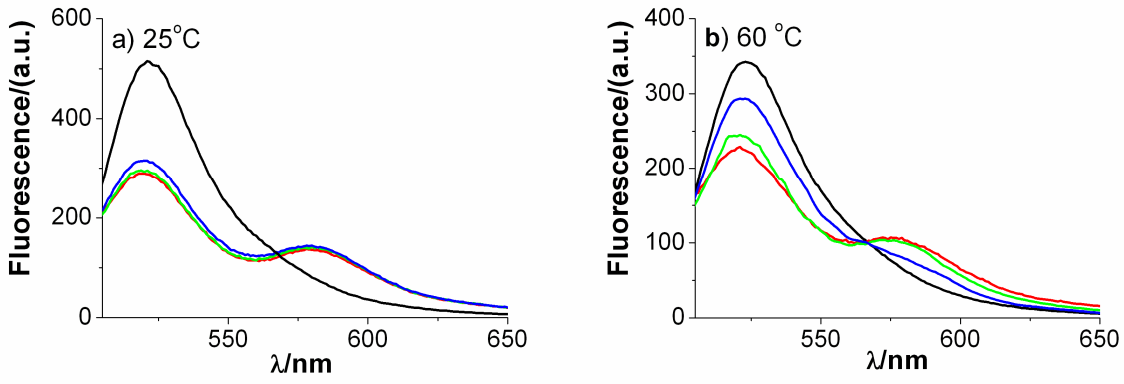

Figure 4.21 Fluorescence spectra of LbL-Flu-PMAA-Probe-Target^n (Rho) at a) 25 °C and b) 60 °C, in which Target ODN without fluorescent label is presented as black line; target ODN (Rho-labelled) containing 0, 1 and 2 mismatches are presented as red, green and blue lines, respectively. Spectra were taken at λ_{ex} = 480 nm, slits width: 5/10 nm.

4.1.4.7 Reusability of the LbL-ODN particles

dsDNA denatures above its melting point, meaning that the target DNA that hybridised onto the LbL-ODN particles can be released when heated up above the melting temperature. Hence, the LbL-ODN particles could be in principle 'recycled' and reused. Therefore, the reusability of our LbL-A_{21} particles was investigated (Figure 4.22). The removal of $RhoT_{20}$ that was bound onto the particle surface was conducted at 75 °C, so that the probe ODNs became again single stranded. After removal of the supernatant and cooling down the particles were again hybridised with $RhoT_{20}$. However, the binding capacity of LbL–A_{21} particles decreased approximately 25% for each binding cycle. One problem was the complete removal of released $RhoT_{20}$, because it involved centrifugation at high temperature and separation of the supernatant as quickly as possible to avoid rehybridisation. Simultaneously, irreversible aggregation of particles occurred during heating at 75 °C which became a severe problem after two heating and cooling cycles. Therefore, the LbL-ODN particles should not be used more than twice for nucleic acid detection. However, for DNA extraction purposes, reuse of the LbL-ODN particles is still feasible.

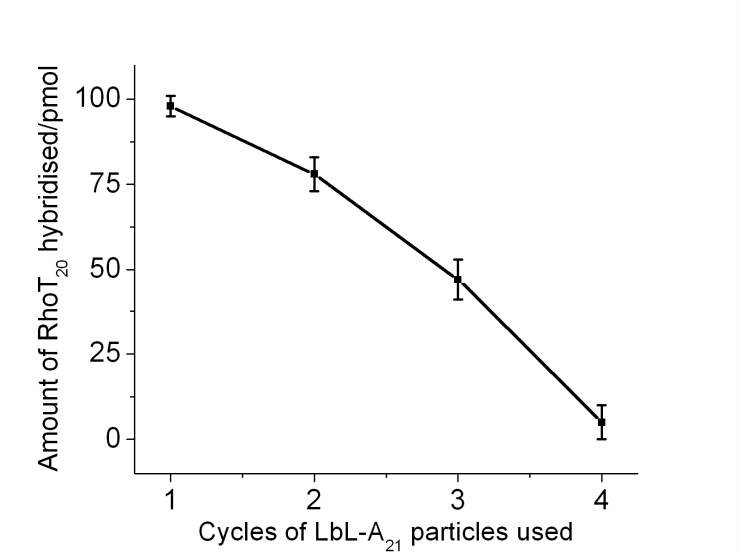

Figure 4.22 Amount of $RhoT_{20}$ hybridised on LbL-A_{21} particles in dependence on the number of hybridisation cycles LbL-A_{21} being used.

4.1.4.8 Cy3-Cy5 FRET pair

Flu-Rho as a FRET pair has been intensively studied by researchers. However, there are several problems in using fluorescein for consistent signal evaluation in serum samples. For example, the fluorescence intensity of fluorescein is highly dependent on the pH, and the dye often undergoes fast photobleaching. Moreover, in serum samples, auto-fluorescence often

exists for excitation at short wavelengths, which hinders a reliable fluorescence reading. Cyanine dyes Cy3-Cy5 are another commonly used FRET pair that offers the advantage of smaller crosstalk between the donor and acceptor as well as longer absorption and emission wavelengths than the Flu-Rho system (Figure 4.23).

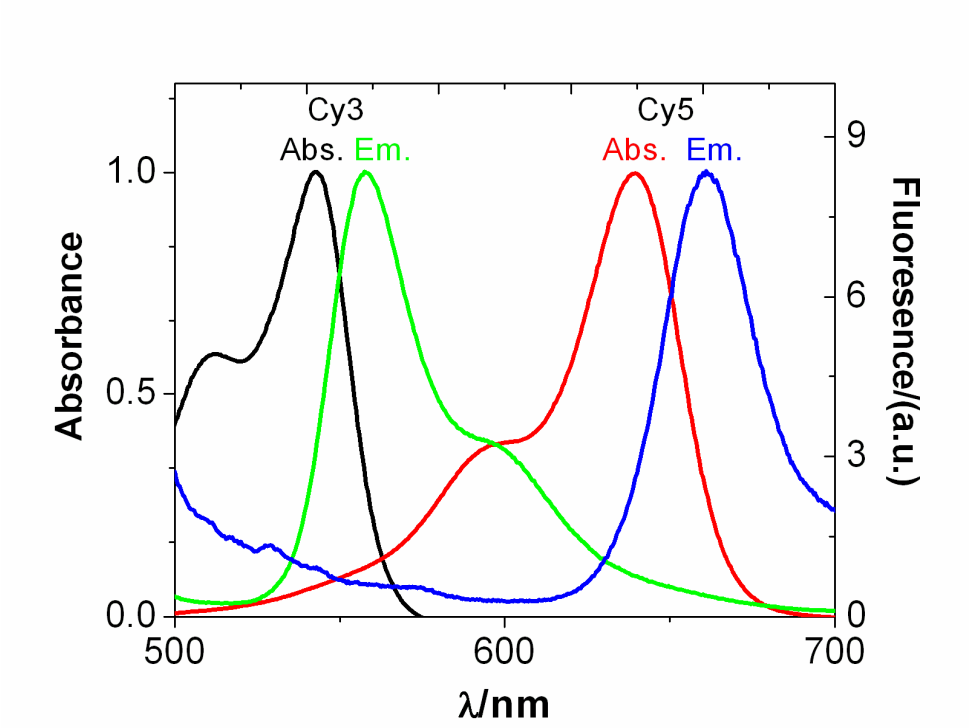

Figure 4.23 Spectra of the FRET pair Cy3 and Cy5: the absorption and emission spectra of Cy3 are shown as black and green lines, respectively; the absorption and emission spectra of Cy5 are shown as red and blue lines, respectively. TRIS buffer (10 mM, pH 7.0) was used as the solvent for the measurement.

For construction of the systems 1 and 2 with Cy3 as the donor, Cy3ODN and Cy3-PMAA were used. As target DNA, the complementary ODN sequence to the probe ODN labelled with Cy5 at the 3' end was used. Similarly to the study based on Flu-Rho pair, two FRET systems, of which donor dye either on the probe ODN (by use of Cy3ODN) or on the polyelectrolyte layer (by usage of Cy3-PMAA) were prepared. However, in contrast to the results obtained from Flu-Rho system, the FRET system 2 (Cy3 on PMAA) yielded a lower FRET efficiency than system 1 (Cy3 on probe ODN), even with a high density of Cy3 on the PMAA layer (Figure 4.24).

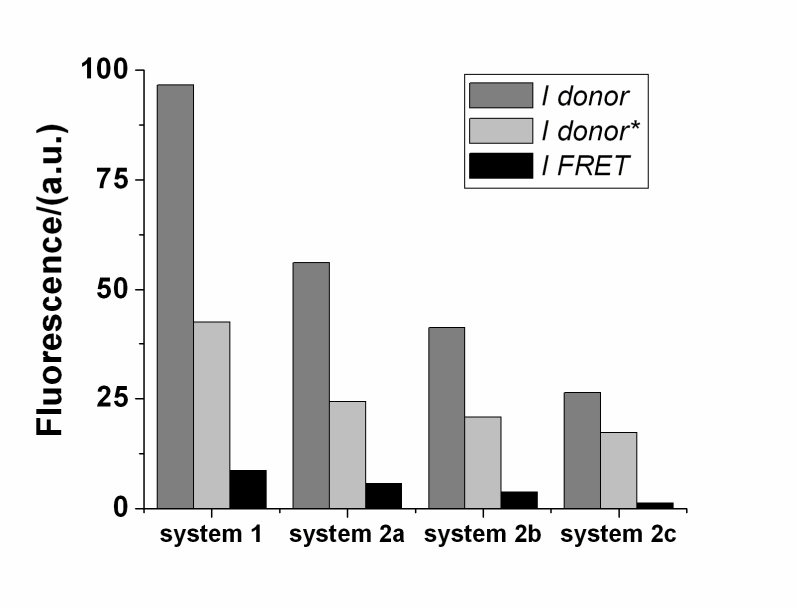

Figure 4.24 Comparison of FRET between system 1 and 2 based on Cy3-Cy5 pair by fluorometry. I_{donor} and I_{donor*} represents the donor fluorescence in the absence and presence of acceptor, respectively. In system 2, Cy3-PMAA with different label degrees of a) 1: 130; b) 1: 260; and c) 1: 500 were used as the outermost layer on LbL particles, respectively.

In system 1, at a coupling density of 100 pmol Cy3ODN per mg LbL particles, the density of Cy3 molecules was estimated to be approximately 120 nmol m^{-2}; whereas in system 2 it was 240 nmol m^{-2} using Cy3-PMAA with a label degree of 1: 130, which was double than in system 1. However, the fluorescence intensity of LbL-Cy3-PMAA particles was remarkably lower.

This can be due to the smaller Förster radius of Cy3-Cy5 (approximately 20% smaller than Flu-Rho), which means a higher demand for a close distance between the two dyes for efficient FRET. In system 1, the Cy3 and Cy5 were labelled at the same end of each dsODN hybrid, which yielded higher FRET than in system 2, where the Cy3 dyes were in a random distance to Cy5 dyes.

Besides, it was found that the fluorescence quantum yield of Cy3 was reduced after immobilisation on the polymer chain or particle surface. Figure 4.25 shows that with the same excitation wavelength and amount of absorbed photons, the quantum yield of Cy3-PMAA was approximately 58% lower than for the free dye Cy3; whereas the quantum yield of Cy3ODN was almost twice as much as for the free dye. In order to clarify the origin of this decreased fluorescence quantum yield of Cy3-PMAA, a deeper investigation of the photophysics of cyanine dyes covalently coupled to polyelectrolytes was carried out (section 4.2).

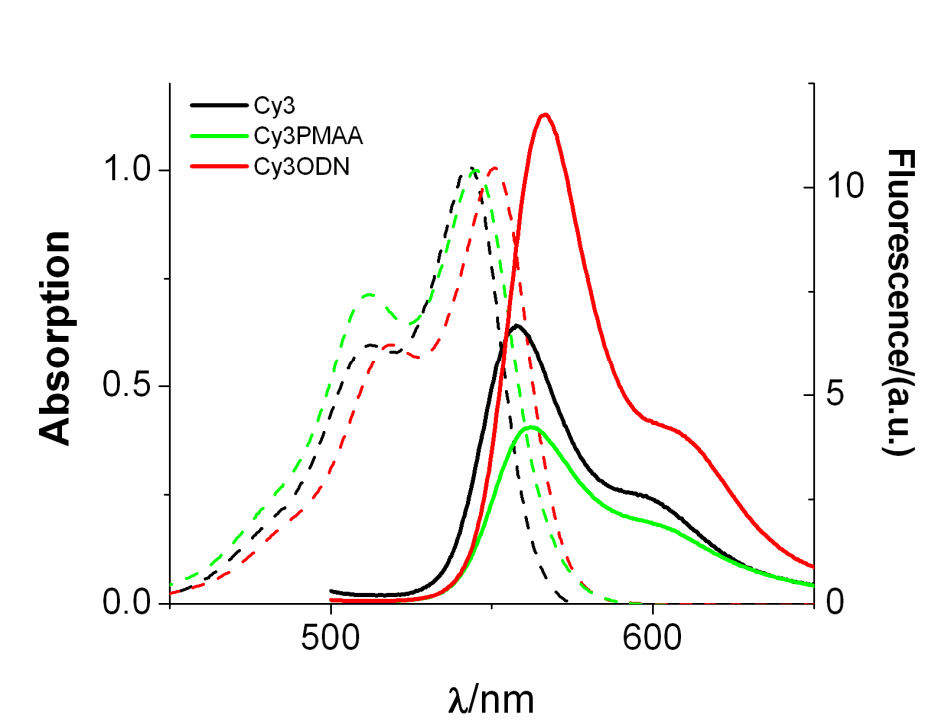

Figure 4.25 Absorbance (dashed lines) and fluorescence (solid lines) spectra of Cy3 dye (black), Cy3ODN (red) and Cy3-PMAA (green) solution with their peak absorption normalised at 1. TRIS buffer (10 mM, pH 7.0) was used as the solvent for the measurement.

4.1.5 Summarising Discussion

4.1.5.1 Advantages of the LbL-ODN particles for DNA detection

A DNA bioconjugation system based on microparticles modified by polyelectrolyte multilayer films has been prepared, which can detect nucleic acids and base pair mismatches by FRET with high sensitivity. A high density of probe molecules could be homogenously immobilised onto the LbL surface by covalent linkage. The system exhibited specific and high binding capacity to a complementary model ssDNA. The covalent coupling of fluorophores to the outermost polyelectrolyte layer yielded a very efficient FRET detection system for which no removal of other DNA molecules from the supernatant by an additional washing step was required.

The LbL-ODN particle system presented several advantages compared to the conventional particle systems thanks to the specific features of the multilayer polyelectrolyte film assembled by the LbL technology (Figure 4.26):

1. The nanoroughness of the LbL surface offered a high concentration of reactive groups available for coupling probe ODNs. Thus, a high binding capacity to the target molecules can be achieved.
2. The use of donor dye-labelled polymer as outermost coating layer offered a high donor density that was independent on the amount of ODNs coupled on the particles. Therefore inexpensive label-free probe ODNs can be applied for detection.
3. With the donor dye conjugated to the most flexible outermost polymer layer, the average distance between donor and acceptor was reduced, increasing the sensitivity of the FRET system and allowing the detection of longer DNA chains.
4. Although the carboxylic acid groups were partly used for coupling, the large remaining amount still ensured sufficient negative charges on the surface, which prevented non-specific binding of other DNAs. Moreover, this LbL-particle based assay can be easily manipulated, and it can offer a high throughput approach e.g. incorporating additional tags such as QDs of different fluorescence and ratios into the LbL structure to allow distinguishing between different samples with different DNA sequences in a particle library.

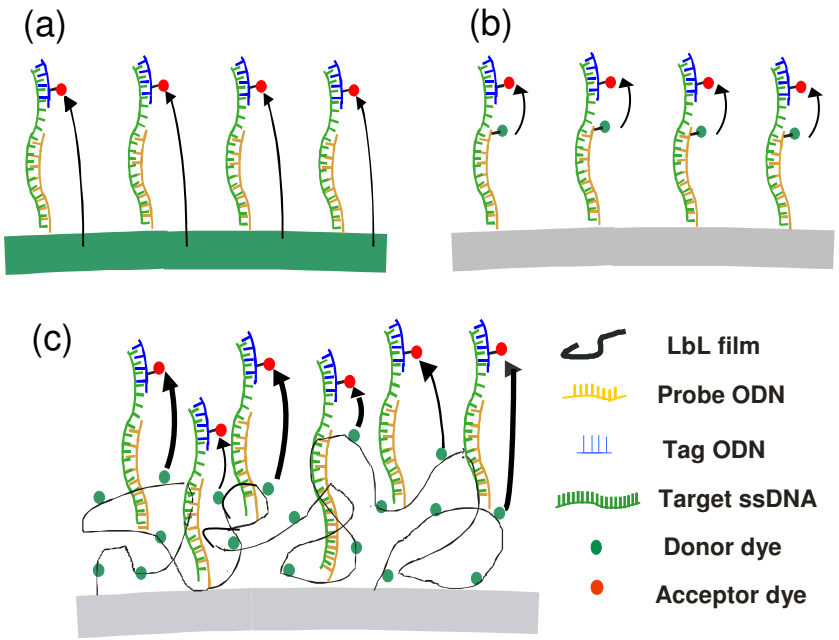

Figure 4.26 Schematic representation of the advantages of LbL film-coated surface (c) for probe ODNs immobilisation and FRET detection compared to plain surfaces: donor molecules in/on the substrate (a) and donor molecules on the probe ODNs (b).

Seradyn Inc. launched dT_{14} magnetic particles (Sera-Mag™) for specific dA_{30} capture, which claimed to offer so far the highest binding capacity in the market: 200 pmol per mg of 1 µm magnetic particles (information available under www.thermo.com). This capacity was in the range of 10^{-19} mole target ODN per particle (1 µm magnetic). Our up-to-date developed LbL-A_{21} particles could capture 10^{-17} mole T_{20} per particle (4.3 µm, silica), which corresponds to $5.4x10^{-19}$ mole target DNA per 1 µm silica particle. Therefore, our LbL-ODN particles exhibited similar binding capacity as the so far best commercially available particles.

The sensitivity of the LbL-ODN system for DNA detection measured by fluorometry was in a comparable range to other fluorescein-based detection systems.[10, 11] Abel *et al.* achieved the highest detection limit of $2.0x10^{-13}$ M (24 fmol) of a fluorescein-labelled complementary 16-mer ODN by applying longer assay cycles, with an incubation time of 60 min. However, it was a heterogeneous assay based on avidin-biotin interactions for the probe ODN immobilisation; and their detection limit as a fluorescence competitive assay was only $1.1x 10^{-9}$ M (132 pmol).[272]

Using advanced techniques such as CLSM and flow cytometry, single LbL-ODN particles carrying 10^{-19}-10^{-17} mol target DNA could be analysed, which presented a much superior detection limit compared to other optical DNA detection systems.[11]

Therefore, microparticles coated with LbL films offered a unique platform for bioconjugation and FRET detection of binding events. The demonstrated advantageous features recommend the developed LbL-ODN particles as a novel efficient system for DNA diagnostic.

4.1.5.2 LbL-ODN system with different FRET pairs (Flu-Rho vs. Cy3-Cy5)

In order to avoid several disadvantages of the FRET pair Flu-Rho, the well-known FRET system Cy3-Cy5 was also tested. However, problems arose from the photophysical properties of the cyanine dyes, such as small Förster radius and strong reduction of the fluorescence quantum yield after coupling to polyelectrolytes and assemble by LbL on surfaces. In order to solve these problems when using Cy3-Cy5 as the FRET pair in the present LbL-ODN particle system, further investigation on the cyanine dyes and their photophysical behaviour after coupling to polyelectrolytes was conducted.

4.1.5.3 LbL-ODN surface as a template for other functional structures

The LbL-ODN system was not only employed for nucleic acid sensing applications, but also presented as a template for the specific assembly of vesicles modified with liphophilic ODNs via DNA hybridisation. Intact liposomes were assembled onto the LbL-ODN surfaces. By addition of triggers such as melittin fusion of liposomes occurred.[267] Different types of vesicles containing specific reactants can be assembled onto LbL particles. Such LbL particles carrying nanocontainers with reactants to be released on demand can offer novel attractive applications for the local delivery of molecules in microfluidic devices or for signal enhancement by triggered fusion of two adjacent liposomes encapsulated with reacting substances for chemi- or bioluminescence.

4.2 Formation of H-aggregates of cyanine dyes covalently attached to polyelectrolytes

As mentioned in section 4.1.5.2, it was observed that the fluorescence quantum yield of Cy3 dye was reduced when coupled onto PMAA. This effect hindered the use of Cy3-Cy5 pair for preparing LbL-ODN FRET systems. Therefore the spectroscopic behaviour of these fluorophores in the free states and when covalently attached to polyelectrolytes was investigated. In particular, Cy5-PAH was selected as a model polymer for investigation because Cy5 has a more extended conjugated π-electron system and shows more pronounced spectral changes in dependence on the environment. The cationic polyelectrolyte PAH is not only an important material used in the LbL technology but can also serve as a simple model for proteins below the isoelectric point. The synthesis of Cy5-PAH is a one-step process so it can be better controlled and fine tuned than the preparation of Cy3-PMAA.

4.2.1 H-aggregates of Cy5 dye molecules on polymer chains

The molecular structure of the Cy5 dye is shown in Figure 4.27. The succinimide group reacting with amine groups enables the covalent labelling of Cy5 on PAH. The reaction was performed with a good yield (label degree of 1: 350). However, the absorption spectrum of the dye coupled to the polymer (Cy5-PAH) was remarkably different from the spectrum of the free dye Cy5 (Figure 4.28). Instead of showing the intrinsic absorption peak at 648 nm, which is normally the case for Cy5, a new absorption band in the Cy5-PAH spectrum at 590 nm close to the vibrational transition of the dye at 602 nm was observed. The emission spectra of the free dye and the dye-labelled polymer had similar shape and peak wavelength, while the free dye yielded almost 50% higher fluorescence intensity (Figure 4.28).

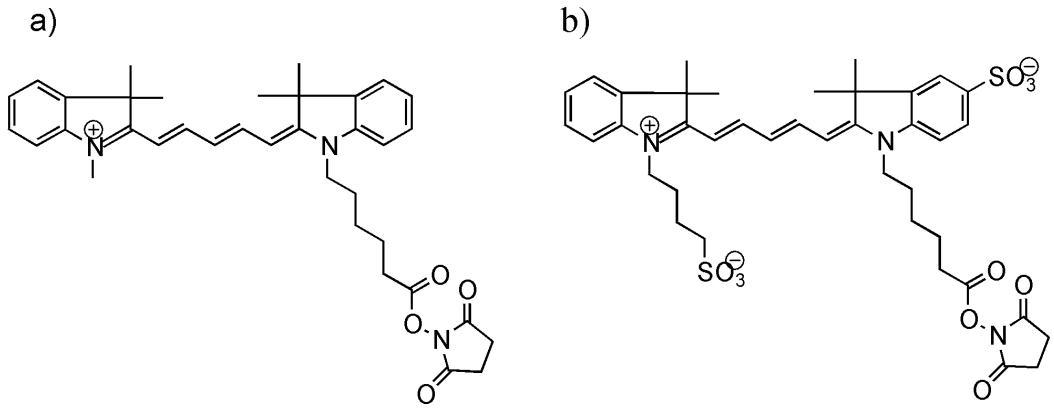

Figure 4.27 Molecular structure of a) Cy5, b) disulfo-Cy5.

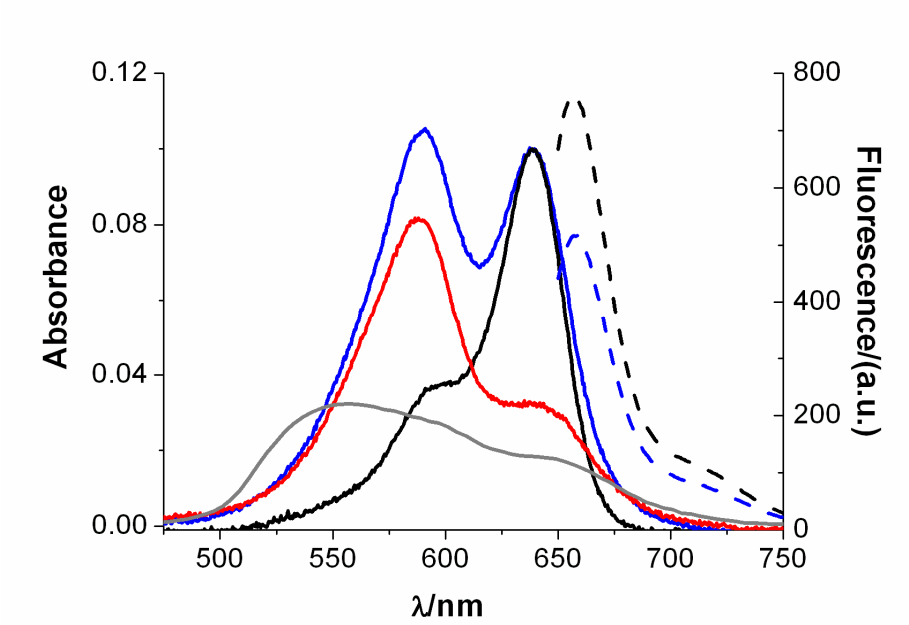

Figure 4.28 Absorption (solid lines) and fluorescence spectra (dash lines) of Cy5-PAH (label degree: 1: 350, blue lines) and Cy5 (black lines). The fluorescence spectra were taken at λ_{ex}= 638 nm close to the absorption maximum. The absorption spectrum of the new species was calculated (red line). For comparison the H-aggregate spectrum of Cy5/PSS was shown (grey line).[273, 274]

A control sample of PAH solution showed no absorption in the UV-Vis range above 300 nm, therefore the peak at 590 nm could have two possible origins: 1. a new species was formed by the labelling procedure; 2. the vibrational structure of the dye changed, which is known for some dyes such as pyrene.[275] In order to verify this, the excitation spectra were measured for the free and the immobillised dye molecules (Figure 4.29).

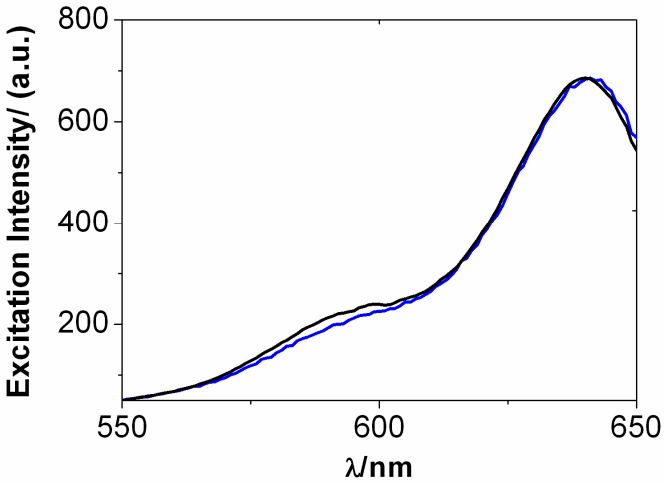

Figure 4.29 Excitation spectra of Cy5 (black line) and Cy5-PAH (blue line). Spectra were taken at λ_{em} = 655 nm, slits width: 5/10 nm.

Both spectra were almost identical and showed only very weak peaks around 590 nm. This indicated that the absorption spectrum of Cy5-PAH was the superposition of the spectrum of Cy5 molecule and a non-fluorescent species.

The spectrum of the new species was determined as the difference between the spectrum of the labelled polymer and that of the free dye (red line in Figure 4.28). This species had an absorption maximum at 588 nm and a broad shoulder at around 645 nm. Such hypsochromic shift of absorption to higher energy is known from H-aggregate or dimer formation of dyes caused by transition dipole interactions.[276] Formation of H-aggregates of Cy5 has been observed earlier by adsorption of the dye to PSS at a 1:1 dye to monomer ratio.[273, 274] However the spectrum of Cy5 H-aggregate on PSS, (Cy5/PSS), had a quite different shape compared to that of Cy5-PAH, pointing to a different arrangement and orientation of the dye molecules to each other (Figure 4.28).

In the case of a statistically even distribution of the dye molecules on the polymer chain, a label degree of 1: 350 and a stretched polymer chain, the chromophores are too far apart for transition dipole interactions to occur. There can be two possible ways in which dyes can come close to each other, leading to formation of H-aggregates (Figure 4.30).

1. The dye molecules were not statistically distributed along the PAH chain. This could be due to a preferred attachment of the dyes in close neighbourhood on the PAH chains during the reaction.

2. The dye molecules were statistically evenly distributed. However, due to entanglement of polyelectrolytes in the aqueous solution, even dye molecules located far from each other could form aggregates.

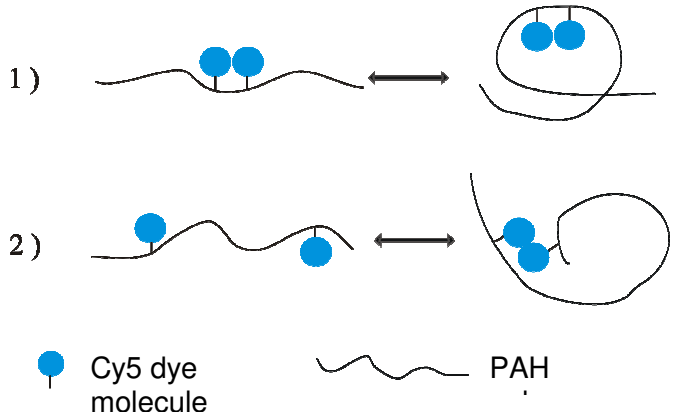

Figure 4.30 Two possible arrangements of dye aggregates on Cy5-PAH: 1) Cy5 dye molecules are adjacent to each other on the polymer chain; 2) Cy5 dye molecues are evenly distributed on the polymer chain.

4.2.2 Spectral changes of Cy5-PAH in dependence on external parameters

In order to find out the origin of the H-aggregates of Cy5, absorption and fluorescence spectra of Cy5-PAH in dependence on label degree, ionic strength and solvent were investigated.

4.2.2.1 Dependence on the label degree

In theory, the lower the density of Cy5 on the polymer is, the less H-aggregates should form. To verify this, Cy5-PAH with lower label degrees were synthesized. Absorption spectra of Cy5-PAH of three different label degrees are shown in Figure 4.31. The aggregate band decreased slightly with decreasing label degree, which proved less dye-dye interactions and aggregate formation at lower dye density on the polymer chain. However, at the low label degree of 1: 840, the H-aggregate effect was already pronounced; even at the label degree of 1: 1500, theoretically with less than half a dye molecule bound per polymer molecule, the aggregates were still present.

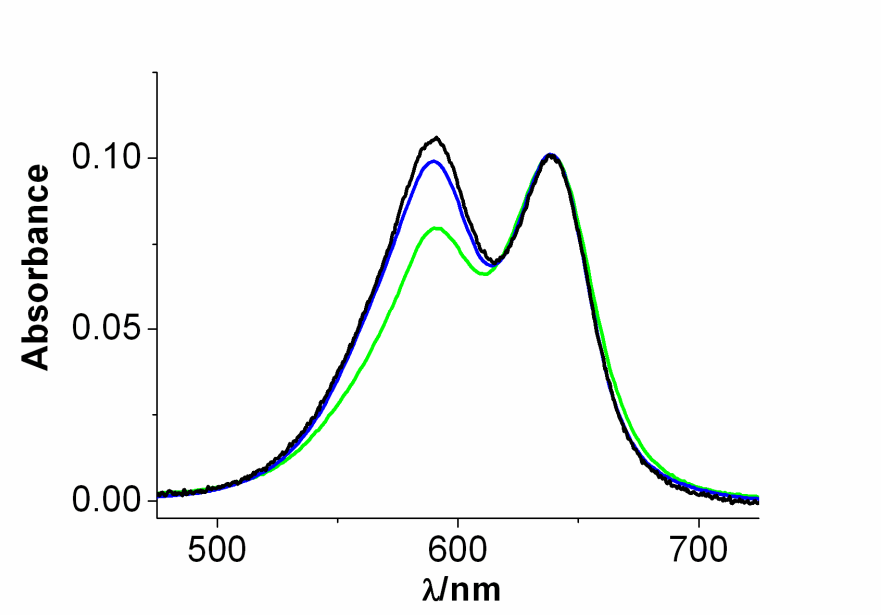

Figure 4.31 Absorption spectra of Cy5-PAH with dye label degree of 1: 1500 (green line), 1: 840 (blue line) and 1: 350 (black line).

4.2.2.2 Influence of the ionic strength

The entanglement level of polyelectrolytes depends highly on the ionic strength of the surrounding aqueous solution due to screening of the charges.[277, 278] In pure water, the polymer chains are stretched, which can keep statistically distributed dye molecules far away

from each other. The absorption spectrum of the Cy5-PAH solution in dependence on the NaCl concentration in the range between 0 and 0.25 M was investigated. No changes in the absorption spectra were observed, which excluded the possibility of through space interactions between the dyes. Hence the dye molecules were obviously bound in close proximity to each other on the PAH chain during the synthesis (Figure 4.30-1). This can be ascribed to the fact that the labelling procedure was performed mainly in aqueous solution that is the preferred medium of dye aggregation.[279, 280]

4.2.2.3 Influence of organic solvent

In order to find out the influence of solvent on the H-aggregates formation, the spectra of the Cy5-PAH were measured in solvent consisted of 75% (v/v) organic solvent DMF and 25% aqueous solution (50 mM borate buffer, pH 8.0). This resulted in an increase of the absorption in the monomer dye region at the cost of the H-aggregate band. Simultaneously, the fluorescence intensity increased by almost three times (Figure 4.32).

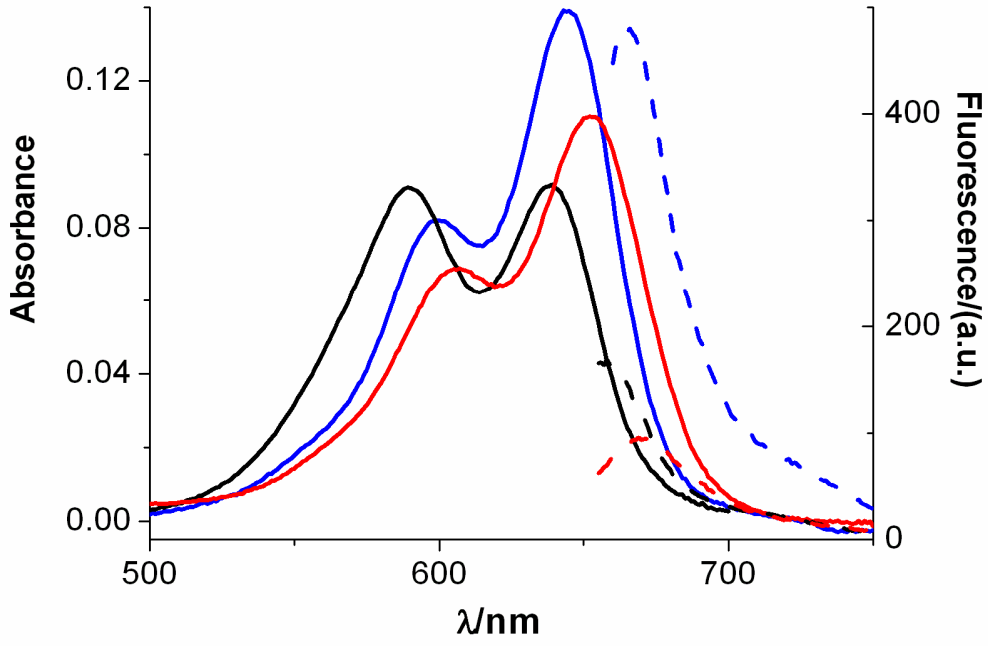

Figure 4.32 Absorption (solid lines) and fluorescence spectra (dashed lines) of Cy5-PAH (1:840) in various solvent: DMF (25% water) (blue lines), H_2O (black lines) and PSS solution (C_{PSS} = 5 mg/ml, monomer ratio between PAH and PSS was 1:12) (red lines). The fluorescence spectra are taken with λ_{ex} = 638 nm and a slit width of 5/10 nm.

4.2.2.4 Influence of the formation of complex with oppositely charged polyelectrolytes

It was also observed that the interactions between Cy5-PAH and PSS yielded a strong decrease of absorption near 588 nm, showing the disappearance of the H-aggregate (Figure 4.32). However the fluorescence intensity decreased as well. This can be explained by the formation of insoluble polyelectrolyte complexes, leading to an increase of dye density and strong self-quenching. Furthermore, a bathochromic shift of absorption energy of the monomer dye molecules was observed, caused by the negative charges of the surrounding PSS molecules (Table 4.3). The same effect was also found on two sulfonate groups modified Cy5. This shift by negative charges was not related to the aggregation phenomena.

Table 4.3 Shift of the main absorption peak, λ_{abs} of Cy5 in different environments.

	λ_{abs} in water	λ_{abs} in DMF	λ_{abs} in PSS solution
Cy5	638	644	648
Cy5-PAH	638	644	652
disulfo-Cy5-PAH	644	650	655

The spectral changes of Cy5-PAH pointed to the conclusion that the dye molecules were non-statistically attached on the PAH chain. It could be caused by the high dye concentration during the labelling procedure in the aqueous environment, leading to formation of H-aggregates well before the covalent attachment on PAH.

4.2.3 Reduction of H-aggregates in Cy5-PAH

In order to minimize the formation of H-aggregates on the PAH chain, attempts were made to reduce the interactions between the Cy5 molecules during the labelling reaction by addition of different organic solvents such as methanol, acetone, DMSO and DMF. The reaction in DMF yielded Cy5-PAH with remarkable lower amount of H-aggregates and a high label degree of 1:230. Figure 4.33 shows that the H-aggregate peak of Cy5-PAH synthesized mainly in DMF (PAHCy5 II) was much smaller compared to that of Cy5-PAH synthesized mainly in aqueous solution. Furthermore, the fluorescence quantum yield was significantly improved for PAHCy5 II. However, the fluorescence quantum yield of the free dye was still 20% higher compared to the immobillised ones in Cy5-PAH II.

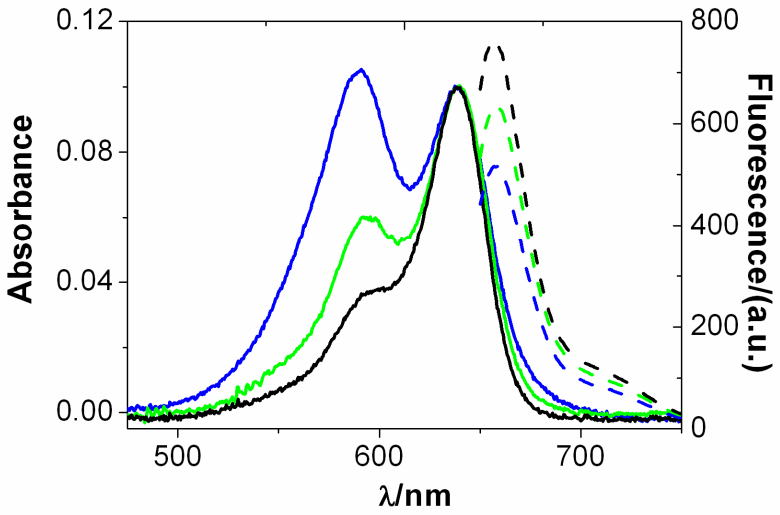

Figure 4.33 Absorption (solid lines) and fluorescence spectra (dashed lines) of Cy5-PAH (blue), Cy5-PAH II (green) and Cy5 free dye (black) measured in aqueous solution. The fluorescence spectra are taken with λ_{ex} = 638 nm and slit widths of 5/5 nm.

For the labelling of biological molecules, Cy5 functionalised with two additional sulfonate groups is often used to increase the solubility in water (disulfo-Cy5). Hence, hydrophobic interactions supporting the formation of dye aggregates were reduced. Disulfo-Cy5 was also used for the labelling procedure in aqueous solution. The formation of H-aggregate was less pronounced compared to the Cy5 without sulfonate groups (Figure 4.34). However, the H-aggregates were still present and it also increased with dye label density.

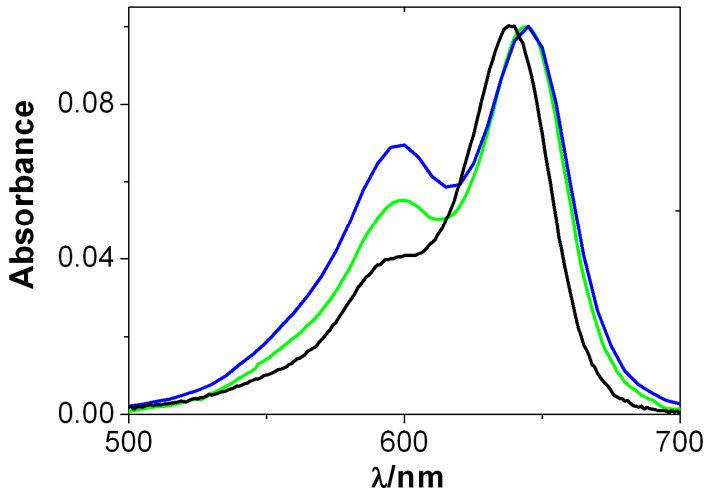

Figure 4.34 Absorption spectra measured from disulfo-Cy5-PAH with label degrees 1: 500 (green line), 1:320 (blue line) and the free dye Cy5 (black line).

4.2.4 Discussion

4.2.3.1 Mechanism of H-aggregates formation and its minimisation

The formation of H-aggregates can be explained by the Kasha-theory and the Davydov-splitting (Figure 4.35).[276, 281, 282] The hypsochromic absorption shift was caused by the transition dipole interactions between two or more chromophores arranged parallel to each other with almost no slip to each other.[10] The interactions between two transition dipoles M1 and M2 yield an energetic splitting of the excited state in two components m_+ and m_-. In the case of parallel alignment of dye molecules, the absorption and emission from one energy level is forbidden because the resulting transition moment $m_- = M1 - M2 = 0$. Only the state $m_+ = M1 + M2$ can be populated. In H-aggregates the allowed m_+ state has a higher energy than the m_- state and the monomer, leading to the observed hypsochromic shift of the absorption energy with respect to the monomer. This state shows no fluorescence due to fast internal conversion process to the non-emitting m_- state, in which the radiative decay is forbidden. In agreement with this, the Cy5 H-aggregates showed no fluorescence.

The two absorption bands for the Cy5-PAH could be caused by a slightly inclined orientation of dye molecules to each other like in a herringbone aggregate. Then, both transitions were permitted and can be observed as Davydov-components at different wavelengths. The intensity ratio between the peaks depends on the angle between the molecule axes (transition dipoles), which caused the observed shoulder at 642 nm.

The difference between the spectrum of Cy5/PSS and Cy5-PAH can be explained firstly by the high 1:1 ratio of dye molecules to monomer units in the dye-polymer complex Cy5/PSS, and secondly by the less spatial constraints of dye molecules in Cy5/PSS compared to the covalently linked Cy5-PAH. The concentration of the dye molecules adsorbed on PSS was more than 600 times higher, resulting in the almost complete vanishing of the monomer absorption and the fluorescence. The dye molecules were obviously all in parallel alignment i.e. the long wavelength absorption was not present. In contrast, the large constraints of covalently linked Cy5 on Cy5-PAH and the lower dye concentration resulted in a relatively high content of non-aggregated dye molecules. The aggregates consist of inclined molecules, producing the shoulder around 640 nm as second Davydov-component.[276]

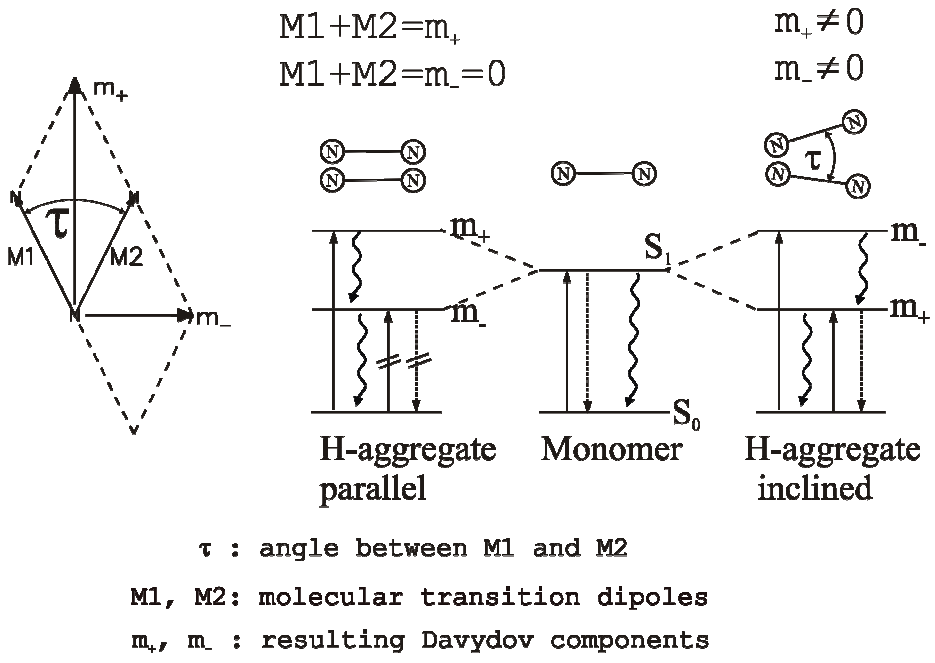

Figure 4.35 Left: scheme of Davydov splitting; Right: model of molecule orientation and transition dipole interactions in dye H-aggregates and their absorption and fluorescence properties. The dumbbells model the dye molecules; solid arrows, broken arrows and wavy arrows show the absorption, the fluorescence and the internal conversion, respectively; Crossed lines are forbidden transitions.

The decrease of the H-band by complexation between Cy5-PAH and a polyanion and by transfer the polymer to organic solvents confirmed the inhomogeneous distribution of the dye molecules on the PAH chain. This is because complexation as well as organic solvent can change the conformation of the polymer and probably destruct the dye aggregates.[283] Based on these findings, the preparation of Cy5-PAH in high content of organic solvent instead of aqueous solution reduced the formation of H-aggregates, resulted in higher label degree and led to a remarkably increased fluorescence quantum yield.

The findings concerning the photophysics of the cyanine dyes on macromolecules can contribute to the establishment of an improved protocol for the nucleic acid sensor preparation based on the LbL-ODN system and the Cy3-Cy5 FRET pair. However, due to the limited time frame of the project, further development of LbL-ODN particles based on the Cy3-Cy5 system was not carried out.

Beyond this, the fundamental aspects of cyanine dye labelled macromolecules, including proteins or DNA/RNA, are of general importance for all fluorescence based analytical techniques such as fluorescence correlation spectroscopy (FCS),[284, 285] single molecule spectroscopy (SMS),[286] CLSM,[287] FRET, fluorescence recovery after photobleaching

(FRAP)[288] or time resolved spectroscopic methods.[289, 290] It should be noted that cyanine dyes are the mostly used fluorescent dyes in fundamental research as well as in applications especially for diagnostics.

4.3 Interaction of the LbL films with cationic surfactants

For the hybridisation between the probe ODN and the ssDNA, high salt concentration, heat and also surfactants are applied. The presence of certain sufactants can prevent hydrophobic interactions to non-target molecules. It is important that the LbL-ODN particles remain stable under these conditions. It is well known that the structure of the polyelectrolyte multilayer films can be influenced by environmental parameters such as pH, ionic strength, solvent, and temperature.[84-118] The structural changes are associated with the film properties such as layer density, permeability and morphology, which might lead to swelling or shrinking of polyelectrolyte films. It is also known that charged surfactants can interact with oppositely charged polyelectrolytes under formation of complexes.[46] Recently, two research groups reported that surfactants such as SDS can also induce changes in the LbL film morphology.[262, 291] The influence of negatively charged surfactants SDS could not be confirmed in our work, but it was found that cationic surfactants induced a much faster and stronger response even at low concentrations. In this section, the influences of cationic surfactants on the LbL films are studied in depths.

Freestanding LbL films without solid support represent a flexible system for investigation because they respond to the environmental changes in 3 dimensions. Such LbL films can be prepared as hollow polyelectrolyte microcapsules by dissolving the template core of the LbL particles. Four types of microcapsules consisted of different polyelectrolyte combinations were prepared to obtain a deeper insight into the interactions between the cationic surfactants and the LbL films.

4.3.1 Preparation of polyelectrolyte capsules

Microcapsules consisted of 4 double layers of (PAH/PSS), (PVA/PSS), (PDA/PSS) and (PAH/PMAA) were prepared on 4.3 µm negatively charged silica templates. To enable visibility for investigation of the changes in the capsules wall structure, the 3rd and 5th polycation layers of the LbL film were labelled with Rho unless specified otherwise.

4.3.2 $(PAH/PSS)_4$ capsules and surfactant DoTAB

4.3.2.1 Interactions between $(PAH/PSS)_4$ capsules and DoTAB

Firstly, the interaction between the cationic surfactant DoTAB and $(PAH/PSS)_4$ capsules was investigated. Addition of 100 mM DoTAB solution in a 1:1 volume ratio to the capsule suspension induced a fast swelling of the capsules in a few seconds (Figure 4.36). The capsules swelled continuously until the diameter increased approximately by a factor of 1.5. At the same time, an increase in the fluorescence intensity of the capsules was observed. Also, the capsules were found to be filled with fluorescent polyelectrolyte (Figure 4.36 b).

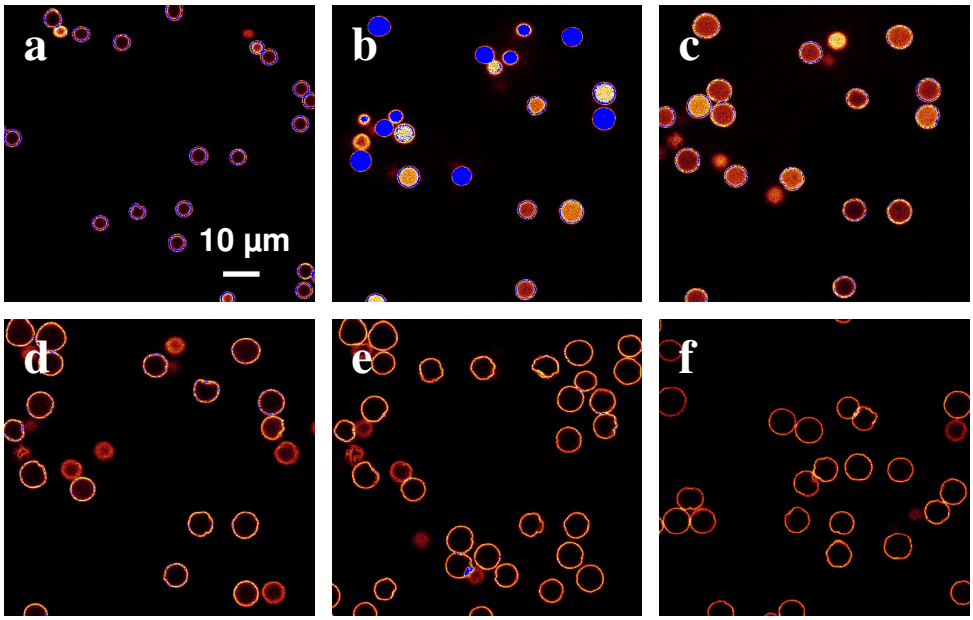

Figure 4.36 CLSM micrographs of $(PAH/PSS)_4$ capsules in 50 mM DoTAB (pH 7.0) with incubation time 0s (a), 30s (b), 60s (c), 120s (d), 600s (e) and 4 days (f). (PMV=750; the blue colour represents very high fluorescence intensity.)

Some PAH-Rho molecules diffused out of the polyelectrolyte film into the interior and also to the exterior of the capsules; the fluorescent polymers in the exterior can not be detected by CLSM due to fast dilution. Thereafter, with continuous increase in the diameter of the capsules, the fluorescence intensity of the capsules slowly decreased until the maximal swelling was reached. The resulting swollen capsules remained spherical and stable up to weeks. This process induced a strong increase in the fluorescence intensity of the capsule suspension by a factor above four as measured by fluorometry (Figure 4.37). This 'turning-on' signal was used for studying the kinetics of the swelling process. It showed that the capsules were swollen approximately from 4 µm to 6 µm in a short time of 60 seconds.

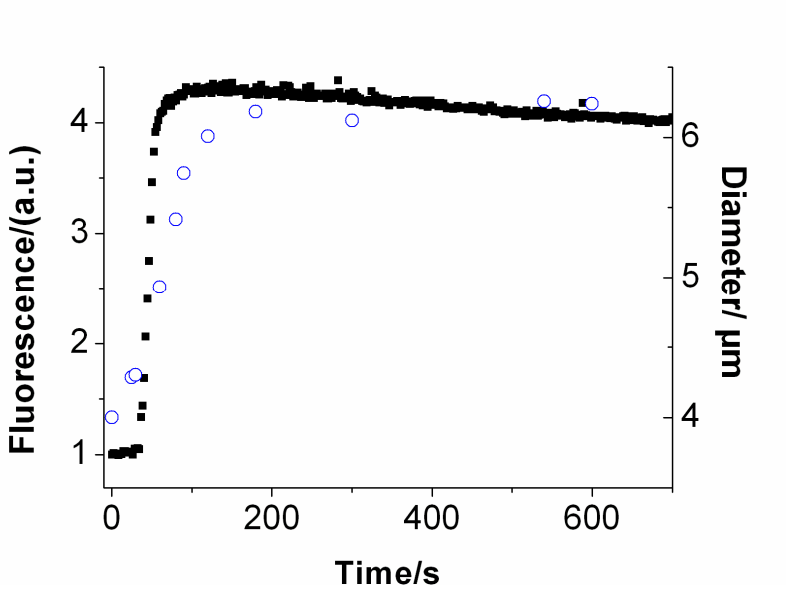

Figure 4.37 Kinetic response of $(PAH/PSS)_4$ capsules to 50 mM DoTAB by fluorescence intensity of the suspension (black squares, left axis) and by diameter of individual capsules (blue circles, right axis, 8 capsules were meausured by CLSM for each point).

4.3.2.2 Influence of the capsule surface charge

It was expected that the interaction with the cationic surfactants was mainly caused by adsorption to the negatively charged surface of the capsules. Therefore, the experiments were repeated after assembling an additional cationic layer of PAH to the capsules. Surprisingly, both the kinetics and the swelling behaviour were almost identical to the negatively charged capsules.

4.3.2.3 Interaction between DoTAB and the outermost polyelectrolyte layer

The outermost polyelectrolyte layer of the capsules is highly charged and it reacts as the first part with environmental changes. Hence, the interaction between this layer and the surfactants can be different from the internal layers. In order to study the influence of the surfactant to the outermost layer of the capsules, PSS-Rho was used as the outermost and only fluorescent layer for preparation of $(PAH/PSS)_4$ capsules. It was observed by CLSM that after addition of 50 mM DoTAB, the capsules were swollen and became non-fluorescent. The outermost PSS layer was completely desorbed from the capsule. In a second experiment, the influence to the PAH layer underneath was studied using PAH-Rho as the only fluorescent layer (the 7^{th} layer). The CLSM images show that the fluorescence intensity was significantly reduced after addition of DoTAB to the capsules. However, the fluorescent layer partially remained in the shell (Figure 4.38 a, b).

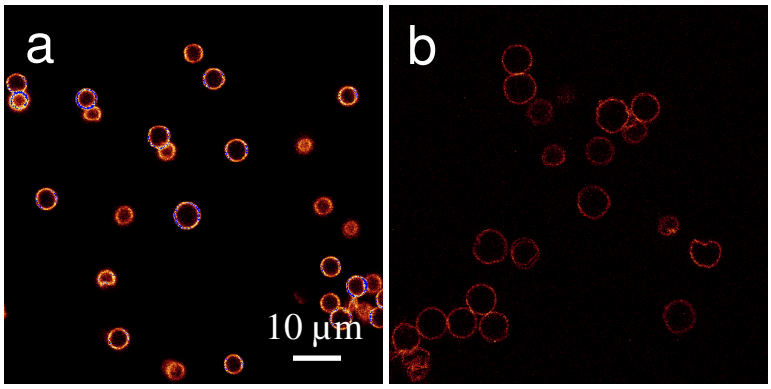

Figure 4.38 CLSM micrographs of $(PAH/PSS)_4$ capsules in a) water (pH 7.0) and b) in 50 mM DoTAB (pH 7.0) after 300s. The 7th layer of the LbL film was labelled with TRITC. (PMV= 850)

4.3.2.4 Permeability changes of the $(PAH/PSS)_4$ capsules

Controlled release of the encapsulated materials is of high interest for pharmaceutical and biomedical applications. The release behaviour of the microcapsules is mainly determined by the permeability of the capsule wall. The influence of the surfactant to the permeability of the capsules was investigated in a solution of 1 mg/ml FITC-dextran (150 kDa). After incubation for 30 min, the confocal images show that the dextran did not enter the interior of the capsules (Figure 4.39 a). After addition of the DoTAB solution, the capsules swelled and the permeability of the capsules increased. Thus, the FITC-dextran entered the capsules within 30s (Figure 4.39 b, c).

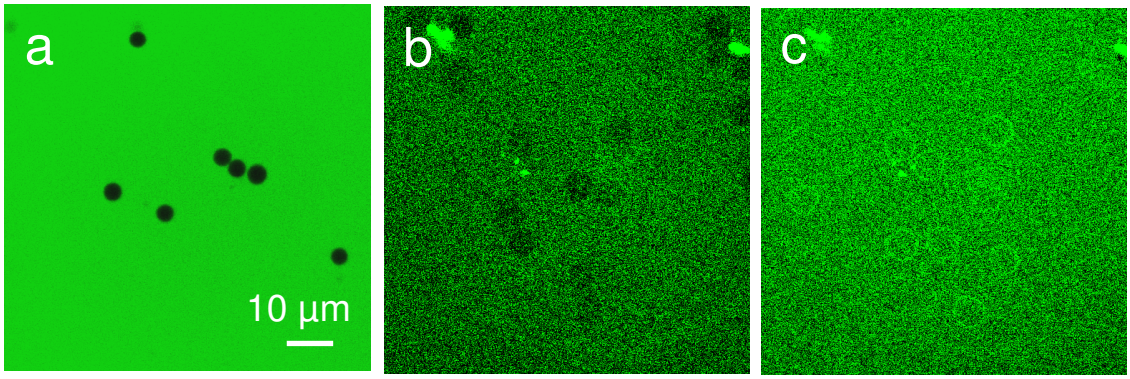

Figure 4.39 CLSM micrographs of $(PAH/PSS)_4$ capsules in 1 mg/ml FITC-dextran solution in the presence of 50 mM DoTAB (pH 7.0) with incubation time 0s (a), 30s (b), and 600s (c). PMV= 750 for (a) and 800 for (b) and (c).

4.3.2.5 Stabilisation of the capsule wall by crosslinking

In order to make the LbL capsules resistant against the decomposing influence by the surfactant DoTAB, the PAH layers were crosslinked by glutaraldehyde either after each Rho-PAH layer or only at the end of the complete LbL film assembly. The fluorescence intensities of the crosslinked $(PAH/PSS)_4$ multilayers after incubation for 15 min in DoTAB solution at different concentrations are shown in Figure 4.40 a. As described earlier, the capsules without crosslinking showed a more than 4-fold increase in fluorescence intensity. In contrast, the fluorescence remained constant when the capsules were crosslinked after each deposited PAH layer. When the crosslinking was performed only once after the final layer of the LbL film was assembled, the fluorescence increased intermediately by a factor of 1.6. The strongly crosslinked capsules remained the same size and impermeable to FITC-dextran (150 kDa) after addition of DoTAB (Figure 4.40 b).

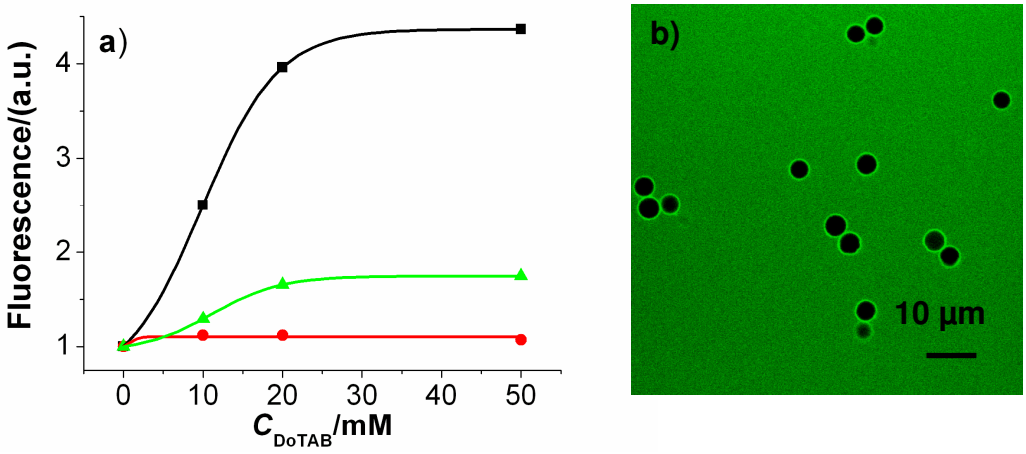

Figure 4.40 a) Fluorescence intensity of $(PAH/PSS)_4$ capsules after 15 min incubation in DoTAB solution at different concentrations. The capsules without crosslinking in the LbL film are shown as black squares; the capsules crosslinked after the 8 layers are shown as green triangles; the capsules crosslinked at each PAH layers are shown as red circles; the lines are fitted for visual guidance. b) CLSM image of the capsules crosslinked at each PAH layer, after 15 min incubation in 50 mM DoTAB and 1 mg/ml FITC-dextran (PMV= 800).

4.3.3 Other polyelectrolyte capsules and DoTAB

4.3.3.1 Interaction between other polyelectrolyte combinations and DoTAB

Microcapsules consisted of other polyelectrolyte pairs were also incubated in 50 mM DoTAB and the kinetic of changes in fluorescence intensity was studied (Figure 4.41). The

most substantial changes were observed for $(PAH/PSS)_4$ and $(PVA/PSS)_4$ capsules, while $(PDA/PSS)_4$ and $(PAH/PMAA)_4$ exhibited negligible changes.

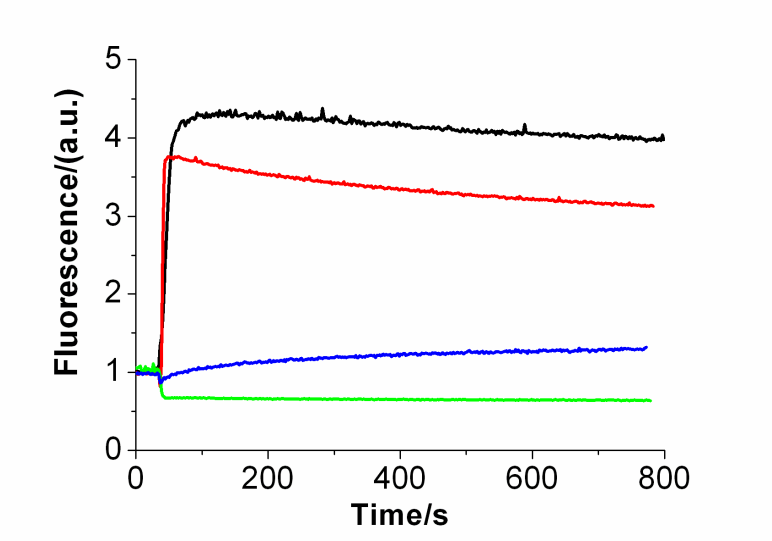

Figure 4.41 Kinetic of fluorescence changes of $(PAH/PSS)_4$ (black line), $(PVA/PSS)_4$ (red line), $(PDA/PSS)_4$ (green line) and $(PAH/PMAA)_4$ (blue line) capsules in the presence of 50 mM DoTAB measured by the fluorescence spectrometry.

The investigation by CLSM showed remarkable differences for all capsules. For $(PVA/PSS)_4$ capsules, the fastest swelling took place, which was consistent with the fluorescence data. The diameter of the capsules increased drastically from 4 µm to above 7 µm within 1 min. The capsules became highly instable and collapsed after 5 min (Figure 4.42, Figure 4.43).

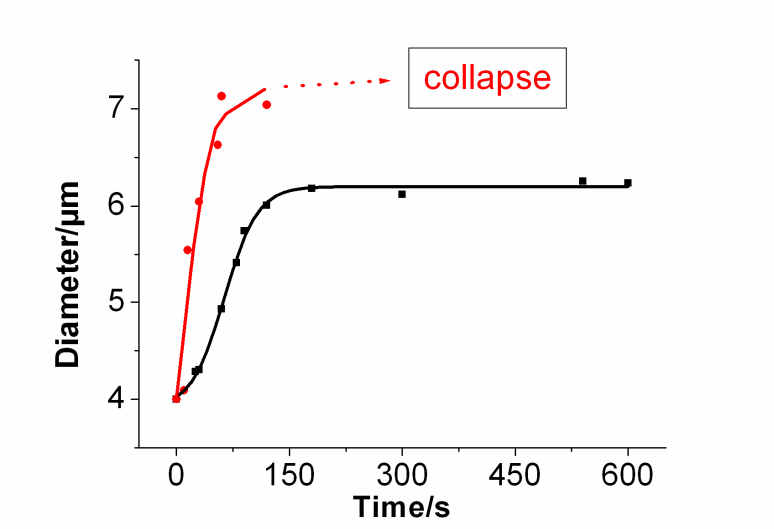

Figure 4.42 Changes of capsules diameter in the presence of 50 mM DoTAB. Measurement on $(PAH/PSS)_4$ capsules are presented as black squares and $(PVA/PSS)_4$ ones as red circles. The lines are fitted for visual guidance.

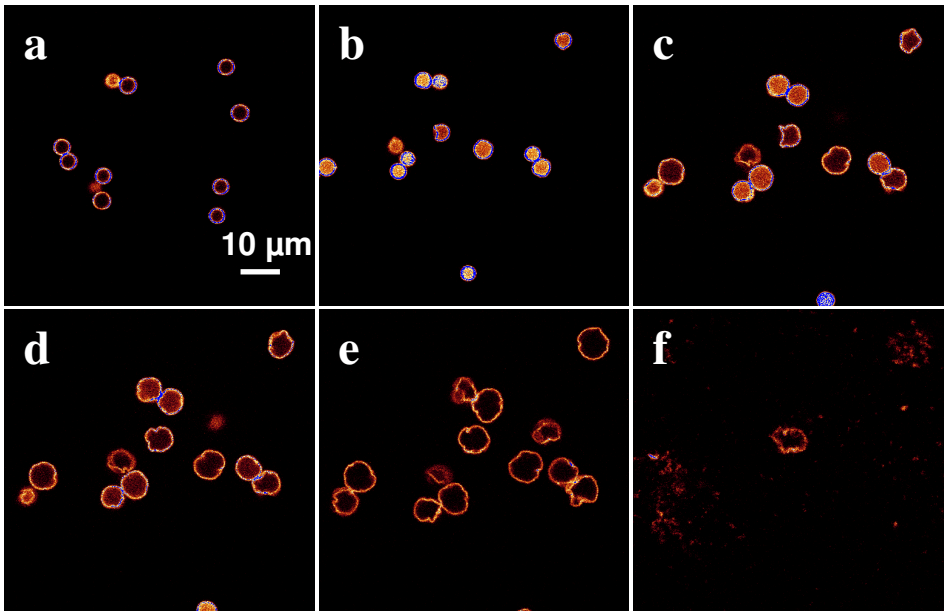

Figure 4.43 CLSM images of $(PVA/PSS)_4$ capsules in presence of 50 mM DoTAB a) 0s, b) 10s, c) 15s, d) 30s, e) 60s, f) 300s. (PMV=850).

For $(PAH/PMAA)_4$ capsules, slight deformation was observed instead of swelling. After addition of DoTAB, they were partially deformed into a 'boat' shape and remained stable in this form (Figure 4.44).

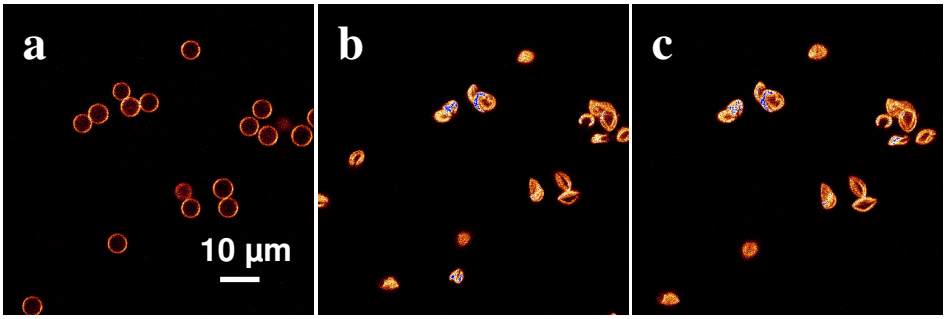

Figure 4.44 CLSM images of $(PAH/PMAA)_4$ capsules in the presence of 50 mM DoTAB at a) 0s, b) 30s and c) 600s. (PMV=1000).

The $(PDA/PSS)_4$ capsules dissolved instantaneously after addition of DoTAB; therefore no CLSM images could be obtained to follow the process.

4.3.3.2 Dependence on the DoTAB concentration

The changes in fluorescence intensity of the LbL film associated with structural changes were investigated as a function of the DoTAB concentration. DoTAB of different concentrations were added to the four types of capsules; then the fluorescence intensities were measured after 15 min (Figure 4.45). Below 5 mM DoTAB, all capsules showed

negligible changes in fluorescence intensity. Between 5 mM and 20 mM the fluorescence of all capsules except $(PDA/PSS)_4$ strongly increased, whereas it became almost independent to the concentrations above 20 mM.

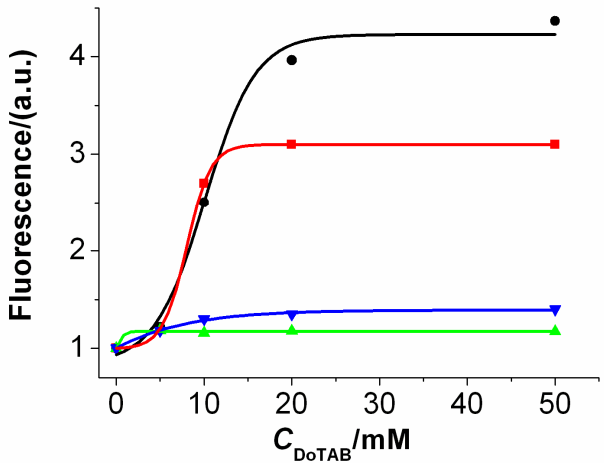

Figure 4.45 Dependence of fluorescence intensity of the capsule suspension on DoTAB concentration. Black circles represent data for $(PAH/PSS)_4$, red squares for $(PVA/PSS)_4$, green triangles for $(PDA/PSS)_4$ and blue triangles for $(PAH/PMAA)_4$ capsules. The lines are fitted for visual guidance.

The dependence of swelling of the capsules on the DoTAB concentration was also studied by CLSM. The diameter of the capsules remained almost unchanged at 5 mM DoTAB, while it increased drastically when they were dispersed in 13 mM and 25 mM DoTAB solution. Initially, the swelling was faster at higher DoTAB concentration. However, it reached similar steady state after 60 s (Figure 4.46).

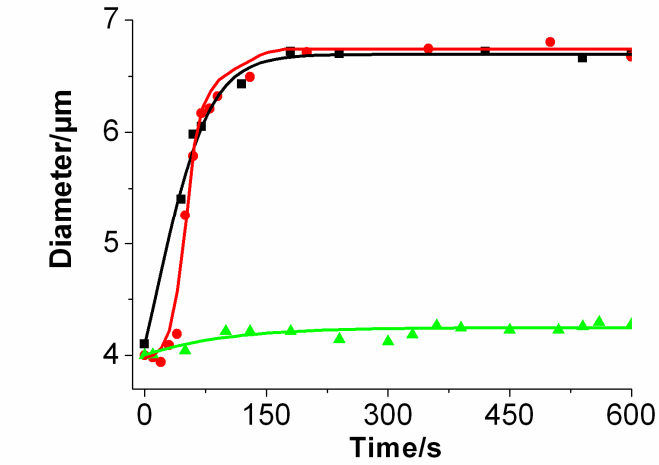

Figure 4.46 Changes in the diameter of $(PAH/PSS)_4$ capsules in the presence of DoTAB at different concentrations: 5 mM (green triangles), 13 mM (red circles) and 25 mM (black squares). The lines are fitted for visual guidance.

4.3.3.3 Interaction of surfactants with the polyelectrolytes

Experiments showed that no interaction was found between the cationic surfactant DoTAB and the polycations Rho-PVA and Rho-PAH in a 1:1 charge ratio in solution. On the contrary, precipitation of complexes between DoTAB and the polyanions PSS or PMAA was observed, while the precipitation was less in the case of PMAA.

4.3.3.4 Stability of polyelectrolyte complexes against DoTAB

In order to compare the stability of complexes Rho-PAH/PSS, Rho-PDA/PSS and Rho-PAH/PMAA with the DoTAB/polyanion complex, polyelectrolyte complexes were prepared in a 1:1 charge ratio. The polyelectrolyte complexes were washed with water until the supernatant was colourless. Thereafter they were incubated in 50 mM DoTAB solution overnight under shaking. The suspension was centrifuged to separate the precipitates and the supernatant. The colour of the precipitates and the supernatant was visually analysed (Table 4.4).

Table 4.4 Colour of the supernatant and precipitates of the polyelectrolyte complexes after treatment with 50 mM DoTAB.

polyelectrolyte complex	colour of precipitates	colour of supernatant
Rho-PDA/PSS	almost colourless	strong red
Rho-PAH/PSS	red (weaker than before)	red
Rho-PAH/PMAA	red (same as before)	almost colourless

The results showed that DoTAB substituted the polycations in different extents. This revealed that the DoTAB/PSS complex was more stable than Rho-PDA/PSS because the PDA was completely removed. A similar behaviour was observed for the Rho-PAH/PSS complex, although there was still Rho-PAH present in the precipitate, pointing to stronger interactions between PAH and PSS than that of PDA/PSS. In contrast, the Rho-PAH/PMAA was more stable than DoTAB/PMAA, because there was no release of the PAH-Rho in the supernatant.

4.3.4 Interaction between $(PAH/PSS)_4$ capsules and other cationic surfactants

The influence of other cationic surfactants on $(PAH/PSS)_4$ capsules was also investigated with CeTAB and BAC (see Figure 3.1). Compared to DoTAB, CeTAB has a larger

hydrophobic part that is bended and more bulky due to a cis-double bond in the alkyl chain. Its *cmc* is approximately 10 times lower than that of DoTAB. The CeTAB treatment caused swelling of the capsules and the increase in fluorescence intensity at a lower concentration below 1 mM (Figure 4.47 a). Although the swelling was initially slower when compared to DoTAB, the diameter of the capsules finally reached nearly 1.8 times the original ones (Figure 4.47 b). The fluorescence intensity of the capsule suspension increased strongly in a small range of CeTAB concentration between 0.5 mM -1.0 mM after incubation for 15 min. Below and above this range the fluorescence was independent on the CeTAB concentrations (Figure 4.47 a).

The cationic surfactant BAC is widely used in pharmaceutical applications as preservatives. It has mixed even-numbered alkyl chain lengths from 8 to 18. BAC caused changes in the diameter of the $(PAH/PSS)_4$ capsules in a remarkably different way compared to other cationic surfactants (Figure 4.47 b). Addition of 5 mM BAC to the capsules also caused initial swelling of the capsules in the first few minutes, thereafter they started to shrink slowly to around half of their original diameter. The shape of the capsules was similar as the (PAH/PMAA) capsules in the presence of DoTAB (see Figure 4.44 c).

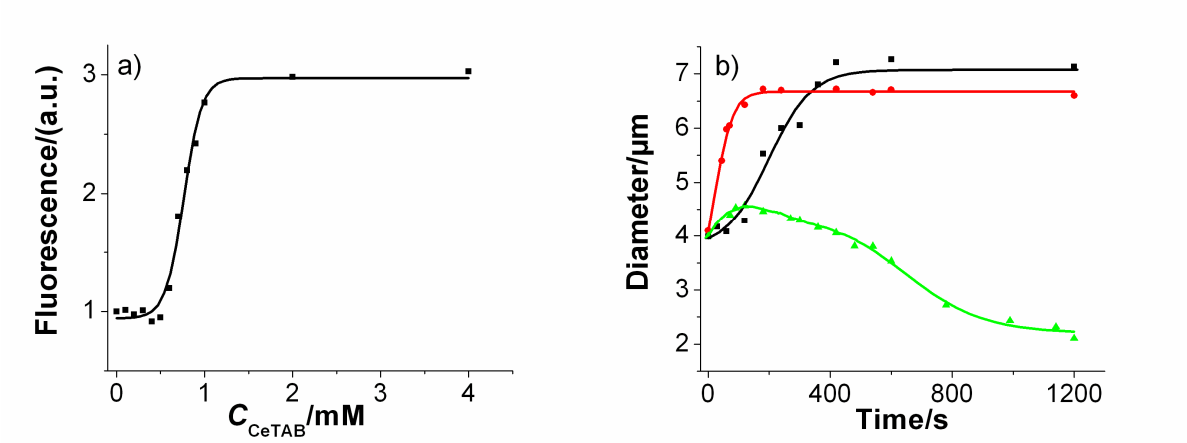

Figure 4.47 a) Fluorescence intensity of a suspension of $(PAH/PSS)_4$ capsules in dependence on the CeTAB concentration (black squares); b) Kinetic change of capsule diameter $(PAH/PSS)_4$ in the presence of 25 mM DoTAB (red circles), 1 mM CeTAB (black squares) and 5 mM BAC (green triangles), respectively. The lines are fitted for visual guidance.

4.3.5 Discussion

4.3.5.1 Mechanism of capsule swelling by cationic surfactant

Based on the experimental results, a schematic presentation of the responsive behaviours of different polyelectrolyte microcapsules upon interaction with the cationic surfactant DoTAB is drawn (Figure 4.48).

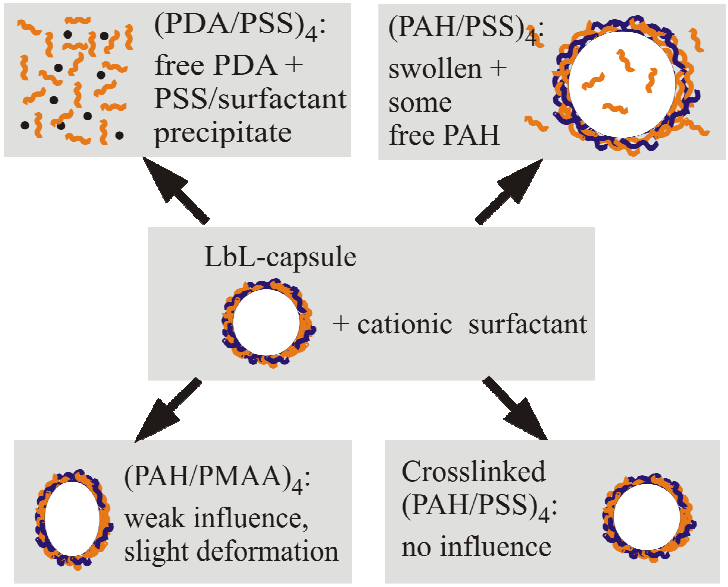

Figure 4.48 Schematic representation of response of different polyelectrolyte capsules upon addition of cationic surfactant DoTAB.

The mechanism explaining the reaction is firstly proposed for the mostly investigated (PAH/PSS) and (PVA/PSS) capsules (Figure 4.49). The original LbL film of $(PAH/PSS)_4$ is internally in a charge balanced state. After addition of DoTAB, the small surfactant molecules diffuse into the film and complex the PSS partially by electrostatic and hydrophobic forces. The partial substitution from the PAH-PSS ionic bonds to PSS-surfactant ionic bonds leads to an excess of positive charges and a high concentration of chloride counterions in the film due to the electroneutrality. This creates a high osmotic pressure leading to the swelling of the wall. The outermost PSS layer with a high negative charge is completely complexed with the surfactant and removed from the capsule surface, whereas the internal layers of the (PAH/PSS) remain intact.

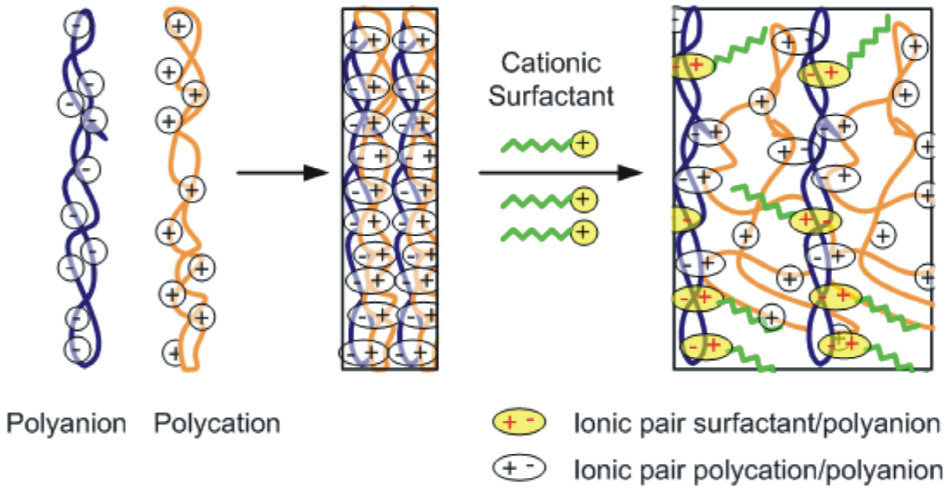

Figure 4.49 Interaction of cationic surfactant DoTAB with the (PAH/PSS) or (PVA/PSS) LbL films.

In contrast to the (PDA/PSS) capsules, of which complete disintegration of the film occurred, the (PAH/PSS) and (PVA/PSS) film remained as spherical capsules. The reason for the higher stability of (PAH/PSS) film could be the additional hydrogen bonding between the sulfonate groups of PSS and the primary amine groups, which is not possible with the quaternary amine groups of PDA due to the missing free electron pair. Despite the hydrogen bonding in (PAH/PSS) capsules, some polycation molecules were also released from the wall, which could be detected initially inside the capsules due to their high concentration compared to the released molecules outside. Due to the increased permeability of the swollen capsules, the polycations in the capsule interior also diffused out within a few minutes (see Figure 4.36 and Figure 4.43). Furthermore, the outermost PSS layer was removed by formation of insoluble PSS-surfactant complexes as also observed for (PDA/PSS). A comparable swelling effect is known from multilayer films composed of weak polyelectrolytes, when free charges are created by a shift of the pH value.[89] However, in contrast to the reversible protonation/deprotonation effect, which relies on the use of weak polyacids or polybases, the interaction between the LbL film and the surfactants is irreversible and is determined by the ratio of the complex stability between the polyanion/polycation and the polyanion/cationic surfactant.

Only for PMAA as the polyanion, the capsules were mainly intact because the stability of DoTAB/PMAA was smaller than that of (PAH/PMAA). The difference between PSS and PMAA in terms of the interaction with cationic surfactants mainly lies in the different

hydrophobicity and the high tendency of hydrogen bonding between PMAA and primary or secondary amines. In contrast to the hydrophilic PMAA, PSS has a hydrophobic backbone due to the phenyl rings, which play an important role for the formation of complexes with the surfactants.[45, 52]

Moya *et al.* have employed the low stability of the (PDA/PSS) film as a protective layer for (PAH/PSS) layers underneath to cationic surfactants.[262] They claimed that the (PAH/PSS) layers were not influenced by the surfactant, which was not confirmed by our experiments. However, the changes in swelling and permeability are difficult to analyse on thin and supported LbL films used by Moya *et al*. The recently published work from Rahim *et al.* on surfactant-LbL-film interactions presented different results.[291] In contrast to the response within seconds observed by us, they investigated the films in the hour and day scale and observed much smaller changes. The reason could be that their detection method was based on the spectroscopic determination of released PSS in the supernatant. At least for cationic surfactants their method is not applicable, because the formation of insoluble PSS/surfactant complexes prevents the detection of released PSS, which can result in wrong conclusions.

4.3.5.2 Fluorescence intensity changes of the LbL film

The strong changes in fluorescence intensity of the multilayer films arise from transition dipole interactions between the dye molecules. If identical dye molecules are assembled in close distance within the Förster radius, self-quenching of the fluorescence can occur. (PAH/PSS) films contain in aqueous environment approximately 30% water and 70% polymer.[36] For a label degree of 1: 100, the average distance between the dye molecules on Rho-PAH in a completely interpenetrated (PAH/PSS) film is calculated to be 2.3 nm. Assuming that the dye molecules are preferentially located in the PAH layer, the distance is even smaller to less than 1 nm. In both cases the distance between the dye molecules is remarkably below the Förster radius, leading to strong self-quenching of the dyes.

The three dimensional swelling of the polyelectrolyte film after addition of surfactants led to an increase of the average distance between the dye molecules and to an increase in the fluorescence intensity. In addition, the released free Rho-PAH molecules also contributed to the increase in fluorescence of the capsule suspension. However, the constant fluorescence intensity during the complete desintegration of the (PDA-Rho/PSS) can hardly be explained. It could be ascribed to the high persistence length of the PDA polyelectrolyte and the relative low label degree of the dye molecules, which resulted in negligible self-quenching of Rho on PDA.

4.3.5.3 Permeability changes of the capsules and its prevention

The cationic surfactants induced a fast and strong permeability increase of $(PAH/PSS)_4$ and $(PVA/PSS)_4$ capsules at a low concentration, e.g. below 1 mM CeTAB. This can be employed as an instantaneously triggered release of encapsulated compounds. However, for some applications e.g. encapsulation of drugs, it is important to control or prevent this sensitivity to cationic surfactants. The LbL films could be stabilised by crosslinking of the polyelectrolyte layers. As demonstrated on the crosslinked $(PAH/PSS)_4$ capsules, fluorescence changes and wall opening for macromolecules permeation was effectively prevented after crosslinking. The grade of crosslinking can be controlled, which enables a fine tuning of the LbL film response to the surfactant.

4.3.5.4 Influence of the surfactant concentration

There was a threshold concentration of DoTAB (around 5 mM) and CeTAB (around 0.5 mM) for an effective interaction between the surfactant and the microcapsules (see Figure 4.45 and Figure 4.47 a). In the concentration range of 5-20 mM for DoTAB and 0.5-2 mM for CeTAB, strong increase of the interactions was observed. No further effect was observed at higher surfactant concentrations. It is well known that surfactant molecules associate at the so called critical micellisation concentration (*cmc*) to large micelles.[43, 44] However, in the presence of oppositely charged polyelectrolytes, the surfactants form small aggregates already at a concentration below the *cmc*, which is referred to as the critical aggregation concentration (*cac*).[39, 48] Obviously, the cationic surfactants start to interact with the multilayer film above its *cac*, and the interaction increases at the surfactant concentration range between the *cac* and *cmc*. Above the *cmc*, which is >15 mM for DoTAB and >0.8 mM for CeTAB,[46, 293] the interactions between the surfactant and the capsules remain almost constant, because the excess free surfactant molecules form micelles that can not enter the multilayer film.

4.3.5.5 Influence of the surfactant structure

The structural changes induced by CeTAB were slower compared to that by DoTAB. However, it yielded similar final state or even more swelling of the capsules (Figure 4.47). The CLSM investigation revealed that the interaction process was almost identical apart from the kinetics. Obviously the longer and bended chain of CeTAB caused a slower diffusion into the LbL film but induced more pronounced structural changes due to higher hydrophobicity.

In contrast, BAC only caused initial swelling of the capsules in the first 2 min; thereafter the capsules shrank to smaller diameters. BAC is a mixture of molecules with different alkyl chain lengths. Therefore the *cmc* of BAC is in a range between 0.34-3.8 mM. The deviation in the capsule behaviour could be caused on one hand by the mixture of different alkyl chain lengths[294] and on the other hand by the additional phenyl rings in BAC, which contribute to further hydrophobic or π–π interactions with the phenyl rings in PSS.

It is important to control the strong influence of BAC for applications of LbL film encapsulated drugs in pharmaceutical or dermatological formulations, because BAC is often used as preservatives. Therefore, one need to ensure that either no such preservatives are present in the formulation or the capsules are stabilised by crosslinking the polyelectrolyte wall as demonstrated so that undesired release of the drugs does not occur prior to use.

5 Conclusions and Outlook

An ODN bioconjugation system based on the LbL film modified microparticles for the detection of DNA hybridisation was developed. Evaluation of multiple parameters including the selection of polyelectrolytes, coupling agent, solvent and activation time enabled stable covalent coupling of probe ODNs onto the particles at high density and with homogeneous distribution. The system exhibited a higher binding capacity to specific target sequences than most of the commercially available particles on the market. Moreover, non-specific interactions with non-complementary DNA were almost completely suppressed.

For detection of the binding events, a FRET-based optical method was employed, where the donor fluorophore was either pre-labelled on the probe ODNs (system 1) or covalently coupled to the polyelectrolyte prior to LbL coating (system 2). The acceptor dye was tagged on the target DNA sequence. In this way, the donor dye molecules were located exclusively on the outermost few nanometers on the particle surface so that the donor-acceptor distance was minimized, which was highly advantageous for FRET detection. Because of the special properties of the LbL films, this LbL-ODN system demonstrated several advantages over other conventional DNA hybridisation assays. The detection limit of the developed LbL-ODN sensing system by conventional fluorometry was 1-5 nM of target ODNs. Moreover, this microparticle-based system allowed analysis of single particles by flow cytometry and CLSM. A single LbL-A_{21} particle could capture 10^{-17} mole of T_{20} ODNs. When 1% target molecule is captured, as little as 10^{-19} mole target ODNs can be detected. This detection limit is superior compared to the hybridisation assays on the market.

The LbL-ODN particles were also successfully applied in single-nucleotide polymorphism (SNP) detection as a mutation assay. A single mismatch in a 25-mer target ssDNA could be distinguished by the FRET method. The sensitivity is comparable other established SNP assays.

The LbL-ODN particles could be recycled several times by melting/washing cycles, although the efficiency of the hybridisation decreased for every cycle. Hence, use of fresh LbL-ODN particles for diagnostic applications is highly recommended. However, for other applications such as specific DNA extraction from a mixture, subsequent reuse of the LbL-ODN particles can be applied.

Beside the promising application of the LbL-ODN particles for nucleic acid sensing, it was demonstrated that liposomes as nanocontainers modified with complementary ODNs could be assembled onto the LbL-ODN particle surface specifically via DNA hybridisation. The liposomes stayed intact on the particle surface and fused only upon trigger. Such specific assembly of filled containers on planar or colloidal surfaces can be broadly varied and widely applied. Especially in the fast developing field of microfluidic and delivery systems, such structures as specific targeted cargos offer a great potential for exploitation.

The preparation of the LbL-ODN structures on planar surface enabled further investigation of the system by AFM. AFM images showed that the roughness of the LbL surface increased drastically after the probe ODNs were coupled. The roughness increase of the LbL-ODN surface was beneficial to achieve a higher FRET efficiency due to reduced overall distance between the FRET pairs.

The assembly process of the LbL-ODN structure and the specific binding of liposomes were also monitored and investigated by QCM. Multilayers of liposomes were assembled on the planar LbL-ODN surfaces. The amount assembled was determined from the mass gain on the surface by QCM. The obtained data was in a good agreement with the results obtained from the particle based system.

For target binding detection, the FRET pair Flu-Rho was mainly used in this study. Two different systems were constructed: in system 1, the donor dye Flu was on the probe ODN in a 1:1 ratio; and in system 2, the donor was on the outermost PMAA layer and its amount was independent on the amount of probe ODNs. While the donor and acceptor ratio and distance is fixed in system 1, the excess and even distribution of the donor dyes in system 2 resulted in a superior FRET efficiency, benefiting from the higher donor density and the multi-interaction between the donor and acceptor dye molecules. In addition, system 2 can be prepared less expensively, since it is not required to fluorescently label all the ODNs.

In contrast, the alternative and widely applied FRET pair Cy3-Cy5 with lower excitation energy showed opposite results: system 2, using Cy3-PMAA, yielded remarkably less FRET efficiency than system 1, even if a high excess of the donor dye Cy3 was used (label degree of Cy3-PMAA 1: 130). This can be explained as follows: 1. the fluorescence quantum yield of Cy3ODN was higher than that of the free dye and Cy3-PMAA; 2. with increased labelling density of Cy3 on PMAA, the fluorescence quantum yield of Cy3-PMAA decreased further; 3. the Cy3-Cy5 has a shorter Förster radius compared to Flu-Rho, which required a smaller separation distance between the dye pairs in order to obtain sufficient FRET. These factors contributed to the quite different behaviours of the Flu-Rho and Cy3-Cy5 FRET pairs.

The fluorescence quantum yield of cyanine dyes is often reduced after they are covalently coupled to polyelectrolytes. The effect was more pronounced for Cy5, whose conjugate structure is more extended than Cy3. The decrease in the quantum yield arose from the partial formation of dye H-aggregates that showed no fluorescence but a hypsochromic shift of the absorption wavelengths, as described by the Kasha-theory.[276] In order to improve the quantum yield of the dye-labelled materials for analytical methods, the origin of the H-aggregates formation was determined. It was found that the aggregates were formed during the labelling reaction by interactions between dye molecules, leading to an inhomogeneous distribution along the polymer chain. The formation of H-aggregates on the polymer could be remarkably reduced by a newly developed synthetic route in organic solvents. At the same time, this improved synthetic approach produced polymers with higher label degrees. These findings can enable a more efficient use of Cy3-Cy5 as the FRET pair in the LbL-ODN particle system.

A well known drawback in the application of LbL films is their lower stability against certain environmental parameters such as high temperature, salt concentration or pH compared to covalently linked polymers. Under the relatively harsh conditions used for hybridisation (0.5 M salt, 70°C, 0.1% SDS, 1 mg/ml BSA) some polyelectrolyte molecules were released from the particle surface. The 'leaking' was successfully prevented by treatment of the LbL particles with borate buffer (50 mM, pH 8.0, 0.5 M NaCl) at 70 ^{o}C for two hours prior to the coupling process.

During the stability study, it was surprisingly found that certain polyelectrolyte films as microcapsules showed strong changes in diameter and permeability in the presence of low concentrations of cationic surfactants (<5 mM). In dependence on the polyelectrolyte composition, the behaviour of the capsules varied from negligible changes to complete disintegration via strong swelling. For example, $(PAH/PSS)_4$ microcapsules swelled with a five-fold volume increase and became permeable for large molecules. In the case of fluorescently labelled films their fluorescence intensity increased by four times. A mechanism explaining the interactions between the cationic surfactants and polyelectrolyte capsules was derived from the experiments: the cationic surfactants diffused into the LbL film, formed complexes with the polyanion and then replaced the polycation partly or completely. The extent of the interaction depended on the relative stability of the polycation/polyanion complex and the surfactant/polyanion complex. The structural shape of the surfactants and their *cmc* or *cac*, determined the kinetics and the threshold of the interaction due to different diffusion rates inside the LbL film, respectively.

The sensitivity of the LbL films to traces of cationic surfactants can limit their applicability, for example in drug encapsulation for pharmaceutical formulations that often contain cationic detergents such as BAC. In this work it was demonstrated that such undesired changes in the capsule properties can be effectively prevented by crosslinking. On the other hand, the remarkable strong and fast response of polyelectrolyte films to cationic surfactants can be exploited for a range of applications such as triggered and fast release of encapsulated materials, sensor development based on strong fluorescence changes or micromechanical devices like valves.

In summary, the LbL-ODN particles exhibited several advantageous features that recommend them for cost effective and versatile FRET systems for DNA diagnostic. Moreover, several other functions can be introduced into the present system for wider applications such as:

1. Incorporating additional tags such as QDs into the LbL structure to distinguish between different target sequences in library high throughput approaches.
2. Using magnetic particles as the core for fast collection of particles and signal amplifications.
3. Bioconjugation of antibodies or antigens on LbL-FRET particles for diagnostic analysis.
4. Chemi/bioluminescent sensors based on the fusion of adjacent liposomes assembled by selective hybridisation on the LbL-ODN particles, one containing the luminescent substance and the other the biocatalyst.
5. Specific assembly of other ODN modified systems onto the LbL-ODN particles via DNA hybridisation.

6. References

1. M. J. Campolongo, S. J. Tan, J. F. Xu, D. Luo, *Adv. Drug Delivery Rev.* **2010**, *62*, 606-616.
2. P. A. Piunno, U. J. Krull, *Anal. Bioanal. Chem.* **2005**, *381*, 1004-1011.
3. A. Mirkin, *Chem. Rev.* **2005**, *105*, 1547-1562.
4. V. Dugas, G. Depret, Y. Chevalier, X. Nesme, E. Souteyrand, *Sens. Actuators, B* **2004**, *101*, 112-121.
5. C. A. Mirkin, R. L. Letsinger, R. C. Mucic, J. J. Storhoff, *Nature* **1996**, *382*, 607-609.
6. K. Suzuki, K. Hosokawa, M. Maeda, *J. Am. Chem. Soc.* **2009**, *131*, 7518-7519.
7. P. Hazarika, F. Kukolka, C. M. Niemeyer, *Angew. Chem., Int. Ed.* **2006**, *45*, 6827-6830**.**
8. Q. Wang, Y. Liu, Y. Ke, H. Yan, *Angew. Chem., Int. Ed.* **2008**, *47*, 316-319.
9. F. Patolsky, Y. Weizmann, E. Katz, I. Willner, *Angew. Chem., Int. Ed.* **2003**, *42*, 2372-2376.
10. X. Zhou, J. Zhou, *Anal. Chem*. **2004**, *76*, 5302-5312.
11. A. Sassolas, B. D. Leca-Bouvier, L. J. Blum, *Chem. Rev.* **2008**, *108*, 109-139.
12. J. J. Goodings, *Electroanalysis* **2002**, *14*, 1149-1156.
13. J. R. Lakowicz, *Principles of fluorescence spectroscopy*, 3rd ed., Springer, New York, **2006**.
14. R. A. Cardullo, S. Agrawal, C. Flores, P. C. Zamecnik, D. E. Wolf, *Biochemistry* **1988**, *85*, 8790-8794.
15. M. Massey, W. R. Alger, U. J. Krull, *Anal. Chim. Acta* **2006**, *568*, 181-189.
16. T. Tuschl, C. Gohlke, T. M. Jovin, E. Westhof, F. Eckstein, *Science* **1994**, *266*, 785-789.
17. O. Naruhisa, K. Hirano, M. Warashina, A. Andrus, B. Mullah, K. Hatanaka, K. Taira, *Nucleic Acids Res.* **1998**, *26*, 735-743.
18. P. Zhang, T. Beck, W. Tan, *Angew. Chem., Int. Ed.* **2001**, *40*, 402-405.
19. S. Tyagi, F. R. Kramer, *Nat. Biotechnol.* **1996**, *14*, 303-308.
20. B. S. Gaylord, A. J. Heeger, G. C. Bazan, *Proc. Natl. Acad. Sci.* **2002**, *99*, 10954-10957.

21. B. Liu, T. T. T. Dan, G. C. Bazan, *Adv. Funct. Mater.* **2007**, *17*, 2432-2438.
22. L. H. Chen, D. W. McBranch, H. L. Wang, R. Helgeson, F. Wudl, D. G. Whitten, *Proc. Natl. Acad. Sci. USA* **1999**, *96*, 12287-12292.
23. F. Feng, F. He, L. An, S. Wang, Y. Li, D. Zhu, *Adv. Mater.* **2008**, *20*, 2959-2964.
24. W. R. Algar, U. J. Krull, *Anal Bioanal. Chem.* **2008**, *391*, 1609-1618.
25. C. Y. Zhang, L. W. Johnson, *Angew. Chem.* **2007**, *119*, 3552-3555.
26. D. Zhou, L. Ying, X. Hong, E. A. Hall, C. Abell, D. Klenerman, *Langmuir* **2008**, *24*, 1659-1664.
27. C. Y. Zhang, H. C. Yeh, M. T. Kuroki, T. H. Wang, *Nat. Mater.* **2005**, *4*, 826-831.
28. C. S. Wu, J. M. Cupps, X. D. Fan, *Nanotechnol.* **2009**, *20*, 305502-305509.
29. X. G. Peng, M. C. Schlamp, A. V. Kadavanich, A. P. Alivisatos, *J. Am. Chem. Soc.*, **1997**, *119*, 7019-7029.
30. J. J. Li, A. Wang, W. Guo, J. C. Keay, T. D. Mishima, M. B. Johnson, X. Peng, *J. Am. Chem. Soc.*, **2003**, *125*, 12567-12575.
31. H. Dautzenberg, W. Jaeger, J. Kötz, B. Philipp, C. Seidel, D. Stscherbina (Eds.), *Polyelectrolytes: Formation, Characterisation and Application*, Hanser Publishers, Munich, **1994**.
32. S. K. Tripathy, J. Kumar, H. S. Nalwa (Eds.), *Handbook of Polyelectrolytes and Their Application*, American Scientific Publishers, Los Angeles, **2002**.
33. G. Decher, J. D. Hong, *Macromol. Chem. Macromol. Symp.* **1991**, *46*, 321-327.
34. G. Decher, J. D. Hong, J. Schmitt, *Thick Solid Films* **1992**, *210/211*, 831-835.
35. G. Decher, *Science* **1997**, *277*, 1232-1237.
36. G. Decher, J. B. Schlenoff, *Multilayer Thin Films* Wiley-VCH Verlag, Weinheim, **2003**.
37. S. Förster, M. Schmidt, *Adv. Polym. Sci.* **1995**, *120*, 51-133.
38. A. Katchalsky, O. Kunzle, W. Kuhn, *J. Polym. Sci.* **1950**, *5*, 283-300.
39. J. Kötz, S. Kosmella, *Polyelectrolytes and Nanoparticles*, Springer Publishers, Heidelberg, **2007**.
40. V. Kabanov, *Multilayer Thin Films* (Eds.: G. Decher, J. B. Schlenoff), Wiley-VCH Verlag, Weinheim, **2003**.
41. K. N. Bakeev, V. A. Izumrudov, S. I. Kuchanov, A. B. Zezin, V. A. Kabanov, *Macromolecules* **1992**, *25*, 4249-4254.
42. H. Dautzenberg, N. Karibyants, *Macromol. Chem. Phys.* **1999**, *200*, 118-125.
43. S. Zhou, B. Chu, *Adv. Mater.* **2000**, *12*, 545-556.

44. E. D. Goddard, *Colloidal Surfaces* **1986**, *19*, 301-329.
45. O. Anthony, R. Zana, *Langmuir* **1996**, *12*, 1967-1975.
46. D. Langevin, *Adv. Colloid Interface Sci.* **2009**, *147-148*, 170-177.
47. P. S. Chelushkin, E. A. Lysenko, T. K. Bronich, A. Eisenbergh, V. A. Kabanov, *Docklady Phys. Chem.* **2004**, *395*, 72-75.
48. a) P. Hansson, M. Almgren, *Langumir* **1994**, *10*, 2115-2124; b) P. Hansson, M. Almgren, *J. Phys. Chem.* **1995**, *99*, 16694-16703.
49. A. R. Khokhlov, E. Y. Kramarenko, E. E. Makhaeva, S. G. Starodubtzev, *Makromol. Chemie. Theory Simul.* **1992**, *1*, 105-118.
50. J. Liu, N. Takisawa, K. Shirahama, *J. Phys. Chem.* **1997**, *101*, 7520-7523.
51. A. Malovikova, K. Hayakawa, *J. Phys. Chem.* **1984**, *88*, 1930-1933.
52. P. Hansson, M. Almgren, *J. Phys. Chem.* **1996**, *100*, 9038-9046.
53. A. Perico, A. Ciferri, *Chem. Eur. J.* **2009**, *15*, 6312-6320.
54. L. Piculell, J. Norrman, A. V. Svensson, I. Lynch, J. S. Bernards, W. Loh, *Adv. Colloid Interface Sci.* **2009**, *147-148*, 228-236.
55. R. K. IIer, *J. Colloid Interface Sci.* **1966**, *21*, 569-594.
56. Y. Lvov, K. Ariga, I. Ichinose, T. Kunitake, *J. Am. Chem. Soc.* **1995**, *117*, 6117-6123.
57. G. B. Sukhorukov, H. Möhwald, G. Decher, Y. M. Lvov, *Thin Solid Films* **1996**, *285*, 220-223.
58. R. Georgieva, S. Moya, S. Leporatti, B. Neu, H. Bäumler, C. Reichle, E. Donath, H. Möhwald, *Langmuir* **2000**, *16*, 7075-7081.
59. Y. Lvov, H. Haas, G. Decher, H. Möhwald, A. Mikhailov, B. Mtchedlishvily, E. Morgunova, B.Vainshtein, *Langmuir* **1994**, *10*, 4232-4236.
60. A. A. Mamedov, N. A. Kotov, M. Prato, D. M. Guldi, J. P. Wicksted, A. Hirsch, *Nat. Mater.* **2002**, *1*, 190-194.
61. K. Ariga, Y. Lvov, T. Kunitake, *J. Am. Chem. Soc.* **1997**, *119*, 2224-2231.
62. J. F. Quinn, A. P. R. Johnston, G. K. Such, A. N. Zelikin, F. Caruso, *Chem. Soc. Rev.* **2007**, *36*, 707-718.
63. W. B. Stockton, M. F. Rubner, *Macromolecules* **1997**, *30*, 2717-2725.
64. J. Anzai, H. Takeshita, Y. Kobayashi, T. Osa, T. Hoshi, *Anal. Chem.* **1998**, *70*, 811-817.
65. Y. L. Liu, M. L. Bruening, D. E. Bergbreiter, R. M. Crooks, *Angew. Chem., Int. Ed.* **1997**, *36*, 2114–2116.

66. A. P. R. Johnston, E. S. Read, F. Caruso, *Nano Lett.* **2005**, *5*, 953-956.

67. T. Serizawa, K. Nanameki, K. Yamamoto, M. Akashi, *Macromolecules* **2002**, *35*, 2184–2189.

68. G. Ladam, P. Schaad, J. C. Vögel, P. Schaff, G. Decher, F. Cuisinier, *Langmuir* **2000**, *16*, 1249-1255.

69. Ph. Lavalle, C. Gergely, F. J. G. Cuisinier, G. Decher, P. Schaaf, J. C. Voegel and C. Picart, *Macromolecules* **2002**, *35*, 4458-4465.

70. G. B. Sukhorukov, E. Donath, H. Lichtenfeld, E. Knippel, M. Knippel, A. Budde, H. Möhwald, *Colloids Surf., A* **1998**, *137*, 253-266.

71. A. Voigt, H. Lichtenfeld, G. B. Sukhorukov, H. Zastrow, E. Donath, H. Bäumler, H. Möhwald, *Ind. Eng. Chem. Res.* **1999**, *38*, 4037-4043.

72. G. B. Sukhorukov, E. Donath, S. A. Davis, H. Lichtenfeld, F. Caruso, V. I. Popov, H. Möhwald, *Polym. Adv. Technol.* **1998**, *9*, 759-767.

73. E. Donath, G. B. Sukhorukov, F. Caruso, S. A. Davis, H. Möhwald, *Angew. Chem., Int. Ed.* **1998**, *37*, 2202-2205.

74. C. S. Peyratout, L. Dähne, *Angew. Chem., Int. Ed.* **2004**, *43*, 3762-3783.

75. a) C. Y. Gao, S. Moya, H. Lichtenfeld, A. Casoli, H. Fiedler, E. Donath, H. Möhwald, *Macromol. Mater. Eng.* **2001**, *286*, 355-361; b) C. Y. Gao, S. Moya, E. Donath, H. Möhwald, *Macromol. Chem. Phys.* **2002**, *203*, 953-960.

76. C. Déjugnat, G. B. Sukhorukov, *Langmuir* **2004**, *20*, 7265-7269.

77. Y. Itoh, M. Matsusaki, T. Kida, M. Akashi, *Chem. Lett.* **2004**, *33*, 1552-1553.

78. T. Mauser, C. Dejugnat, G. B. Sukhorukov, *Macromol. Rapid Commun.* **2004**, *25*, 1781-1785.

79. K. Köhler, D. G. Shchukin, G. B. Sukhorukov, H. Möhwald, *Macromolecules* **2004**, *37*, 9546-9550.

80. O. Kreft, R. Georgieva, H. Baumler, M. Steup, B. Muller-Rober, G. B. Sukhorukov, H. Möhwald, *Macromol. Rapid Commun.* **2006**, *27*, 435-440.

81. N. G. Balabushevitch, G. B. Sukhorukov, N. A. Moroz, D. V. Volodkin, N. I. Larionova, E. Donath, H. Möhwald, *Biotechnol. Bioeng.* **2001**, *76*, 207-213.

82. D. O. Grigoriev, T. Bukreeva, H. Möhwald, D. G. Shchukin, *Langmuir* **2008**, *24*, 999-1004.

83. D. G. Shchukin, K. Kohler, H. Möhwald, G. B. Sukhorukov, *Angew. Chem., Int. Ed.* **2005**, 44, 3310-3314.

84. S. A. Sukhishvili, *Curr. Opin. Colloid Interface Sci.* **2005**, *10*, 37-44.

85. L. Krasemann, B. Tieke, *J. Membr. Sci.* **1998**, *150*, 23-30.

86. J. E. Wong, F. Rehfeldt, P. Hänni, M. Tanaka, R. Klitzing, *Macromolecules* **2004**, *37*, 7285-7289.

87. G. B. Sukhorukov, A. Fery, M. Brumen, H. Möhwald, *Phys. Chem. Chem. Phys.* **2004**, *6*, 4078-4089.

88. A. A. Antipov, G. B. Sukhorukov, S. Leporatti, I. L. Radtchenko, E. Donath, H. Möhwald, *Colloids Surf. A Physicochem Eng. Asp.* **2002**, *198*, 535-541.

89. J. D. Mendelsohn, C. J. Barret, V. V. Chan, A. J. Pal, A. M. Mayes, M. F. Rubner, *Langmuir* **2000**, *16*, 5017-5023.

90. A. J. Chung, M. F. Rubner, *Langmuir* **2002**, *18*, 1176-1183.

91. E. Kharlampieva, S. A. Sukhishvili, *Langmuir* **2004**, *20*, 9677-9685.

92. S. E. Burke, C. J. Barret, *Macromolecules* **2004**, *37*, 5375-5384.

93. M. K. Park, S. Deng, R. C. Advincula, *J. Am. Chem. Soc.* **2004**, *126*, 13723-13731.

94. J. Hiller, M. F. Rubner, *Macromolecules* **2003**, *36*, 4078-4083.

95. G. Ibarz, L. Dähne, E. Donath, H. Möhwald, *Adv. Mater.* **2001**, *13*, 1324-1327.

96. A. A. Antipov, G. B. Sukhorukov, H. Möhwald, *Langmuir* **2003**, *19*, 2444-2448.

97. K. Glinel, G. B. Sukhorukov, H. Möhwald, V. Khrenov, K. Tauer, *Macromol. Chem. Phys.* **2003**, *204*, 1784-1790.

98. J. A. Jaber, J. B. Schlenoff, *Macromolecules* **2005**, *38*, 1300-1306.

99. J. F. Quinn, F. Caruso, *Macromolecules* **2005**, *38*, 3414-3419.

100. J. F. Quinn, F. Caruso, *Langmuir* **2004**, *20*, 20-22.

101. C. Y. Gao, S. Leporatti, S. Moya, E. Donath, H. Möhwald, *Chem. Eur. J.* **2003**, *9*, 915-920.

102. G. Ibarz, L. Dähne, E. Donath, H. Möhwald, *Chem. Mater.* **2002**, *14*, 4059-4062.

103. a) K. Köhler, D. G. Shchukin, H. Möhwald, G. B. Sukhorukov, *J. Phys. Chem. B.* **2005**, *109*, 18250-18259; b) K. Köhler, H. Möhwald, G. B. Sukhorukov, *J. Phys. Chem., B.* **2006**, *47*, 24002-24010.

104. K. Köhler, G. B. Sukhorukov, *Adv. Func. Mater.* **2007**, *17*, 2053-2061.

105. A. G. Skirtach, B. G. De Geest, A. Mamedov, A. A. Antipov, N. A. Kotov, G. B. Sukhorukov, *J. Mater. Chem.* **2007**, *17*, 1050-1054.

106. D. A. Gorin, D. G. Shchukin, A. L. Mikhailov, K. Köhler, S. A. Sergeev, S. A. Portnov, I. V. Taranov, V. V. Kislov, G. B. Sukhorukov, *Tech. Phys. Lett.* **2006**, *32*, 70-72.

107. X. Tao, J. M. Su, *Curr. Nanosci.* **2008**, *4*, 308-313.

108. a) M. Bedard, A. G. Skirtach, G. B. Sukhorukov, *Macromol. Rapid Commun.* **2007**, *28*, 1517-1521; b) M. Bedard, B. G. De Geest, A. G. Skirtach, G. B. Sukhorukov, H. Möhwald, *Adv. Colloid Interface Sci.* **2010**, *158*, 2-14.
109. A. G. Skirtach, A. A. Antipov, D. G. Shchukin, G. B. Sukhorukov, *Langmuir* **2004**, *20*, 6988-6992.
110. a) B. Radt, T. A. Smith, F. Caruso, *Adv. Mater.* **2004**, *16*, 2184-2189; b) A. S. Angelatos, B. Radt, F. Caruso, *J. Phys. Chem., B.* **2005**, *109*, 3071-3076.
111. K. Katagiri, A. Matsuda, F. Caruso, *Macromolecules* **2006**, *39*, 8067-8074.
112. D. A. Gorin, S. A. Portnov, O. A. Inozemtseva, Z. Luklinska, A. M. Yashchenok, A. M. Pavlov, A. G. Skirtach, H. Möhwald, G. B. Sukhorukov, *Phys. Chem. Chem. Phys.* **2008**, *10*, 6899-6905.
113. M. Fang, P. S. Grant, M. J. McShane, G. B. Sukhorukov, V. O. Golub, Y. M. Lvov, *Langmuir* **2002**, *18*, 6338-6344.
114. Z. H. Lu, M. D. Prouty, Z. H. Guo, V. O. Golub, Ch. S. S. R. Kumar, Y. M. Lvov, *Langmuir* **2005**, *21*, 2042-2050.
115. T. Borodina, E. Markvicheva, S. Kunizhev, H. Möhwald, G. B. Sukhorukov, O. Kreft, *Macromol. Rapid Commun.* **2007**, *28*, 1894-1899.
116. H. Inoue, K. Sato, J. I. Anzai, *Biomacromolecules* **2005**, *6*, 27-29.
117. T. Serizawa, M. Yamaguchi, M. Akashi, *Angew. Chem., Int. Ed.* **2003**, *115*, 1147-1150.
118. A. A. Antipov, G. B. Sukhorukov, *Adv. Colloid Interface Sci.* **2004**, *111*, 49-61.
119. G. B. Sukhorukov, D. V. Volodkin, A. M. Gunther, A. L. Petrov, D. B. Shenoy, H. Möhwald, *J. Mater. Chem.* **2004**, *14*, 2073-2081.
120. L. Dähne, B. Baude, Patent WO/2005/089727, 2005.
121. A. D. Price, A. N. Zelikin, Y. J. Wang, F. Caruso, *Angew. Chem., Int. Ed.* **2009**, *48*, 329-332.
122. A. L. Petrov, D. V. Volodkin, G. B. Sukhorukov, *Biotech. Progress* **2005**, *21*, 918-925.
123. C. Y. Wang, C. Y. He, Z. Tong, X. X. Liu, B. Y. Ren, F. Zeng, *Int. J. Pharm.* **2006**, *308*, 160-167.
124. O. Kreft, M. Prevot, H. Möhwald, G. B. Sukhorukov, *Angew. Chem., Int. Ed.* **2007**, *46*, 5605-5608.
125. V. S. Trubetskoy, A. Loomis, J. E. Hagstrom, V. G. Budker, J. A. Wolff, *Nucleic Acid Res.* **1999**, *27*, 3090-3095.

126. Y. Urabe, T. Shiomi, T. Itoh, A. Kawai, T. Tsunoda, F. Mizukami, K. Sakaguchi, *ChemBioChem* **2007**, *8*, 668-674.

127. L. Dähne, S. Leoporatti, E. Donath, H. Möhwald, *J. Am. Chem. Soc.* **2001**, *123*, 5431-5436.

128. I. L. Radtchenko, G. B. Sukhorukov, S. Leoporatti, G. B. Khomutov, E. Donath, H. Möhwald, *J. Colloid Interface Sci.* **2000**, *230*, 272-280.

129. I. L. Radtchenko, M. Giersig, G. B. Sukhorukov, *Langmuir* **2002**, *18*, 8204-8208.

130. B. G. De Geest, R. E. Vandenbroucke, A. M. Guenther, G. B. Sukhorukov, W. E. Hennik, N. N. Sanders, J. Demeester, S. C. De Smedt, *Adv. Mater.* **2006**, *18*, 1005-1009.

131. Y. Itoh, M. Matsusaki, T. Kida, M. Akashi, *Biomacromolecules* **2006**, *7*, 2715-2718.

132. X. F. Su, B. S. Kim, S. R. Kim, P. T. Hammond, D. J. Irvine, *ACS Nano* **2009**, *3*, 3719-3729.

133. S. H. Hu, C. H. Tsai, C. F. Liao, D. M. Liu, S. Y. Chen, *Langmuir* **2008**, *24*, 11811-11818.

134. Gil. P. Rivera, L. L. der Mercato, P. del-Pino, A. Munoz-Javier, W. J. Parak, *Nano Today* **2008**, *3*, 12-21.

135. W. J. Tong, Y. Zhu, Z. P. Wang, C. Y. Gao, H. Möhwald, *Macromol. Rapid Commun.* **2010**, *31*, 1015-1019.

136. G. B. Sukhorukov, A. L. Rogach, B. Zebli, T. Liedl, A. G. Skirtach, K. Köhler, A. A. Antipov, N. Gaponic, A. S. Susha, M. Winterhalter, W. J. Parak, *Small* **2005**, *2*, 194-200.

137. E. M. Rosenbauer, M. Wagner, A. Musyanovych, K. Landfester, *Macromolecules* **2010**, *43*, 5083-5093.

138. R. Palankar, A. G. Skirtach, O. Kreft, M. Bedard, M. Garstka, K. Gould, H. Möhwald, G. B. Sukhorukov, M. Winterhalter, S. Springer, *Small* **2009**, *19*, 2168-2176.

139. A. Zhuk, S. Pavlukhina, S. A. Sukhishvili, *Langmuir* **2009**, *25*, 14025-14029.

140. P. Gil Rivera, S. De Koker, B. G. De Geest, W. J. Parak, *Nano Lett.* **2009**, *9*, 4398-4402.

141. M. Bedard, S. Sadasivan, G. B. Sukhorukov, A. G. Skirtach, *J. Mater. Chem.* **2009**, *19*, 2226-2233.

142. C. M. Jewell, D. M. Lynn, *Adv. Drug Delivery Rev.* **2008**, *60*, 979-999.

143. A. G. Skirtach, P. Karageorgiev, M. Bedard, G. B. Sukhorukov, H. Möhwald, *J. Am. Chem. Soc.* **2008**, *130*, 11572-11573.

144. B. G. De Geest, A. G. Skirtach, T. R. M. De Beer, G. B. Sukhorukov, L. Bracke, W. R. G. Baeyens, J. Demeester, S. C. De Smedt, *Macromol. Rapid Commun.* **2007**, *28*, 88-95.

145. A. P. R. Johnston, G. K. Such, F. Caruso, *Angew. Chem., Int. Ed.* **2010**, *49*, 2664-2666.

146. U. Manna, S. Patil, *Langmuir* **2009**, *25*, 10515-10522.

147. B. G. De Geest, N. N. Sanders, G. B. Sukhorukov, J. Demeester, S. C. De Smedt, *Chem. Soc. Rev.* **2007**, *36*, 646-649.

148. V. A. Sinani, D. S. Koktysh, B. G. Yun, L. Matts, T. C. Pappas, M. Motamedi, S. N. Thomas, N. A. Kotov, *Nano Lett.* **2003**, *3*, 1177-1182.

149. K. Kadowaki, M. Matsusaki, M. Akashi, *Langmuir* **2010**, *8*, 5670-5678.

150. S. Y. Wong, Q. Li, J. Veselinovic, B. S. Kim, A. M. Klibanov, P. T. Hammond, *Biomater.* **2010**, *31*, 4079-4087.

151. X. Liu, B. Dai, L. Zhou, J. Sun, *J. Mater. Chem.* **2009**, *19*, 497-504.

152. D. G. Shchukin, M. Zheludkevich, K. Yasakau, S. Lamaka, M. G. S. Ferreira, H. Möhwald, *Adv. Mater.* **2006**, *18*, 1672-1678.

153. P. Podsiadlo, L. Sui, Y. Elkasabi, P. Burgardt, J. Lee, A. Miryala, W. Kusumaatmaja, M. R. Carman, M. Shtein, J. Kieffer, J. Lahann, N. A. Kotov, *Langmuir* **2007**, *23*, 7901-7906.

154. L. Zhang, Z. A. Qiao, M. A. Zheng, Q. S. Huo, J. Q. Sun, *J. Mater. Chem.* **2010**, *20*, 6125-6130.

155. X. Wang, S. Y. Zhou, Y. Lai, J. Q. Sun, J. C. Shen, *J. Mater. Chem.* **2010**, *3*, 555-560.

156. W. Chen, T. J. McCarthy, *Macromolecules* **1997**, *30*, 78-86.

157. F. Van Ackern, L. Krasemann, B. Tieke, *Thin Solid Films* **1998**, *327*, 762-766.

158. X. M. Liu, J. H. He, *J. Phys. Chem., C* **2009**, *113*, 148-152.

159. Z. Tang, Y. Wang, P. Podsiadlo, N. A. Kotov, *Adv. Mater.* **2006**, *18*, 3203-3224.

160. T. Boudou, T. Crouzier, K. Ren, G. Blin, C. Picart, *Adv. Mater.* **2010**, *22*, 441-467.

161. H. Ai, S. A. Jones, Y. M. Lvov, *Cell Biochem. Biophys.* **2003**, *39*, 23-43.

162. W. J. Tong, C. Y. Gao, *J. Mater. Chem.* **2008**, *18*, 3799-3812.

163. W. Zhao, J. J. Xu, H. Y. Chen, *Electroanalysis* **2006**, *18*, 1737-1748.

164. K. Ariga, J. P. Hill, Q. Ji, *Phys. Chem. Chem. Phys.* **2007**, *9*, 2319-2340.

165. J. R. Siqueira Jr., L. Caseli, F. N. Crespilho, V. Zucolotto, O. N. Oliveira Jr., *Biosens. Bioelectron.* **2010**, *25*, 1254-1263.
166. J. A. Jaber, J. B. Schlenoff, *Curr. Opin. Colloid Interface Sci.* **2006**, *6*, 324-329.
167. C. Picart, *Curr. Med. Chem.* **2008**, *15*, 685-697.
168. L. Z. Zheng, X. Yao, J. H. Li, *Curr. Anal. Chem.* **2006**, *3*, 279-296.
169. P. T. Hammond, *Curr. Opin. Colloid Interface Sci.* **1999**, *6*, 430-442.
170. J. W. Ostrander, A. A. Mamedov, N. A. Kotov, *J. Am. Chem. Soc.* **2001**, *123*, 1101-1110.
171. P. Yager, G. J. Domingo, J. Gerdes, *Annu. Rev. Biomed. Eng.* **2008**, *10*, 107-144.
172. A. Mirkin, *Chem. Rev.* **2005**, *105*, 1547-1562.
173. W. H. Scouten, J. H. T. Luong, R. S. Brown, *Trends Biotechnol.* **1995**, *13*, 178-185.
174. M. Dufva, *Biomol. Eng.* **2005**, *22*, 173-184.
175. X. C. Zhou, L. Q. Huang, S. F. Y. Li, *Biosens. Bioelectron.* **2001**, *16*, 85-95.
176. S. D. Conzone, C. G. Pantanot, *Mater. Today* **2004**, *7*, 20-26.
177. M. Wilchek, E. A. Bayer, O. Livnah, *Immunol. Lett.* **2006**, *103*, 27-32.
178. X. H. Fang, X. J. Liu, S. Schuster, W. H. Tan, *J. Am. Chem. Soc.* **1999**, *121*, 2921-2922.
179. Y. Sakao, F. Nakamura, N. Ueno, M. Hara, *Colloids Surf., B* **2005**, *40*, 149-152.
180. G. Legay, E. Finot, R. Meunier-Prest, M. Cherkaoui-Malki, N. Latruffe, A. Dereux, *Biosens. Bioelectron.* **2005**, *21*, 627-636.
181. S. G. Wang, R. L. Wang, P. J. Sellin, Q. Zhang, *Biochem. Biophys. Res. Commun.* **2004**, *325*, 1433-1437.
182. H. Gu, X. D. Su, K. P. Loh, *J. Phys. Chem., B* **2005**, *109*, 13611-13618.
183. M. Fuentes, C. Mateo, A. Rodriguez, M. Casqueiro, J. C. Tercero, H. H. Riese, R. Fernandez-Lafuente, J. M. Guisan, *Biosens. Bioelectron.* **2006**, *21*, 1574-1580.
184. T. De Lumley-Woodyear, C. N. Campbell, A. Heller, *J. Am. Chem. Soc.* **1996**, *118*, 5504-5505.
185. H. Korri-Youssoufi, A. Yassar, *Biomacromolecules* **2001**, *2*, 58-64.
186. C. Kocum, S. D. Ulgen, E. Cubukcu, E. Piskin, *Ultramicroscopy* **2006**, *106*, 326-333.
187. B. P. Corgier, L. J. Blum, *J. Am. Chem. Soc.* **2005**, *127*, 18328-18332.
188. B. P. Corgier, A. Laurent, P. Perriat, L. J. Blum, C. A. Marquette, *Angew. Chem., Int. Ed.* **2007**, *46*, 4108-4110.
189. A. Janshoff, H. J. Galla, C. Steinem, *Angew. Chem., Int. Ed.* **2000**, *39*, 4004-4032.

190. Y. Okahata, Y. Matsunobu, K. Ijiro, M. Mukae, A. Murakami, K. Makino, *J. Am. Chem. Soc.* **1992**, *114*, 8299-8300.
191. D. J. Monk, D. R. Walt, *Anal. Bioanal. Chem.* **2004**, *379*, 931-945.
192. X. Wang, U. J. Krull, *Bioorg. Med. Chem. Lett.* **2005**, *15*, 1725-1729.
193. J. Y. Hu, X. Meng, S. Schacher, *J. Neurosci.* **2002**, *22*, 2669-2678.
194. K. Wang, Z. Tang, C. J. Yang, Y. Kim, X. Fang, W. Li, Y. Wu, C. D. Medley, Z. Cao, J. Li, P. Colon, H. Lin, W. Tan, *Angew. Chem., Int. Ed.* **2009**, *48*, 856-870.
195. N. E. Broude, *Trends Biotechnol.* **2002**, *20*, 249-256.
196. P. J. Santangelo, B. Nix, A. Tsourkas, G. Bao, *Nucleic Acid Res.* **2004**, *32*, 57-57.
197. H. J. Tanke, R. W. Dirks, T. Raap, *Curr. Opin. Biotechnol.* **2005**, *16*, 49-54.
198. W. R. Algar, A. J. Tavares, U. J. Krull, *Anal. Chim. Acta* **2010**, *673*, 1-25.
199. E. R. Goldman, I.L. Medintz, J. L. Whitley, A. Hayhurst, A. R. Clapp, H.T. Uyeda, J. R. Deschamps, M. E. Lassman, H. Mattoussi, *J. Am. Chem. Soc.* **2005**, *127*, 6744-6751.
200. S. Pathak, M. C. Davidson, G.A. Silva, *Nano Lett.* **2007**, *7*, 1839–1845.
201. E. Chang, J. S. Miller, J. Sun, W. W. Yu, V. L. Colvin, R. Drezek, J. L. West, *Biochem. Biophys. Res. Commun.* **2005**, *334*, 1317–1321.
202. D. Gerion, F. Q. Chen, B. Kannan, A. H. Fu, W. J. Parak, D. J. Chen, A. Majumdar, A. P. Alivisatos, *Anal. Chem.* **2003**, *75*, 4766-4772.
203. H. Peng, J. J. Zhang, T. H. M. Kjallman, C. Soeller, J. T. Sejdic, *J. Am. Chem. Soc.* **2007**, *129*, 3048-3049.
204. W. R. Algar, U. J. Krull, *Anal. Chim. Acta* **2007**, *581*, 193-201.
205. S. W. Thomas, G. D. Joly, T. M. Swager, *Chem. Rev.* **2007**, *107*, 1339-1386.
206. L. Chen, D. W. McBranch, H. L. Wang, R. Helgeson, F. Wudl, D. G. Whitten, *Proc. Natl. Acad. Sci. USA* **1999**, *96*, 12287-12292.
207. S. A. Kushon, K. D. Ley, K. Bradford, R. M. Jones, D. McBranch, D. G. Whitten, *Langmuir* **2002**, *18*, 7245-7249.
208. S. A. Kushon, K. Bradford, V. Marin, C. Suhrada, B. A. Armitage, D. W. Mcbranch, D. G. Whitten, *Langmuir* **2003**, *19*, 6456-6464.
209. a) R. M. Jones, T. S. Bergstedt, C. T. Buscher, D. W. Mcbranch, D. G. Whitten, *Langmuir* **2001**, *17*, 2568-2571; b) L. D. Lu, R. Helgeson, R. M. Jones, D. W. Mcbranch, D. G. Whitten, *J. Am. Chem. Soc.* **2002**, *124*, 483-488.
210. Y. Tang, K. E. Achyuthan, D. G. Whitten, *Langnuir* **2009**, *26*, 6832-6837.

211. H. A. Ho, M. Boissinot, M. G. Bergeron, G. Corbeil, K. Dore, D. Boudreau, M. Leclerc, *Angew. Chem., Int. Ed.* **2002**, *41*, 1548-1551.

212. a) M. Bera-Aberem, H. A. Ho, M. Leclerc, *Tetrahedron* **2004**, *60*, 11169-11173; b) K. Dore, S. Dubus, H. A. Ho, I. Levesque, M. Brunette, G. Corbeil, M. Boissinot, G. Boivin, M. Leclerc, M. G. Bergeron, D. Boudreau, M. Leclerc, *J. Am. Chem. Soc.* **2004**, *126*, 4240-4244; c) H. A. Ho, M. Leclerc, D. Boudreau, *J. Fluoresc.* **2006**, *16*, 259-265.

213. H. A. Ho, K. Dore, M. Boissinot, M. G. Bergeron, R. M. Tanguay, D. Boudreau, M. Leclerc, *J. Am. Chem. Soc.* **2005**, *127*, 12673-12676.

214. B. S. Gaylord, A. J. Heeger, G. C. Bazan, *J. Am. Chem. Soc.* **2003**, *125*, 896-900.

215. B. Liu, S. Wang, G. C. Bazan, A. Mikhailovsky, *J. Am. Chem. Soc.* **2003**, *125*, 13306-13307.

216. S. Wang, B. S. Gaylord, G. C. Bazan, *J. Am. Chem. Soc.* **2004**, *126*, 5446-5451.

217. Q. H. Xu, S. Wang, D. Korystov, A. Mikhaiovsky, G. C. Bazan, D. Moses, A. J. Heeger, *Proc. Natl. Acad. Sci. USA* **2005**, *102*, 530-535.

218. F. He, Y. Tang, M. Yu, F. Feng, L. An, H. Sun, S. Wang, Y. Li, D. Zhu, G. C. Bazan, *J. Am. Chem. Soc.* **2006**, *128*, 6764-6765.

219. J. W. Hong, W. L. Hemme, G. E. Keller, M. T. Rinke, G. C. Bazan, *Adv. Mater.* **2006**, *18*, 878-882.

220. B. S. Gaylord, M. R. Massie, S. C. Feinstein, G. C. Bazan, *Proc. Natl. Acad. Sci. USA* **2005**, *102*, 34-39.

221. M. Wang, D. Q. Zhang, G. X. Zhang, Y. L. Tang, S. Wang, D. B. Zhu, *Anal. Chem.* **2008**, *16*, 6443-6448.

222. T. Vo-Dinh, K. Houck, D. Stokes, *Anal. Chem.* **1994**, *66*, 3379-3383.

223. T. Niazov, V. Pavlov, Y. Xiao, R. Gill, I. Willner, *Nano Lett.* **2004**, *4*, 1683-1687.

224. T. A. Taton, G. Lu, C. A. Mirkin, *J. Am. Chem. Soc.* **2001**, *123*, 5164-5165.

225. H. Berney, K. Oliver, *Biosens. Bioelectron.* **2005**, *21*, 618-626.

226. N. Y. Yang, X. Su, V. Tjong, W. Knoll, *Biosens. Bioelectron.* **2007**, *22*, 2700-2706.

227. T. Förster, *Naturwissenschafte*n **1946**, *6*, 166-195.

228. T. Förster, *Ann. Phys.* **1948**, *2*, 55-75.

229. N. D. Huebsch, D. J. Mooney, *Biomater.* **2007**, *28*, 2424-2437.

230. G. Baneyx, L. Baugh, V. FN. Vogel, *Proc. Natl. Acad. Sci. USA* **2002**, *99*, 5139–5143.

231. C. Berney, G. Danuser, *Biophy. J.* **2003**, *84*, 3992-4010.

232. a) C. Gutierrez-Merino, *Biophy. Chem.* **1981**, *14*, 247-257; b) C. Gutierrez-Merino, *Biophy. Chem.* **1982**, *14*, 259-266.
233. M. C. Doody, L. A. Sklar, H. J. Pownall, J. T. Sparrow, A. M. Gotto-Jr, L. C. Smith, *Biophy. Chem.* **1983**, *17*, 139-152.
234. E. A. Jares-Erijman, T. M. Jovin, *Nat. Biotechnol.* **2003**, *21*, 1387-1395.
235. M. A. Cooper, *J. Mol. Recognit.* **2004**, *17*, 286-315.
236. K. E. Sapsford, L. Berti, I. L. Medintz, *Minerva Biotecnologica* **2004**, *16*, 247-273.
237. H. Wallrabe, A. Periasamy, *Curr. Opin. Biotech.* **2005**, *16*, 19-27.
238. J. A. Swanson, *Mol. Cell. Microbiol.* **2002**, *31*, 1-18.
239. S. S. Varghess, Y. G. Zhu, T. J. Davis, S. C. Trowell, *Lab on a Chip* **2010**, *10*, 1355-1364.
240. R. Zhao, D. Rueda, *Methods* **2009**, *49*, 112-117.
241. F. Ciruela, *Curr. Opin. Biotech.* **2008**, *19*, 338-343.
242. E. Haas, *ChemPhysChem* **2005**, *6*, 858-870.
243. G. T. Hermanson, *Bioconjugate techniques*, Elsevier Science, San Diego, **1996**.
244. A. Kurz, A. Bunge, A. K. Windeck, M. Rost, W. Flasche, A. Arbuzova, D. Strohbach, S. Müller, J. Liebscher, D. Huster, A. Herrmann, *Angew. Chem.* **2006**, *113*, 4550-4554; *Angew. Chem., Int. Ed.* **2006**, *45*, 4440-4444.
245. P. W. Atkins, *Physical Chemistry* Oxford University Press, **2002**.
246. N. S. Claxton, T. J. Fellers, M. W. Davidson, *Laser Scanning Confocal Microscopy* retrieved on 20/09/2010 from the world wide web: http://www.olympusfluoview.com/theory/LSCMIntro.pdf
247. J. R. Sheppard, D. M. Shotton, *Confocal Laser Scanning Microscopy* Bios Scientific Publishers, Oxford, **1997**.
248. H. M. Shapiro, *Practical Flow Cytometry* Wiley Liss, New York, **2003**.
249. C. Lu, A. W. Czanderna, *Applications of Piezoelectric Quartz Crystal Microbalances* Elsevier, New York, **1984**.
250. G. Sauerbrey, *Zeitschrift. Physik* **1959**, *155*, 206-222.
251. F. Caruso, E. Rodda, D. N. Furlong, *J. Colloid Interface Sci.* **1996**, *178*, 104-115.
252. K. O. Evans, *Int. J. Mol. Sci.* **2008**, *9*, 498-511.
253. K. Katagiri, R. Hamasaki, K. Ariga, J. Kikuchi, *Langmuir* **2002**, *18*, 6709-6711.
254. G. Binnig, C. F. Quate, C. Gerber, *Phy. Rev. Lett.* **1986**, *56*, 930-933.
255. R. A. Wilson, H. A. Bullen, *Introduction to Scanning Probe Microscopy (SPM)* retrieved on 20/09/2010 from the World Wide Web:

http://asdlib.org/onlineArticles/ecourseware/Bullen/SPMModule_BasicTheorySTM.pdf.

256. E. Spyratou, E. A. Mourelatou, M. Makropoulou, C. Demetzos, *Expert Opin. Drug Delivery* **2009**, *6*, 305-317.
257. S. R. Cohen, A. Bitler, *Curr. Opin. Colloid Interface Sci.* **2008**, *13*, 316-325.
258. A. Simon, M. C. Durrieu, *Micron* **2006**, *37*, 1-13.
259. J. Loos, *Adv. Mater.* **2005**, *17*, 1821-1833.
260. J. N. Israelachvili, *Intermolecular and Surface Forces* Academic Press, London, **2002**.
261. Personal communication with Dr. Nitzsche from Malvern Instruments Ltd., Germany, **2009**.
262. J. J. I. Ramos, I. Llarena, L. Fernandez, S. E. Moya, E. Donath, *Macromol. Rapid Commin.* **2009**, *30*, 1756-1761.
263. D. Voet, J. G. Voet, *Biochemistry*, 3rd ed., Wiley-VCH, Weinheim, **2004,** Ch. 5.
264. P. Yin, H. M. Choi, C. R. Calvert, N. A. Pierce, *Nature* **2008**, *451*, 318-322.
265. D. Nykypanchuk, M. M. Maye, D. van der Lelie, O. Gang, *Nature* **2008**, *451*, 549-552.
266. S. Y. Park, A. K. Lytton-Jean, B. Lee, S. Weigand, G. C. Schatz, C. A. Mirkin, *Nature* **2008**, *451*, 553-556.
267. Y. He, T. Ye, M. Su, C. Zhang, A. E. Ribbe, W. Jiang, C. Mao, *Nature* **2008**, *452*, 198-201.
268. M. Loew, J. Kang, L. Dähne, R. Altenburger, O. Kaczmarek, J. Liebscher, D. Huster, K. Ludwig, C. Böttcher, A. Herrmann, A. Arbuzova, *Small* **2009**, *5*, 320-323.
269. K. M. Parkhurst, L. Parkhurst, *Biochemistry*, **1995**, *34*, 285-292.
270. B. Dubertret, M. Calame, A. J. Libchaber, *Nature Biotech.* **2001**, *19*, 365-370.
271. W. J. Qin, L. Y. L. Yung, *Biosen. Bioelectron.* **2009**, *25*, 313-319.
272. A. P. Abel, M. G. Weller, G. L. Duveneck, M. Ehrat, H. M. Widmer, *Anal. Chem.* **1996**, *68*, 2905-2912.
273. C. S. Peyratout, E. Donath, L. Dähne, *J. Photochem. Photobiol., A* **2001**, *142*, 51-57.
274. C. S. Peyratout, E. Donath, L. Dähne, *Phys. Chem. Chem. Phys.* **2002**, *4*, 3032-3039.
275. F. M. Winnik, *Chem. Rev.* **1993**, *93*, 587-614.
276. A. S. Davydov, *Theor. Mol. Exc*. McGraw-Hill, New York, **1962.**
277. A. Fery, B. Scholer, T. Cassagneau, *Langmuir* **2001**, *17*, 3779-3783.
278. R. Georgieva, R. Dimova, G. Sukhorukov, *J. Mater. Chem.* **2005**, *15*, 4301-4310.

279. E. E. Jelly, *Nature* **1936**, *138*, 1009-1010.

280. a) G. Scheibe, *Angew. Chem.* **1936**, *49***,** 563-563; b) W. West, S. P. Lovell, W. Cooper, *Photogr. Sci. Eng.* **1970**, *14*, 52-62.

281. M. Kasha, H. R. Rawls, M. A. El-Bayoumi, *Pure Appl. Chem.* **1965**, *11*, 371-392.

282. D. Moebius, *Adv. Mater.* **1995**, *7*, 437- 444.

283. A. Mishra, G. B. Behera, M. M. G. Krishna, N. Periasamy, *J. Lumin.* **2001**, *92*, 175-188.

284. D. Pristinski, V. Kozlovskaya, S. A. Sukhishvili, *J. Chem. Phys.* **2005**, *122*, 014907.

285. C. Reznik, Q. Darugar, A. Wheat, T. Fulghum, R. C. Advincula, C. F. Landes, *J. Phys. Chem., B* **2008**, *112*, 10890-10897.

286. K. Becker, J. M. Lupton, *J. Am. Chem. Soc.* **2006**, *128*, 6488-6479.

287. A. P. R. Johnston, A. N. Zelikin, L. Lee, F. Caruso, *Anal. Chem.* **2006**, *16*, 5913-5919.

288. V. E. Keuren, W. Schrof, *Macromol.* **2003**, *13*, 5002-5007.

289. K. Ray, H. Nakahara, A. Sakamoto, M. Tasumi, *Chem. Phys. Lett.* **2001**, *342*, 58-64.

290. K. Becker, J. M. Lupton, J. Feldmann, B. S. Nehls, F. Galbrecht, D. Q. Gao, U. Scherf, *Adv. Funct. Mater*. **2006**, *16*, 364-370.

291. M. A. Rahim, W. S. Choi, H. J. Lee, I. C. Jeon, *Langmuir* **2010**, *26*, 4680-4686.

292. J. Kang, O. Kaczmarek, J. Liebscher, L. Dähne, *Inter. J. Polym. Sci.* **2010**, 264781.

293. N. El. Kadi, F. Martin, D. Clausse, P. C. Schulz, *Colloid Polym. Sci.* **2003**, *281*, 353-362.

294. J. W. Ledbetter, J. R. Bowen, *Anal. Chem.* **1969**, *41*, 1345-1347.

List of Publications

M. Loew, J. Kang, L. Dähne, R. Altenburger, O. Kaczmarek, J. Liebscher, D. Huster, K. Ludwig, C. Boettcher, A. Herrmann, A. Arbuzova, *Controlled Assembly of Vesicle-based Nanocontainers on Layer-by-Layer Particles via DNA Hybridisation*, Small**, 2009**, *5*, 320-323.

A. Bunge, M. Loew, P. Pescador, A. Arbuzova, N. Brodersen, J. Kang, L. Dähne, J. Liebscher, A. Herrmann, G. Stengel, D. Huster, *Lipid membranes carrying lipophilic cholesterol-based oligonucleotides--characterisation and application on layer-by-layer coated particles*, J. Phys. Chem. B, **2009**, *113*, 16425-16434.

J. Kang, M. Loew, A. Arbuzova, I., Andreou, L. Dähne, *Nucleic acid diagnostic FRET particles based on Layer-by-Layer tenchmology*, Advanced Materials, **2010**, *22*, 3548-3552.

J. Kang, O. Kaczmarek, J. Liebscher, L. Dähne, *Prevention of H-aggregates formation in Cy5 labelled macromolecules*, International Journal of Polymer Science, **2010**, 264781-264787.

J. Kang, L. Dähne, *Strong response of polyelectrolyte films to cationic surfactants*, Langmuir, **2011,** accepted.